Gas Turbine Laboratory
Department of Aeronautics and Astronautics
Massachusetts Institute of Technology
Cambridge, MA 02139-4307

A Final Technical Report

for research supported under NASA Grant #NAG3-2222

entitled

STATOR LOADING MEASUREMENTS BEHIND A FAN WITH TRAILING EDGE BLOWING

submitted to

NASA Glenn Research Center
21000 Brookpark Avenue
Cleveland, OH 44135

Attn: Dennis Huff, Program Manager

INVESTIGATORS: Ian A. Waitz
Associate Professor of
Aeronautics & Astronautics

Margarita C. Brito
Graduate Research Assistant

January 2000

CONTENTS

List of Figures

List of Tables

CHAPTER 1

INTRODUCTION

1.1 Motivation and Objectives

The problem of aircraft noise pollution around airports has become increasingly important as those areas have become more densely populated. Currently, the removal of older noisier aircraft from operation is reducing noise levels around airports [2]; however, with air traffic projected to increase by about 5% over the next decade the number of commercial aircraft operating in the world is expected to be about 17,700 by the year 2007 [1]. To keep noise levels around airports from increasing as a result of traffic increases, it is important to investigate new methods of noise reduction.

The main sources of aicraft noise are airframe noise and engine noise with the engine being the largest contributor. In many high-bypass-ratio turbofans, the total perceived noise is dominated by fan noise [15]. One of the major components of fan noise is rotor-stator interaction noise. This type of noise results from the interaction of the stator row with the unsteady gusts produced by the rotor. Rotor-stator interaction produces two types of noise— tonal noise and broadband noise. Tonal noise stems from stator interaction with the harmonic components of gusts produced by the rotor wake. This type of noise appears in discrete tones which correspond to multiples of blade passing frequency. Broadband noise is a result of stator interaction with gusts produced by turbulence in the flow.

Typical methods for reducing rotor-stator interaction noise include choosing appropriate blade-to-vane ratios to cut off tones with the most energy, and increasing blade-to-vane spacing to allow greater mixing of the wake. More recently new methods for rotor-stator interaction noise reduction have been investigated. These have included studies on the effects of leaning and sweeping of the stator vanes [8] [14] as well as investigations of wake management techniques. This thesis addresses the latter category.

Wake management refers to techniques, such as trailing edge blowing and boundary layer suction, which are designed to reduce the magnitude of the wake through addition or removal of fluid. Preliminary studies by Waitz et al. [22] indicate that noise reductions can be obtained through either trailing edge blowing or boundary layer suction, but suggest that trailing edge blowing is more attractive because it is relatively easier to implement. Subsequently, three-dimmensional rig experiments by Brookfield [3] and Brookfield et al. [4], have shown significant reductions in the wake harmonics as a result of trailing edge blowing. However, Brookfield [3] found that changes in stator unsteady pressure measurements did not always correlate well with changes in the wake harmonics. He suggested that further investigations be conducted.

The objective of this work is to provide a better understanding of the effects that trailing edge blowing has on stator unsteady loading. This is done by presenting flowfield and stator loading data from experiments conducted with and without trailing edge blowing. Additionally, computational data from the BBN/PW V072 rotor-stator interaction noise prediction code and from the viscous cascade code MISES [6] is used to help interpret the experimental results.

In the next section a brief overview of previous research in the area of rotor stator interaction and trailing edge blowing will be given. A description of the experimental facility is given in Chapter 2. Chapter 3 describes modifications that were made to the trailing edge blowing distribution. In Chapter 4 the flow field measurements are presented. Stator loading measurements are presented in Chapter 5 and discussed in

Chapter 6. Finally, conclusions and recomendations are given in Chapter 7.

1.2 Previous Research

Because this thesis focuses on the stator unsteady loading response to changes in the wake harmonics due to trailing edge blowing, it is appropriate to provide a brief overview of research regarding airfoil response to unsteady gusts as well as an overview of research on trailing edge blowing. Section 1.2.1 deals with airfoil response to unsteady gusts, while Section 1.2.2 discusses trailing edge blowing research.

1.2.1 Airfoil Response to Unsteady Gusts

The response of airfoils to unsteady gusts has long been the object of study. In 1941, Sears [20] developed an analytical model for the unsteady lift of a flat plate under transverse gusts. In 1968, Horlock [9] looked at the effects of longitudinal gusts on a flat plate and determined that the unsteady lift response could be significant, and in some cases greater than the response caused by transverse gusts, at high angles of attack and high lift. By combining his results with the Sears model, Horlock obtained an expression for the unsteady lift response of a flat plate to a general gust. The effects of camber were first considered by Naumann and Yeh in 1973 [16]. In 1976, Goldstein and Atassi [7] formulated a complete second order theory for the unsteady lift which includes the effects of longitudinal and transverse gusts, the effects of angle of attack, camber and thickness as well as all of the coupling effects. One of the elements included in this theory is the distortion of the gust by the steady-state airfoil response. This distortion proves to have a significant impact on the unsteady lift response. Furthermore, it introduces nonlinearities which prevent the effects of thickness, camber and angle of attack from being considered separately and then superposed.

1.2.2 Trailing Edge Blowing Research

Early experiments with trailing edge blowing demonstrated the ability to reduce the mean wake deficit [5] [17] [18]. Later, two-dimensional cascade experiments by Sell [21] investigated the effects of adding different amounts of mass as well as the effects of different injection port geometries. Noise reduction estimates were made based on amplitude reductions of the wake profile spatial harmonics. The noise estimates showed the greatest reductions when momentumeless wakes were produced and injection was done at the deviation angle. The results also showed that not fully eliminating the momentum deficit produced larger harmonic reductions than exceeding the momentum deficit by the same amount.

Experiments by Leitch [12] (see also Ref. [13]) showed that trailing edge blowing can be used to effectively reduce radiated noise generated by stator wake-rotor interaction. Trailing edge blowing was applied to four inlet guide vanes located upstream of a rotor and tests were conducted at 40%, 60% and 88% of the design speed. For all cases, acoustic far-field measurements showed reductions in the overall sound pressure level. Reductions in the blade passing tone ranged from 2.6dB at 88% speed to 8.9dB at 40% speed.

Finally, an existing fan design was modified to incorporate trailing edge blowing and tested by Brookfield in a realistic three-dimensional environment [3] (see also Ref. [4]). Flow field measurements were taken at 0.1 and 1.5 rotor chords downstream of the the rotor. These locations correspond to just downstream of the rotor trailing edge and just upstream of the stator leading edge. The flow field measurements showed that both the wake harmonic amplitude and the wake harmonic phase can be manipulated. Up to 80% reductions in the wake harmonic amplitudes were seen at 1.5c and the harmonic amplitudes at 0.1c with blowing were found to be up to 40% smaller than those without blowing at 1.5c. Shifts of approximately 180 degrees were seen in the harmonic phase when the wake was overfilled. The stator pressure measurements showed that changes in the stator harmonics did not correlate well with changes in the wake harmonics and further study was recommended. Finally,

due to changes in the radial mode content, the duct wall acoustic measurements were inconclusive.

CHAPTER 2

EXPERIMENTAL SETUP

This chapter describes the experimental setup. First a description of the blowdown compressor facility will be given. This will be followed by a description of the instrumentation. Next, the test section geometry will be discussed, and finally, a brief description of the wake management system will be given.

2.1 Blowdown Compressor Facility

The experiments were conducted in the blowdown compressor facility in the Gas Turbine Laboratory at MIT. The facility was developed by Kerrebrock, and details of the theory and development of the facility can be found in [11]. The basic facility consists of a supply tank(100 ft^3) and a dump tank(300 ft^3) connected by a tube 2 ft in diameter (23.25" inside diameter) and approximately 5 ft long. As seen in the schematic diagram in Figure 2-1, the front part of the connecting tube allows for removal of the casing boundary layer and the aft part of the tube contains the test section. Finally, the supply tank is separated from the test section and dump tank by a fast acting valve. A full description of the valve's design and operation can be found in [23].

The basic procedure used to conduct a test in the blowdown compressor is as follows: 1) the entire facility is brought down to vacuum (less than 200 milliTorr)

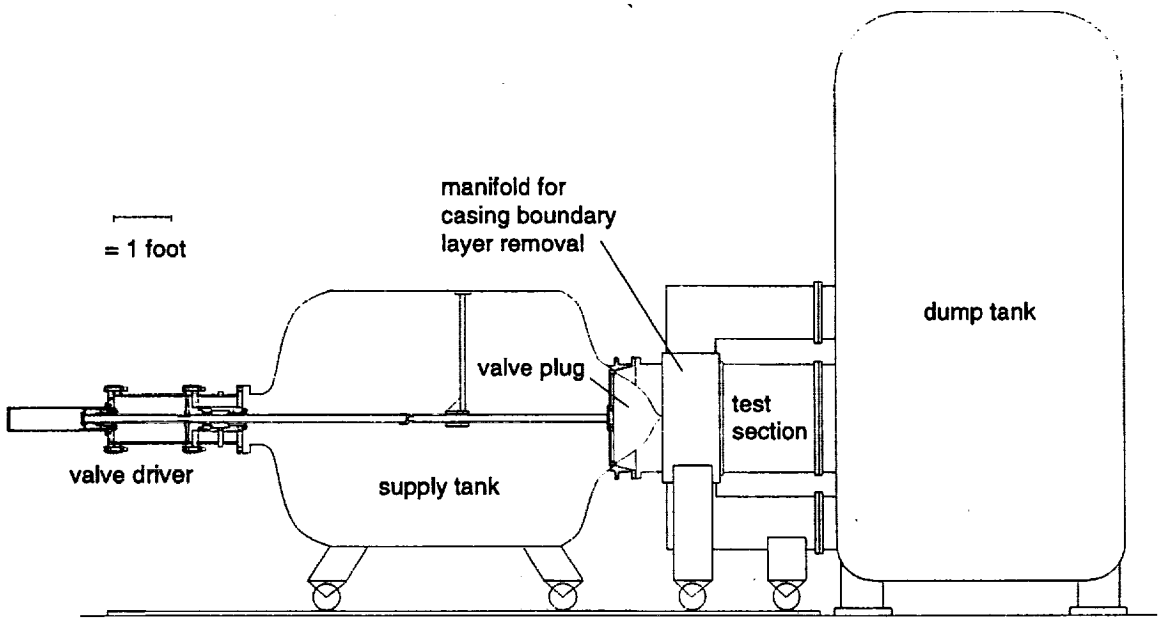

Figure 2-1: Blowdown compressor facility

with the fast acting valve closed, 2) the supply tank is filled with a gas mixture of 61.7% CO_2 and 38.3% Ar by mass fraction, this mixture was chosen to match, at the test conditions for this study, the specific heat ratio of air, 3) an electric motor is used to bring the fan to a speed higher than the desired test speed, 4) the motor is turned off and the fan spins freely with the speed slowly decaying due to frictional forces, 5) when the fan reaches the target speed, the fast acting valve opens and the data acquisition system begins to take data.

During the test, the speed of the rotor decreases as it does work on the flow. The rate of decay of the rotor speed depends on the inertia of the rotor and the amount of work done on the flow. At the same time, the pressure and temperature in the supply tank decay as the gas in the supply tank expands isentropically. By proper matching of the initial supply tank pressure to the rotor inertia for a given operating point, the change in speed of sound can be matched to the change in rotor speed to within 1% resulting in constant Mach numbers and flow angles. The test lasts approximately 300 milliseconds from the time when the valve is opened until the data acquisition system stops taking data. However, the time during which the Mach number and flow

angles remain constant is about 80 milliseconds. This time is equivalent to about 8 rotor revolutions or 200 flow through times. For flow phenomena on the time scale of blade passing this condition corresponds to steady-state. The time during which the facility is in steady-state and the measurement probes are in place is about 60 milliseconds, in this study the equivalent of 6 rotor revolutions or 96 blade passing periods [11].

2.2 Instrumentation

This section describes the instrumentation and the data acquisition system used in this study. The main sources of data were the four-way probe described in Section 2.2.1 and the instrumented stator described in Section 2.2.2. The rest of the instrumentation used is briefly described in Section 2.2.3. The data acquisition system is described in Section 2.2.4.

2.2.1 Four-way Probe

Flow field measurements behind the rotor were made using a probe instrumented with four flush-mounted Kulite differential pressure transducers (XCQ-093-25D) with vacuum reference. The transducers are thermally compensated and the probe includes water cooling to help prevent thermal drift from the transducers heating up in vacuum.

The four transducers are arranged on the probe such that the total and static pressures as well as the radial and tangential flow angles can be determined. From these four quantities the flow Mach number and its components (radial, tangential and axial) can be determined. As seen in Figure 2-2, the probe head is an elliptical cylinder with the tip cut off at a 45 degree angle. Detailed drawings of the probe can be found in Reijnen [19]. Transducer 1 faces the flow, transducers 2 and 3 are at $\pm$ 45 degrees in the tangential direction, and transducer 4 is at 45 degrees in the radial direction. Not shown in Figure 2-2 is a permanent fin which was attached to

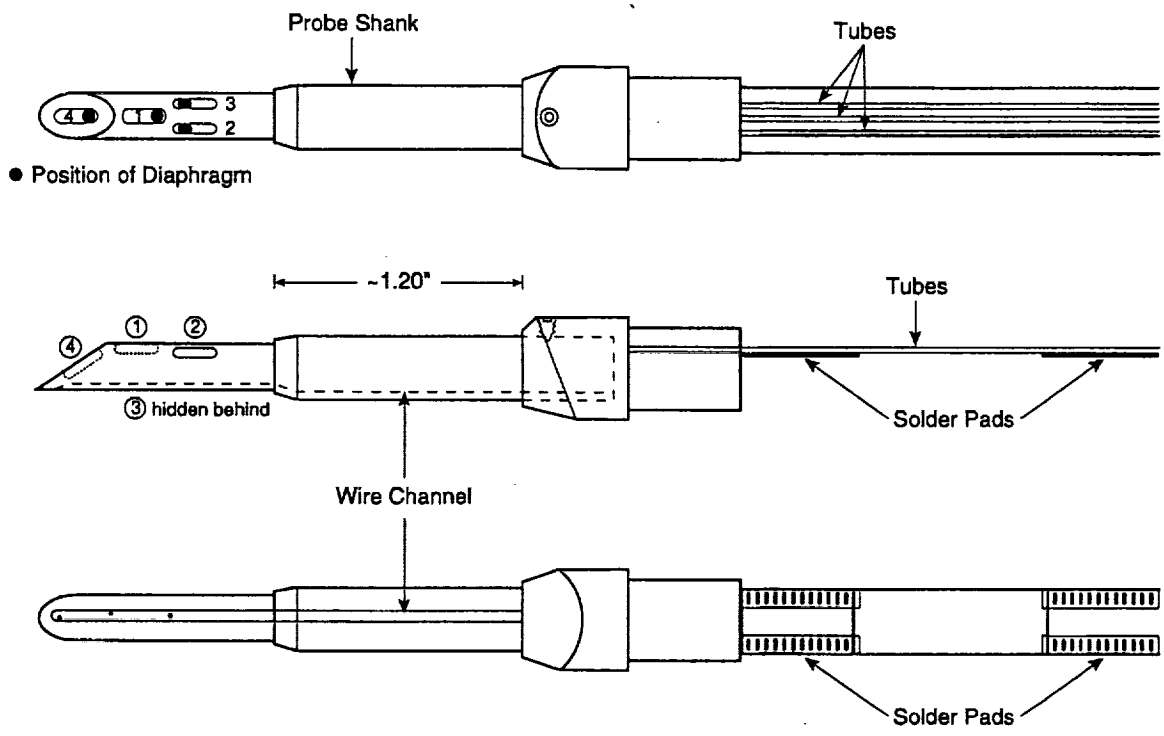

Figure 2-2: Four-way probe

the back of the probe to reduce errors due to unsteady vortex shedding as explained in Brookfield [3]. A schematic of the probe cross-section with the fin attached is shown in Figure 2-3.

The probe was calibrated at Boeing in a 1" free jet facility. Errors were found to be ± 1 degree in flow angles and $\pm 1\%$ in Mach numbers and total pressure over the normal operating range. Detailed explanations of the calibration process and the data reduction procedures can be found in Reijnen [19].

The probe was mounted on a translator which traveled in the radial direction and was actuated pneumatically. The actuator was connected to a timer circuit which delayed firing of the probe into the flow to prevent damage to the transducers during tunnel start-up. The final position of the probe was set by stoppers made of 1" OD rubber tubing and calibrated in length to position the probe at the desired radial location. To determine the time history of the probe position, a linear potentiometer was connected to the probe translator. When measurements were taken closer to the hub than 25% span, the pneumatic actuator was not used and the translator was

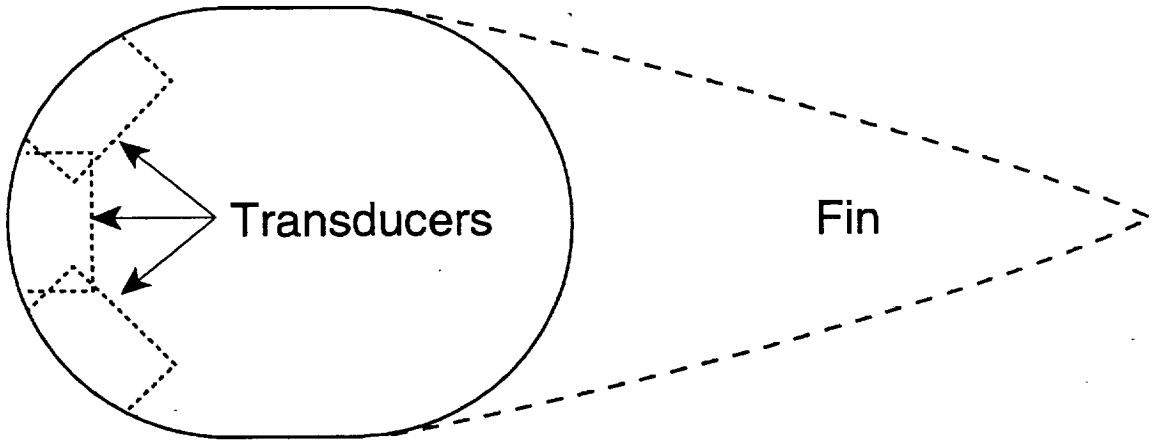

Figure 2-3: Four-way probe cross-section with fin

clamped in place in order to prevent the probe head from hitting the hub when fired.

2.2.2 Instrumented Stator

Stator loading measurements were taken using a stator blade instrumented with 13 flush-mounted Kulite differential pressure transducers (XCQ-093-15D) with vacuum reference. As shown in Figure 2-4, there are seven transducers on the suction side and six transducers on the pressure side. The instrumented blade was made extra long and fitted with a detachable extension equal to 50% of the stator span. These features allow the row of transducers to be positioned at any point along the stator span. A schematic of the instrumented stator blade is shown in Figure 2-5. A more detailed description of the instrumented stator design can be found in Brookfield [3].

2.2.3 Other Instrumentation

Pressure transducers

Absolute pressure transducers were used in the supply and dump tanks as well as in the hub. A 35 psi differential pressure transducer was used to measure the total pressure of the wake management tank.

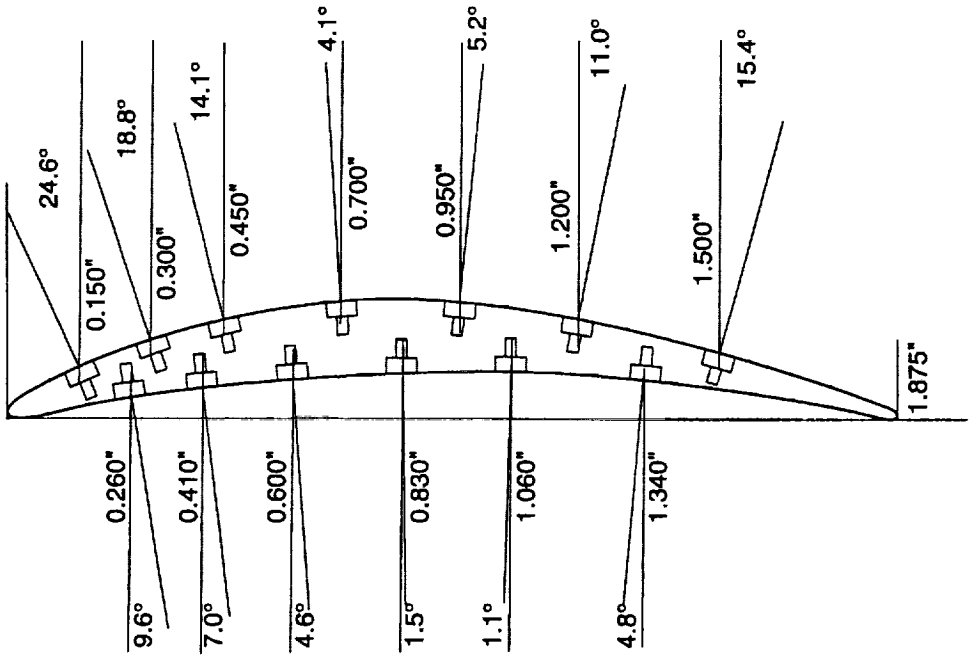

Figure 2-4: Instrumented stator blade transducer locations

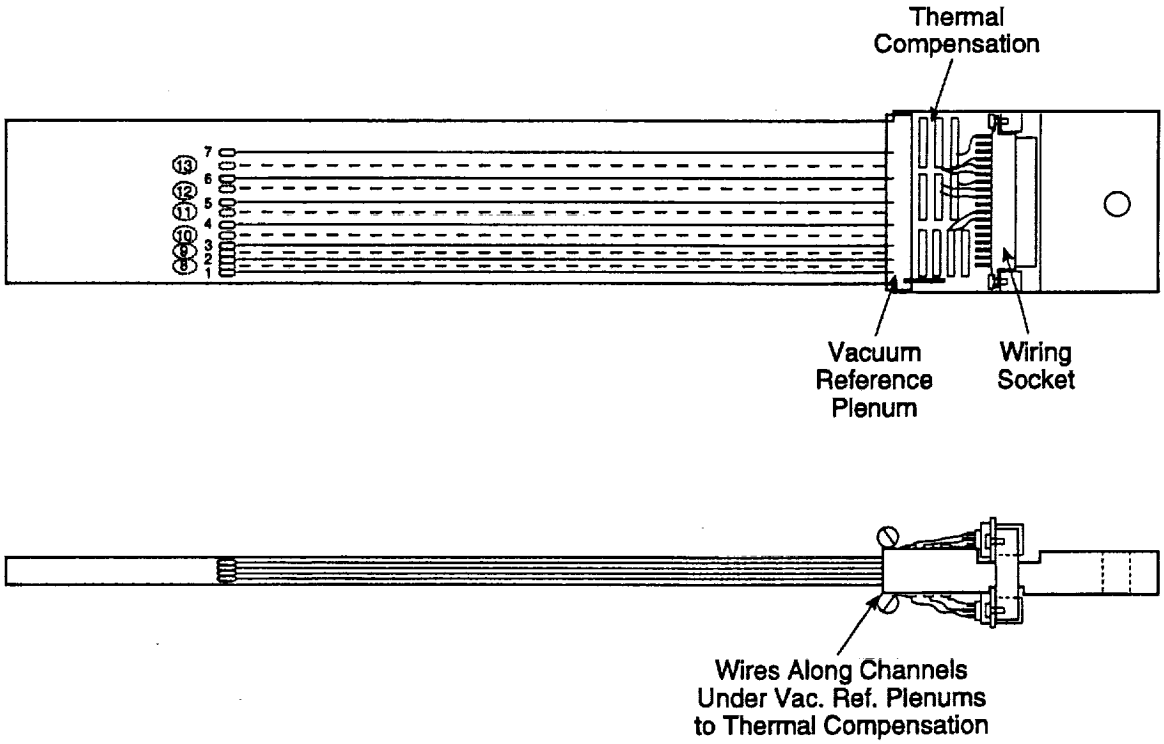

Figure 2-5: Schematic of instrumented stator blade

Gauges and thermocouples

Absolute pressure gauges were used to measure pressures in the supply tank, the dump tank, and the vacuum reference system. A gage pressure pressure transducer was used in the wake management tank. Thermocouples in the supply tank were used to measure the temperature in the supply tank at the beginning of each run.

Optical encoder

An optical shaft encoder which outputs a 400 pulse per revolution signal was used to determine the speed of the rotor. Additionally, the encoder produces a one pulse per revolution index signal which was used to ensure the data analyzed for each run was always with the rotor in the same location.

2.2.4 Data Aquisition System

The data acquisition system used consists of a DELL 450DE 80486 32 MB RAM EISA with three 12-bit 8 channel ADTEK A/D boards. The A/D boards accept signals in the range of ± 10 volts. The data was sampled at a rate of 333kHz.

Except for the 6 pressure side transducers on the stator blade and the supply and dump tank transducers, all transducers were driven by 10 Pacific Instruments model 3210 transducer conditioning amplifiers. The excitation voltage was set at 15 volts DC and the gain was set to maximize the A/D input range. The signals were filtered through 50kHz low-pass filters internal to the amplifiers. The 6 pressure side stator transducers were driven by Pacific Instruments model 8650, F2, J transducer amplifiers. The signals were filtered through a separate 25kHz low-pass filter bank. The excitation voltage was set at 15 volts DC except for transducer eleven. The gain and zero offset were set to maximize the filter input signal range which is ± 5 volts. The excitation voltage for transducer eleven was initially set at 15 volts but was changed to 13 volts mid-way through the testing due to thermal drift problems.

As stated in Brookfield [3], the linearity of the transducers was checked up to one atmosphere pressure difference. The microphone and stator transducers were not linear over one atmosphere and correction factors had to be applied during data reduction.

The transducers were calibrated on a daily basis by calculating the slope from zero pressure differential to one atmosphere pressure differential. The slope variation during the testing was less than one percent. The calibrations were also compared to calibrations taken more than one year earlier and were found to be consistent to within one percent.

2.3 Fan Stage Test Geometry

The test section used in this study was designed by Brookfield and first used in the studies presented in [3] [4]. The engineering drawings and a full description of the test section design can be found in [3]. As in the Brookfield experiment, the stator leading edge is located 1.7 midspan rotor chords behind the rotor trailing edge and a choke-plate is located two stator chords behind the stator trailing edge. See Figure 2-6 for a drawing of the test section layout.

The test fan is 22 inches in diameter and has a hub to tip ratio of approximately 0.45. It features 16 wide chord blades with 40 degrees of twist from hub to tip. The outer blade geometry is a scaled version of the 17 inch Pratt and Whitney Advanced Ducted Propulsor but, as part of the wake management design, has a modified trailing edge. The inner blade geometry incorporates five passages— one for every 20 percent of the span. The flow through each of the five passages can be managed using a throttle plate placed at the base of the blade over the inlets to each of the passages. Each passage ends in seven discrete injection ports that open to the suction surface of the blade. Additionally, each passage has two internal vanes to help turn the flow and provide structural support. A stagger angle view of the blade is shown in Figure 2-7.

The stator row used in the tests consists of 40 blades which are uniform along

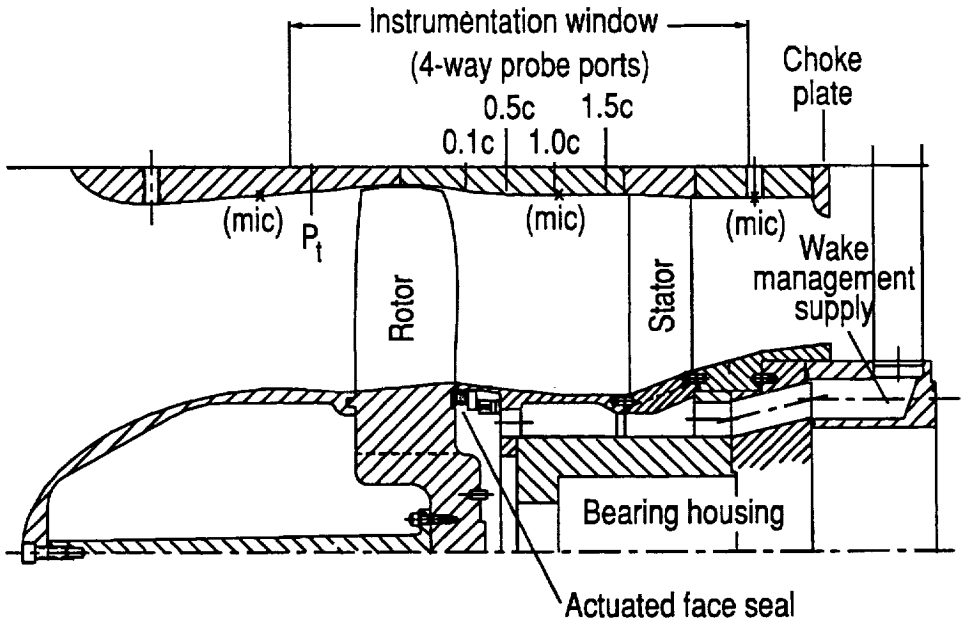

Figure 2-6: Test section layout in blowdown compressor

the span. The airfoil of the stator blades is the same as the midspan airfoil of the stator designed for the ADP fan but with a slightly modified leading edge.

2.4 Blowing System

This section provides a brief overview of the system used to provide the gas for trailing edge blowing. More details can be found in [3]. Like the main gas flow, the gas used for trailing edge blowing was a mixture of CO_2 and Ar. It was held in a cylindrical tank with approximately 356 cubic inches of effective volume. The flow was initiated by a single fast acting valve which led the gas through a 1" diameter pipe to a settling chamber of approximately 73 cubic inches. From the settling chamber, eight 1/2" copper tubes connected to wake management tubes located at 45 degree increments along the circumference of the tunnel. The wake management tubes led the flow through the outer tunnel casing and the outer part of the motor/bearing housing to the area under the hub. This is illustrated in Figure 2-6. The gas then flowed under the hub to the back face of the rotor where it fed into the blades. To minimize leakage through the gap between the rotor back face and the hub, a graphite face seal was

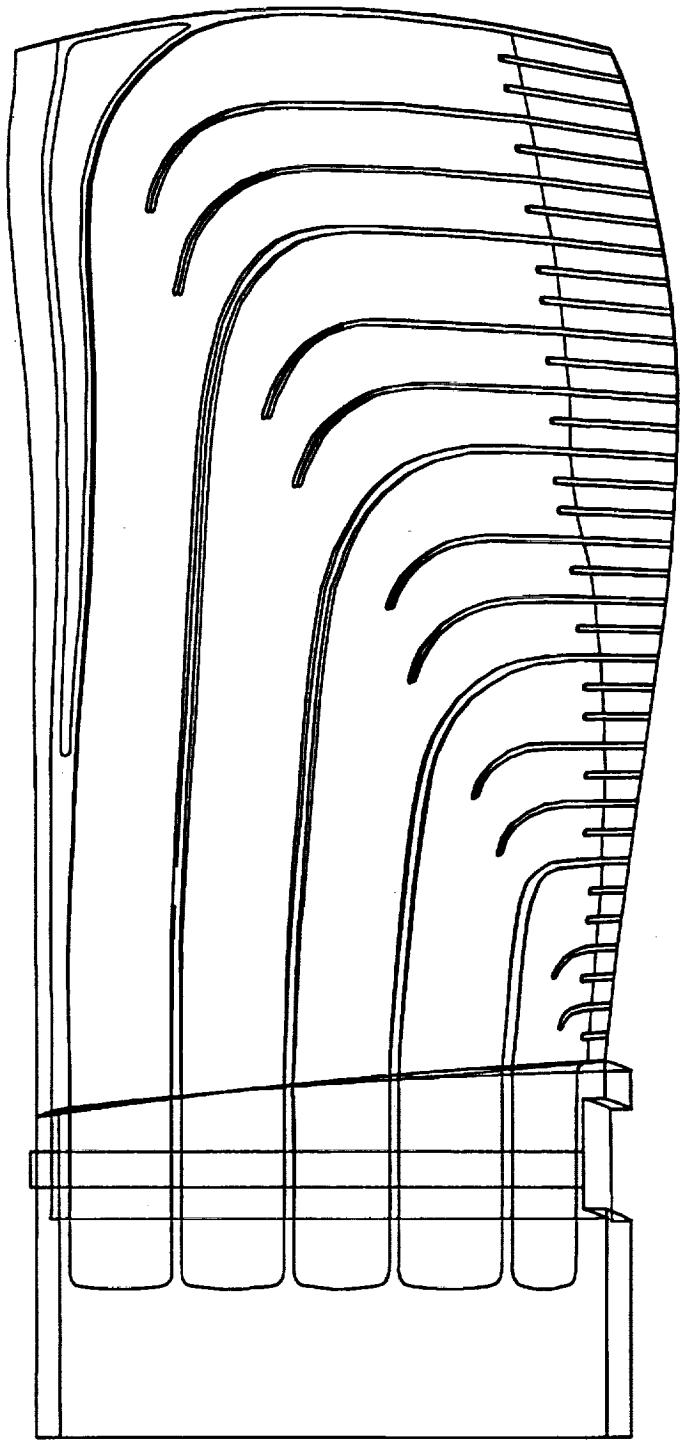

Figure 2-7: Trailing edge blowing blade, stagger view

used (see Figure 2-6). The seal was mounted on eight miniature pneumatic actuators and was held back while the rotor was brought up to speed. This was done to prevent the seal from overheating. When the main flow through the tunnel was initiated, the seal was seated. Subsequently it was pulled back after the tunnel unchoked.

CHAPTER 3

MODIFICATIONS TO BLOWING DISTRIBUTION

The trailing edge blowing distribution used in this study differs from the distributions used by Brookfield. Brookfield tested two different trailing edge blowing distributions, a tip-weighted case and a midspan-weighted case. In the tip-weighted case the wake was momentumless at about 80 percent span but was overfilled at the tip and underfilled at the hub. The midspan-weighted case was underfilled at both the tip and the hub regions and overfilled at 50% span. The tip-weighted distribution resulted when throttle plates were placed at the base of the blades. The midspan-weighted distribution was obtained when no throttle plates were used [3]. The blowing distribution in the experiments presented in this thesis is a compromise between the two Brookfield distributions. The present blowing distribution was obtained by using a set of throttle plates designed with the aid of data from Brookfield's experiments as well as data from a set of experiments which will be described shortly. The goal of the throttle plate modification was to achieve a spanwise uniform momentumless wake. Although this was not achieved, the resulting distribution has less spanwise variation than either of the distributions presented in Brookfield [3].

In the following sections, the methods used to design new throttle plates are described. Section 3.1 details the parametric studies which were carried out to gather data needed for the throttle plate design. In Section 3.2, the metric used to evaluate

the wake reduction is explained. Section 3.3 explains how losses in the blowing system were estimated. This is followed by a description of the throttle plate design method in Section 3.4. Finally, the resulting blowing distribution is presented in Section 3.5.

3.1 Parametric Studies

Data from the pressure transducers in the wake management tank and the hub, in combination with four-way probe data, provided the opportunity to better estimate the conditions needed for a momentumless wake while eliminating the need to estimate the pressure losses incurred from the wake management tank to the hub. To expand on the information provided by Brookfield's data, a set of experiments using Brookfield's midspan-weighted blowing distribution was carried out. The midspan-weighted distribution was chosen because it does not incorporate throttle plates. Flowfield measurements were taken at 1.5 midspan rotor chords downstream of the rotor trailing edge at the following radial locations: 15%, 25%, 50%, 75% and 87.5% of span. At each location, measurements were taken with increasing initial pressures in the wake management tank until a "flat" or an overfilled wake was obtained. For this reason, the number of runs at each location varied.

The parametric experiments provided four major pieces of information. First, they showed that momentumless wakes could be achieved at all the spanwise locations where measurements were taken. Second, the experiments proved that the wake management system had the capacity to provide the hub pressures needed to obtain momentumless wakes at each span. Third, injection was found to be off-center at locations near the hub, i.e. 15% and 25% span, resulting in an increased 2*BPF harmonic when a momentumless wake was achieved. At these locations, the highest reductions in wake harmonics were achieved at a hub pressure close to that needed for a momentumless wake at 87.5% span. Finally, the parametric studies showed that the hub pressure rate of decay was not matched well to the main supply tank pressure rate of decay. During the length of the usable data window, the hub pressure

to supply pressure ratio changed by close to 60% resulting in wakes that were not uniformly filled in time. By opening the wake management tank 100 msec earlier to allow time to fill the hub before the flow through the tunnel was initiated, the hub pressure to supply pressure ratio variation was reduced to about 17%. Because the wake variation during the run was found to be comparable to that found in the cases without blowing, efforts to further reduce the hub pressure to supply pressure ratio variation were not pursued.

3.2 Momentum Thickness Calculations

The metric used to measure wake reduction is the fraction of momentum thickness filled. The changes in temperature and density between the free stream and the wake were small so speed of sound and density were assumed constant. Thus the momentum thickness equation was reduced to:

$$\theta = \int_b^e \frac{M}{M_\infty}(1 - \frac{M}{M_\infty})dy \tag{3.1}$$

where θ is momentum thickness, M indicates Mach number, and the ∞ subscript indicates free stream values. Due to the unsteadiness inherent in the flow, equation 3.1 was only applied to the portion of the flow containing the wake as indicated by the integral limits b and e. The method used to identify the wakes is described in Appendix A. The free stream Mach number was calculated by mass-averaging the Mach number of the flow outside the wake limits.

To determine the fraction of momentum thickness filled, the momentum thickness of the wakes with trailing edge blowing was compared to the momentum thickness of wakes with no trailing edge blowing. For the parametric studies, the no blowing measurements taken by Brookfield at 25%, 50%, 75%, and 87.5% span were used. Because Brookfield did not include measurements at 15% span, measurements without blowing were taken at 15% span during the parametric studies.

3.3 Loss Calculations

During the design of the initial set of throttle plates, Brookfield estimated the losses in the blowing system to obtain pressure values at the hub and at the base of the blades. The need to estimate the losses from the wake management tank to the hub was eliminated once experiments were conducted because pressure measurements at the hub were taken. However, the pressure losses incurred from the hub to the base of the blade passages still had to be estimated. Two types of losses were considered in the estimate. The first were turning losses resulting from a 90 degree turn into the blade passages, the second were losses introduced by the throttle plates at the base of the blades. The losses through the blade were not considered because hub pressure measurements and flow field measurements were available. It was assumed that matching the conditions at the base of the blade passages would result in matching the conditions at the exit of the blade passages.

Before estimating the turning losses it was necessary to calculate the Mach number at the base of each blade passage. The total pressure of the flow before it turned into the blade passages was assumed to be equal to the pressure measured at the hub, the mass flow was set equal to the amount of mass needed to fully eliminate the momentum deficit, and the following equation was solved numerically for the Mach number:

$$\dot{m} = P_t M A \sqrt{\frac{\gamma}{RT_t}} (1 + \frac{\gamma - 1}{2} M^2)^{-\frac{1+\gamma}{2(\gamma-1)}} \tag{3.2}$$

where $\dot{m}$ is mass flow, P_t is total pressure, γ is the specific heat ratio, R is the gas constant, T_t is total temperature, M is Mach number, and A is area. Once the Mach number was computed, Equation 3.3 was used to compute the total pressure after losses.

$$P_{t2} = \frac{P_{t1}}{(1 + \frac{\gamma-1}{2} M^2)^{\frac{\gamma}{(\gamma-1)}}} \tag{3.3}$$

P_{t1} and P_{t2} are the total pressures before and after the turning loss is applied. As indicated equation 3.3, the turning loss was assumed to be equal to the difference between total and static pressure.

To estimate the throttle plate losses, the flow was modelled as flow from one infinite area to another through a beveled orifice facing the flow direction, and the ratio of orifice thickness to hydraulic diameter was estimated as greater than 0.16. In such a case, the loss coefficient is given as ζ =0.18 [10]. ζ is defined as the pressure loss over the dynamic pressure of the jet, $\zeta = \delta P_t / q_{jet}$. Since the pressure loss needed was prescribed, the following equations could be solved simultaneously to determine the orifice area needed.

$$A_o = \frac{\dot{m}}{M P_{tjet}} \sqrt{\frac{RT_t}{\gamma}} (1 + \frac{\gamma - 1}{2} M^2)^{\frac{1+\gamma}{2(\gamma-1)}} \tag{3.4}$$

$$q_{jet} = \frac{1}{2} \gamma P_{tjet} M_{jet}^2 (1 + \frac{\gamma - 1}{2} M_{jet}^2)^{\frac{\gamma}{\gamma-1}} \tag{3.5}$$

The total pressure of the jet was assumed to be equal to P_{t2} from Equation 3.3. As before, $\dot{m}$ represents mass flow, but in this case it was set equal to the mass flow needed for each individual passage.

3.4 Throttle Plate Design

To obtain a new blowing distribution, a modified set of throttle plates was designed. Information from the parametric studies described in Section 3.1 as well as from Brookfield's experiments was used to aid in the design of the new throttle plates. The parametric studies indicated that a momentumless wake at 15% span resulted in an increase of the 2*BPF harmonic. Furthermore, it was seen that the largest reductions in the 1*BPF and 2*BPF harmonics were seen at a hub pressure similar

to that needed to achieve a momentumless wake at 87.5% span. For the reasons just mentioned, the passages responsible for the 0-20% and the 80-100% sections of span were left unthrottled. The process followed to determine the size of the throttling holes for the middle three passages is described in the following paragraphs.

First, the pressure needed at the base of each blade passage was established. Using data from the parametric studies, the hub pressures needed to produce momentumless wakes at each spanwise section was established. Then, turning losses were calculated, as described in Section 3.3, to provide an estimate for the total pressure required at the base of each blade passage. As previously mentioned, the throttle plate losses were not considered at this point because the data used for this purpose was taken without throttle plates.

The next step was to establish the design hub pressure. Since the passage responsible for the 80-100% section of span was left unthrottled, the design hub pressure was set to be that which produced a momentumless wake at the 87.5% span location. Once the hub pressure was established, turning losses were once again calculated and the "feed" pressure at the base of each passage was determined.

Finally, the difference between the feed pressure and the required pressure was used to establish the throttle plate hole sizes. Losses through the throttle plate were calculated as described in Section 3.3. The size of each hole was set to produce the pressure drop needed to obtain adequate pressures at the base of each blade passage.

3.5 Results of Throttle Plate Modifications

Figure 3-1 shows the blowing distribution achieved with the new set of throttle plates along with the two distributions tested by Brookfield. The thicker line marked with asterisks represents the new distribution. The lines marked with circles and crosses represent the tip-weighted and mid-weighted distributions respectively. Although the new distribution did not achieve a spanwise uniform reduction in momentum thickness, the spanwise variation was reduced.

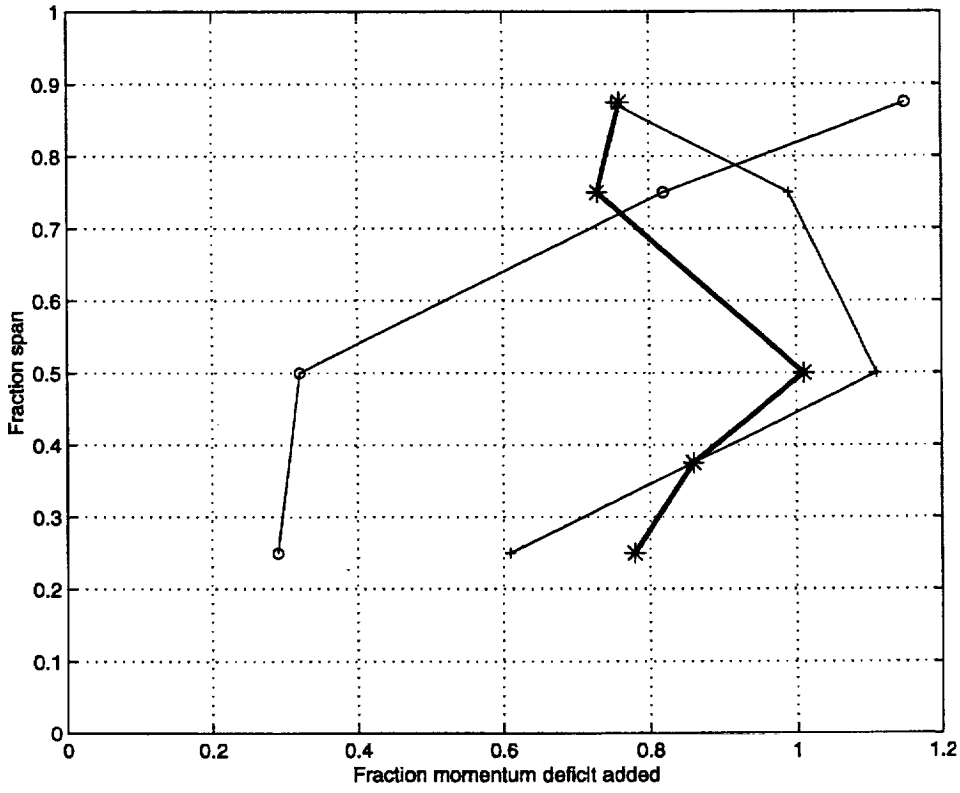

Figure 3-1: Fraction momentum thickness filled at 1.5c. Modified distribution(*), tip-weighted distribution(o), mid-weighted distribution(+)

CHAPTER 4

FLOW FIELD MEASUREMENTS AND STATOR UNSTEADY LOADING PREDICTIONS

This chapter is divided into two main parts, the first part (Sections 4.1 and 4.2) presents flow field data with and without trailing edge blowing. The data presented illustrates the flow field changes caused by trailing edge blowing. The second part (Sections 4.3 and 4.4) presents stator unsteady loading predictions based on the measured wake data that were calculated using the noise prediction program BBN/PW V072. The unsteady loading predictions will later be compared with the stator measurements presented in Chapter 5.

4.1 Overview of Flow Field Measurements

Flow field measurements were taken using the four-way probe described in Chapter 2. Measurements were taken at 1.5c downstream of the rotor trailing edge at the following five radial locations: 25%, 37.5%, 50%, 75% and 87.5% span. All data is presented as an ensemble average on blade passing period and is shown along with 95% confidence intervals. For the cases without blowing, the average consists of one run with 96 blade passing periods. For the cases with blowing, two runs with 96 blade passing periods were averaged. For the blowing case at 37.5% span the runs averaged

contained only 80 blade passing periods.

For each radial location, two sets of figures are presented. The first is used to illustrate the degree to which trailing edge blowing reduced the wake, the second provides information more directly relevant to understanding the stator response. The first set of figures shows the rotor relative Mach number, the relative Mach number blade passing frequency (BPF) harmonics, and the rms of the non-harmonic component of the relative Mach number. The latter is largely a measure of the turbulence intensity; although it also includes other disturbances not harmonic on the blade passing period such as those caused by blade-to-blade differences. The second set of figures shown for each radial location will present the harmonic amplitudes of the axial, tangential, longitudinal and transverse Mach number components. The components of the absolute Mach number (axial, tangential, radial), the flow angles, and the static and total pressures are presented in Appendix B.

4.2 Flow Field Measurements

25% span

As seen in Figure 4-1, the no blowing wake width exceeds 60% of the rotor pitch and the maximum velocity deficit is greater than 15% of the freestream value. The relative Mach number in the trailing edge blowing case has a velocity excess on the pressure side of the wake and a velocity deficit on the suction side. This indicates that the blowing mass addition did not occur at the center of the wake, but rather toward the pressure side. The velocity deficit is equal to about 6% of the freestream value and the velocity excess is about 4%.

At this spanwise location, reductions in the relative Mach number harmonics are only seen for the first two multiples of BPF (Figure 4-1b). At 1*BPF a reduction of close to 60% is seen. At less than 20%, the reduction at 2*BPF is more modest. Changes in the axial and longitudinal Mach number harmonics (Figure 4-2a,c) follow

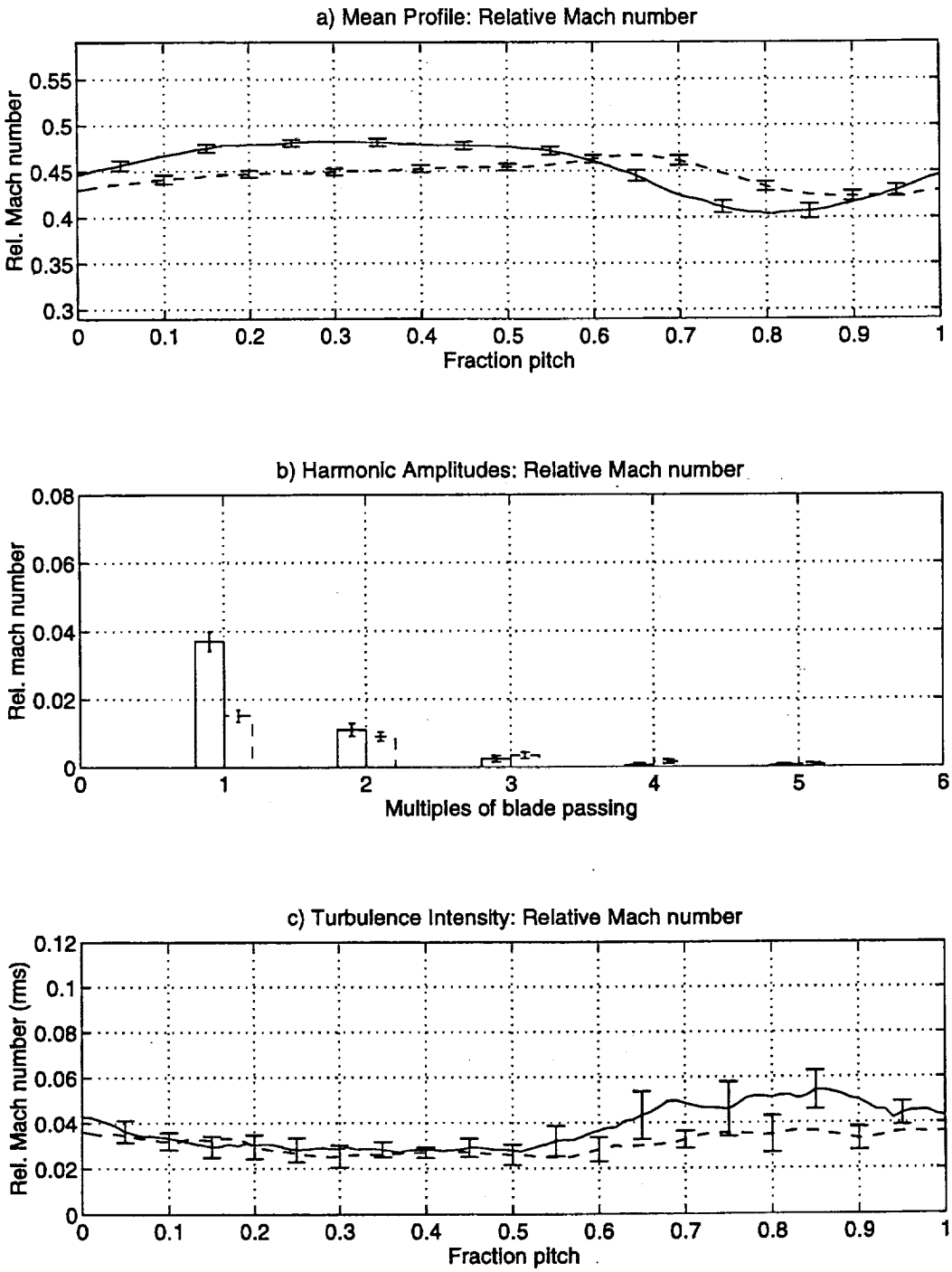

Figure 4-1: Relative Mach number data at 1.5c, 25% span. (—)w/o blowing, (- -)w/ blowing

the same trend as the changes in the relative harmonics. However, in the tangential and transverse harmonics, reductions are seen at each of the first five multiples of blade passing frequency. It is necessary to note, however, that there is a strong overlap in the confidence intervals of the higher harmonics.

37.5% span

At 37.5% span, the unaltered wake has a maximum velocity deficit equal to about 11% of the free stream value. In the blowing case, mass was added near the center of the wake resulting in a velocity excess with velocity deficits on either side (see Figure 4-3). Each of the velocity deficits and the velocity excess is equal to about 2% of the freestream value.

The relative harmonics show reductions of 90% and 87% for the first two multiples of BPF respectively. The 3*BPF harmonic increases by over 80%. The 4*BPF and 5*BPF harmonics also increase. As in the relative harmonics, the longitudinal harmonics show strong decreases in the first two multiples of BPF and an increase in the 3*BPF harmonic. The transverse harmonics, however, also show an increase in the 2*BPF harmonic (see Figure 4-4).

50% span

The 50% span case without blowing has a maximum velocity deficit of about 10% of the freestream value (see Figure 4-5). In the blowing case, the maximum velocity deficit is reduced to about 1% of the freestream value; however, a jet component with a velocity excess of about 2% of the freestream value is also present in the wake. This indicates that the mass addition was slightly off-center.

Large reductions in the relative Mach number harmonics are seen in the blowing case. The 1*BPF harmonic is reduced by almost 95% and the 2*BPF harmonic is reduced by close to 85%. The 3*BPF and 4*BPF harmonics are reduced by over 60% and 40% respectively. Reductions of about 80%, 75%, 70% and 55% are seen for the

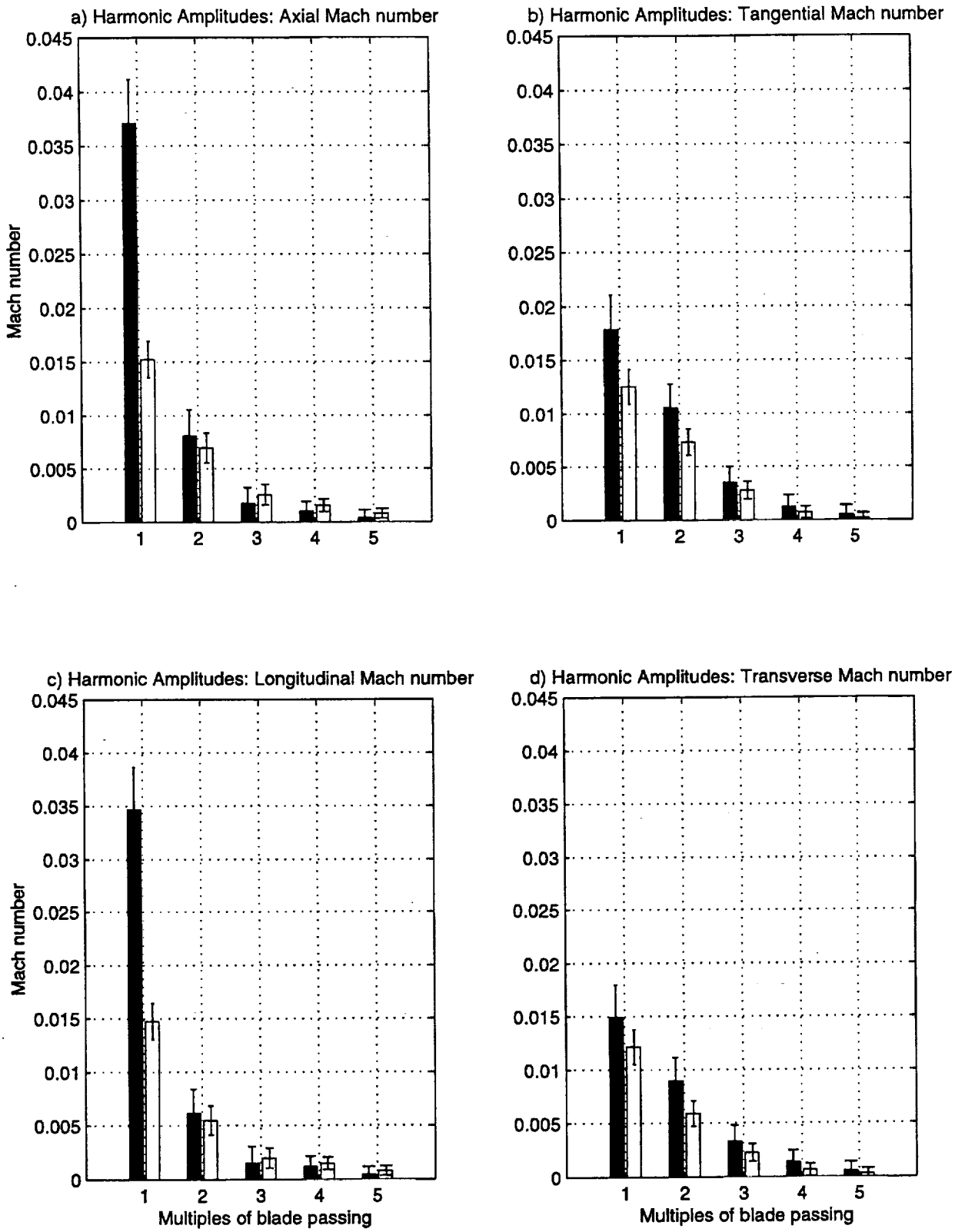

Figure 4-2: Wake harmonic data at 1.5c, 25% span. (shaded)w/o blowing, (open)w/ blowing

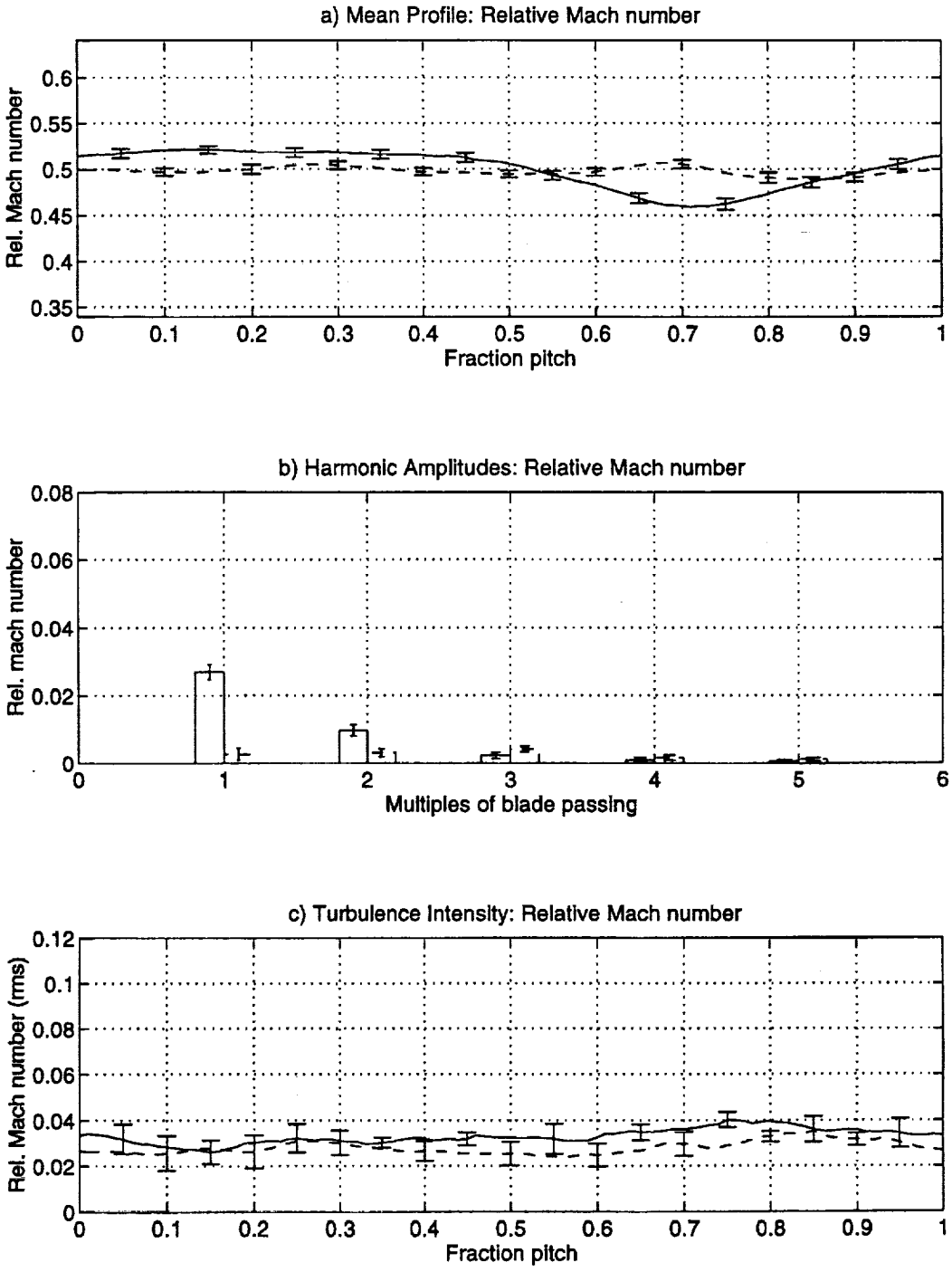

Figure 4-3: Relative Mach number data at 1.5c, 37.5% span. (—)w/o blowing, (- -)w/ blowing

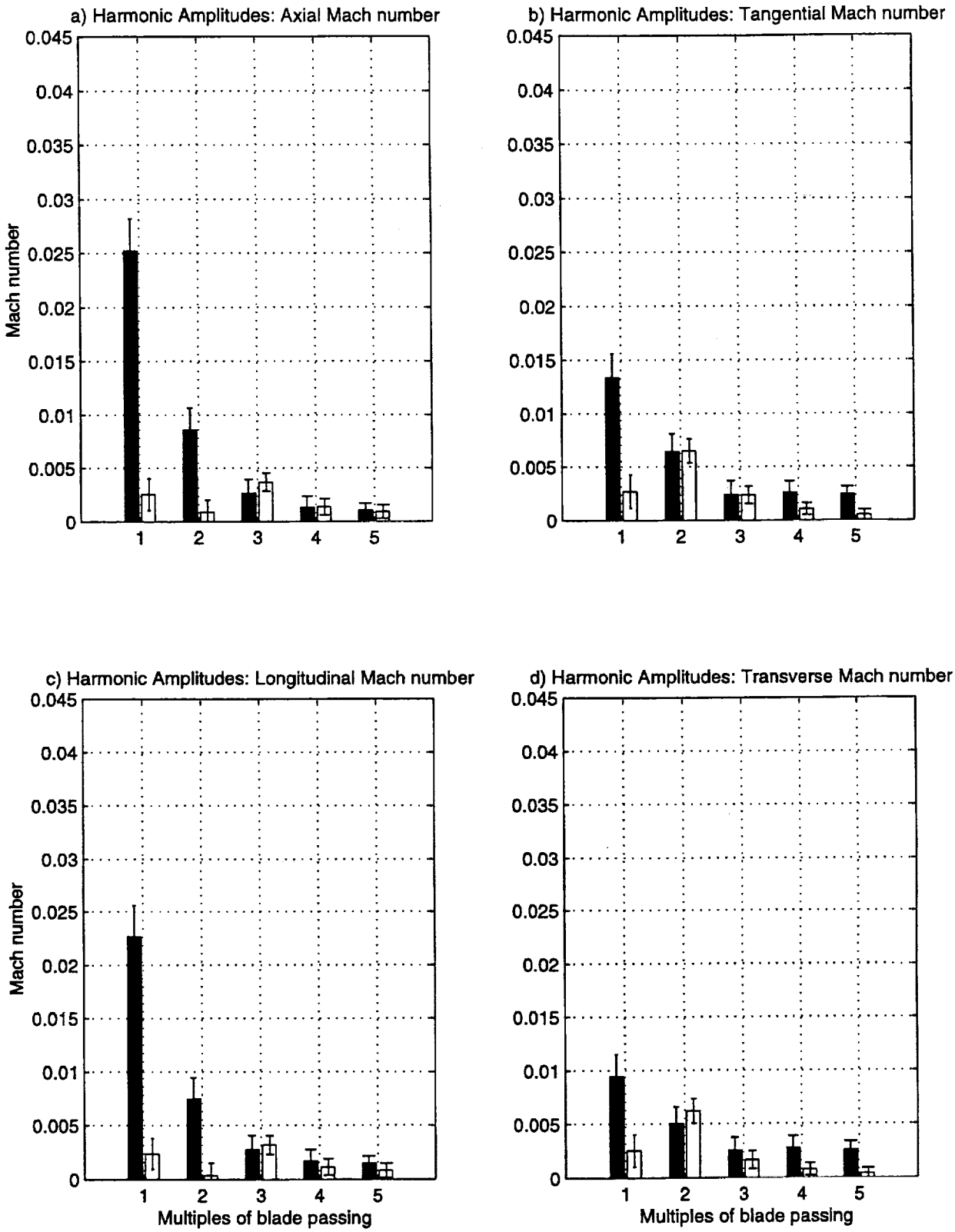

Figure 4-4: Wake harmonic data at 1.5c, 37.5% span (shaded)w/o blowing, (open)w/ blowing

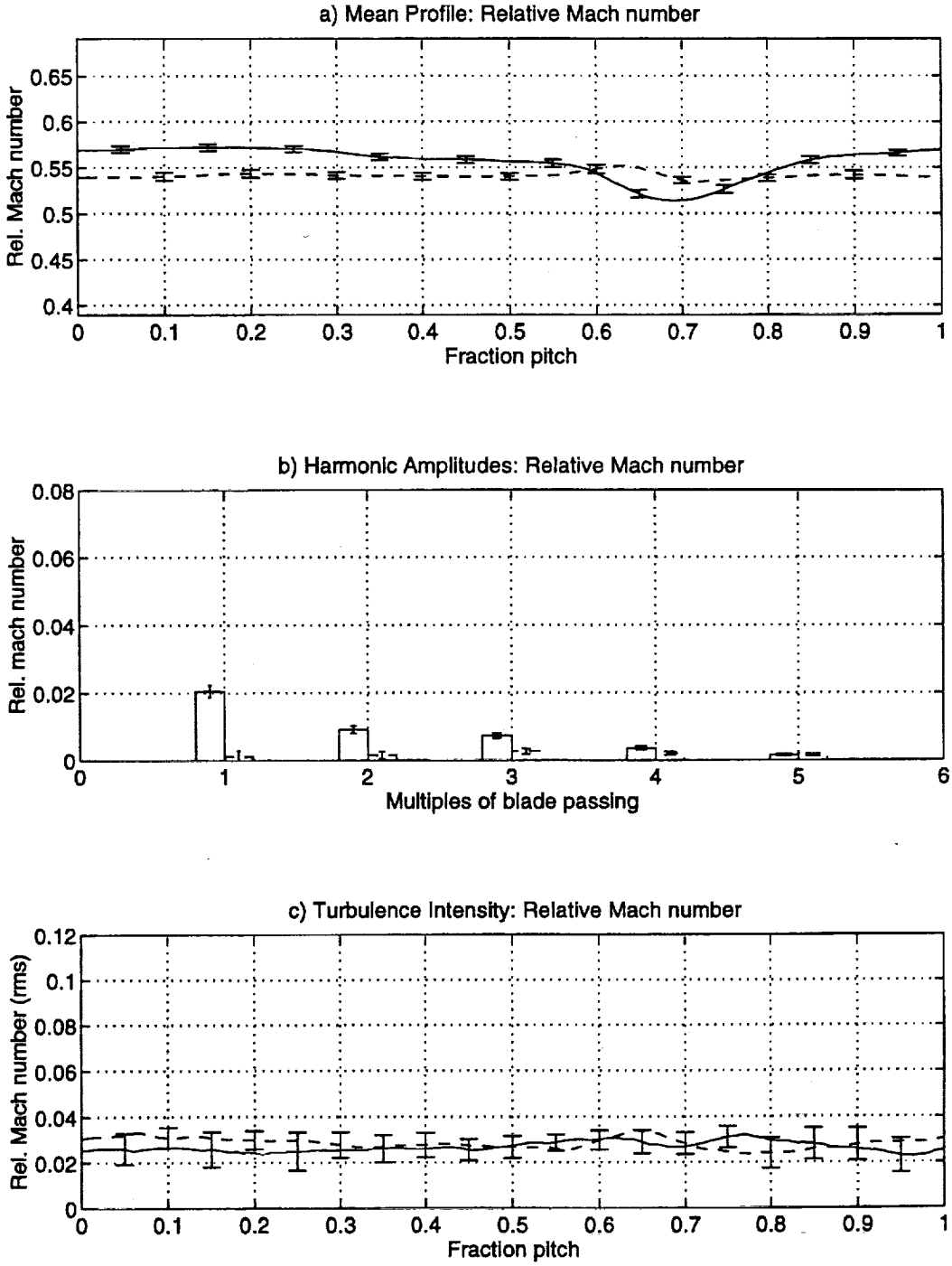

Figure 4-5: Relative Mach number data at 1.5c, 50% span. (—)w/o blowing, (- -)w/ blowing

1,2,3 and 4*BPF longitudinal harmonics (see Figure 4-6). For the transverse harmonics, the first two multiples of BPF show reductions of 47% and 80% respectively but slight increases are seen in the higher harmonics.

75% span

At 75% span the wake without trailing edge blowing has a maximum velocity deficit equal to about 10% of the freestream value. In the trailing edge blowing case the deficit is reduced to a little over 2% of the freestream value. However, as seen in Figure 4-7a, there is a slight (about 1%) velocity excess on the suction side of the wake.

The relative Mach number harmonics seen in Figure 4-7b show significant decreases in the first four multiples of BPF. The 1*BPF and 2*BPF harmonics were both reduced by about 74% while the 3*BPF and the 4*BPF harmonics were reduced by about 63% and 47% respectively. Reductions in the longitudinal harmonics are similar to those in the relative harmonics except for the 1*BPF harmonic where a reduction of about 98% is seen. In the transverse harmonics, reductions of about 43% and 80% are seen in the first two multiples of BPF but increases are seen in the higher harmonics (see Figure 4-8).

87.5% span

At 87.5% span the wake deficit was reduced from about 10% of the freestream value in the case without blowing to a little over 3% in the case with blowing (see Figure 4-9a). Unlike the wakes measured at the other radial locations, the wake at 87.5% span does not have a component with a velocity excess. However, the wake appears to be more filled-in on the suction side indicating that, like the case at 75% span, the blowing mass was most likely injected toward the suction side of the wake.

In the blowing case, reductions in the relative Mach number harmonics of 72% and 57% are seen in the first two multiples of BPF (see Figure 4-9). An increase of about

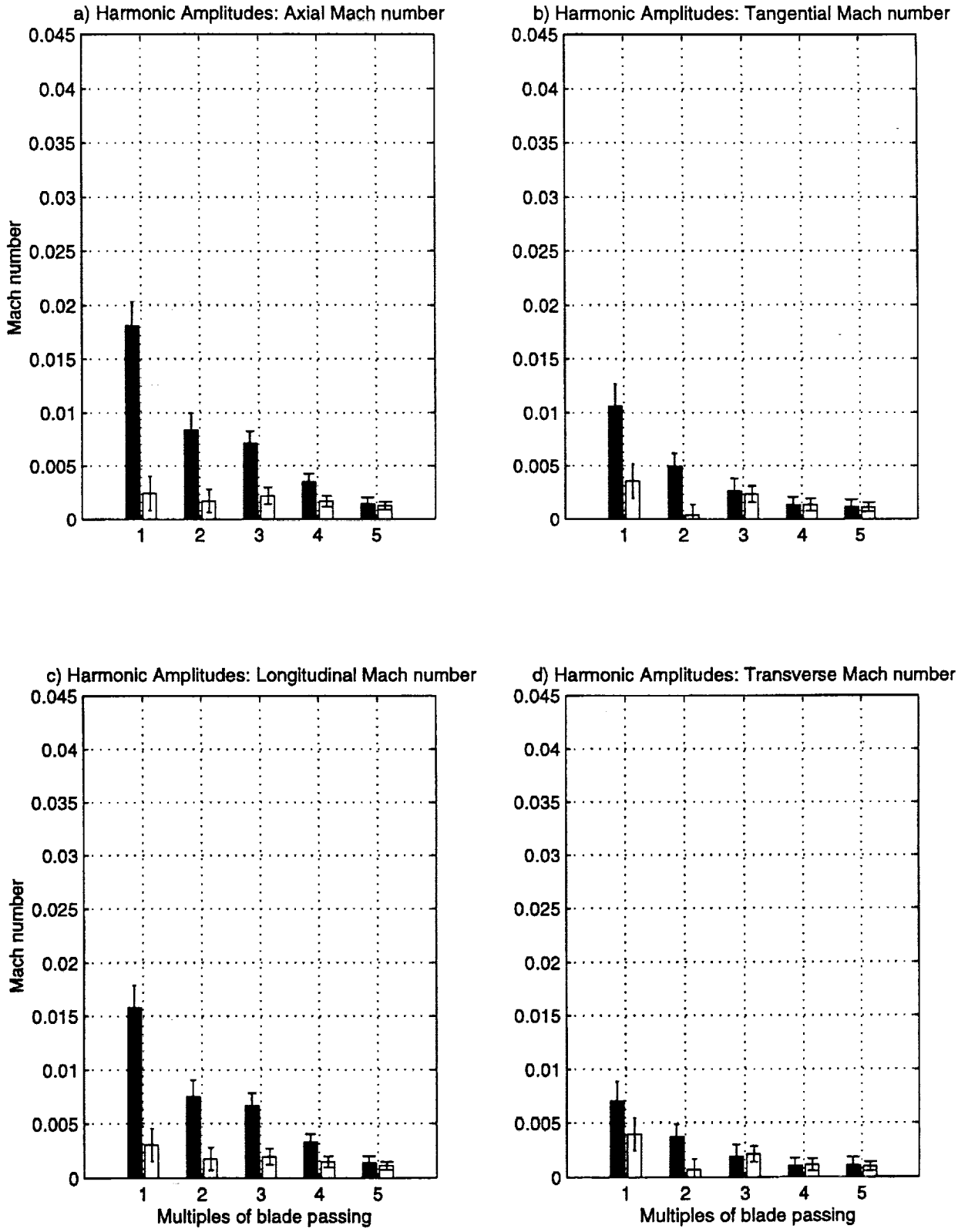

Figure 4-6: Wake harmonic data at 1.5c, 50% span (shaded)w/o blowing, (open)w/ blowing

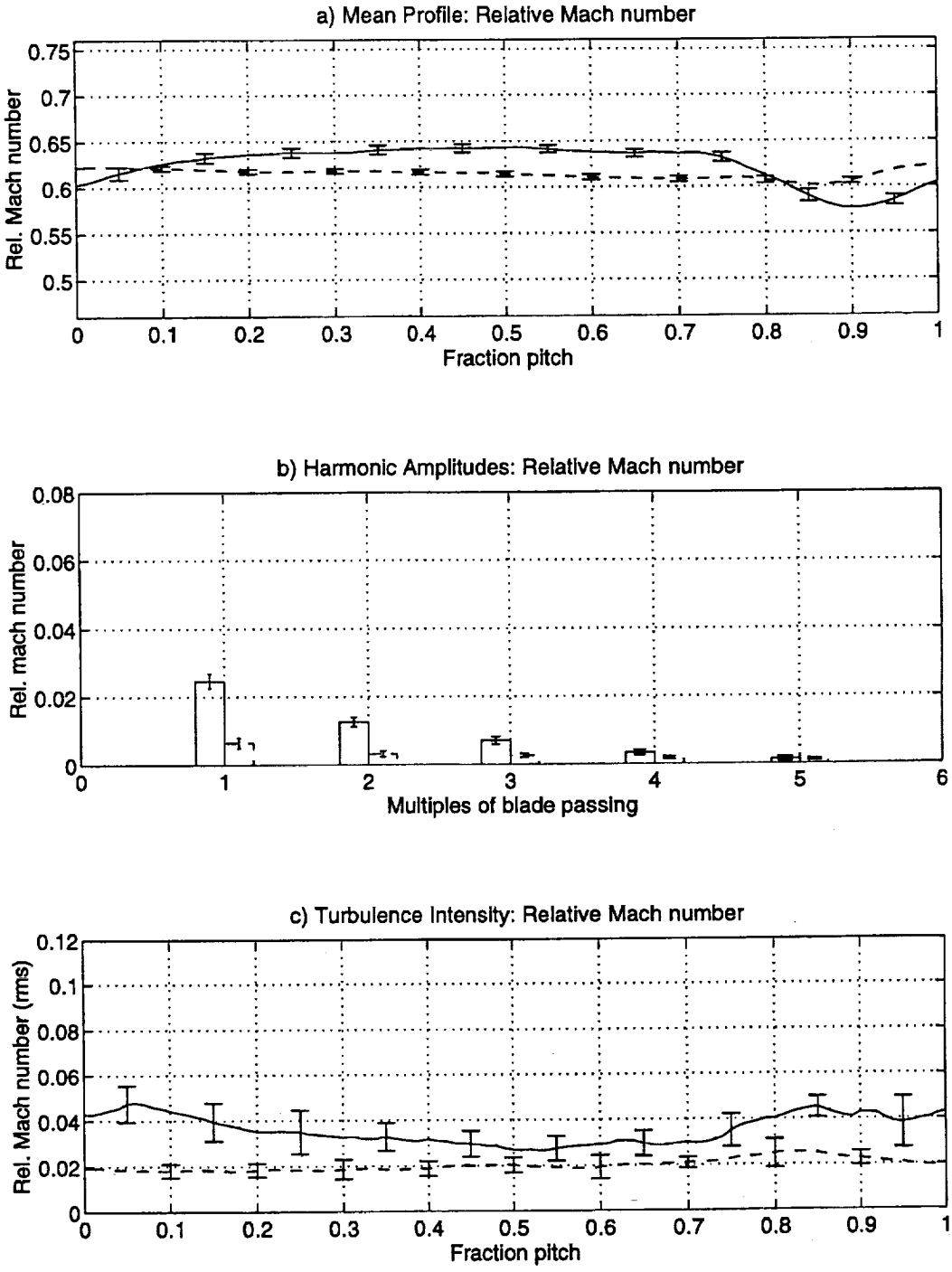

Figure 4-7: Relative Mach number data at 1.5c, 75% span. (—)w/o blowing, (- -)w/ blowing

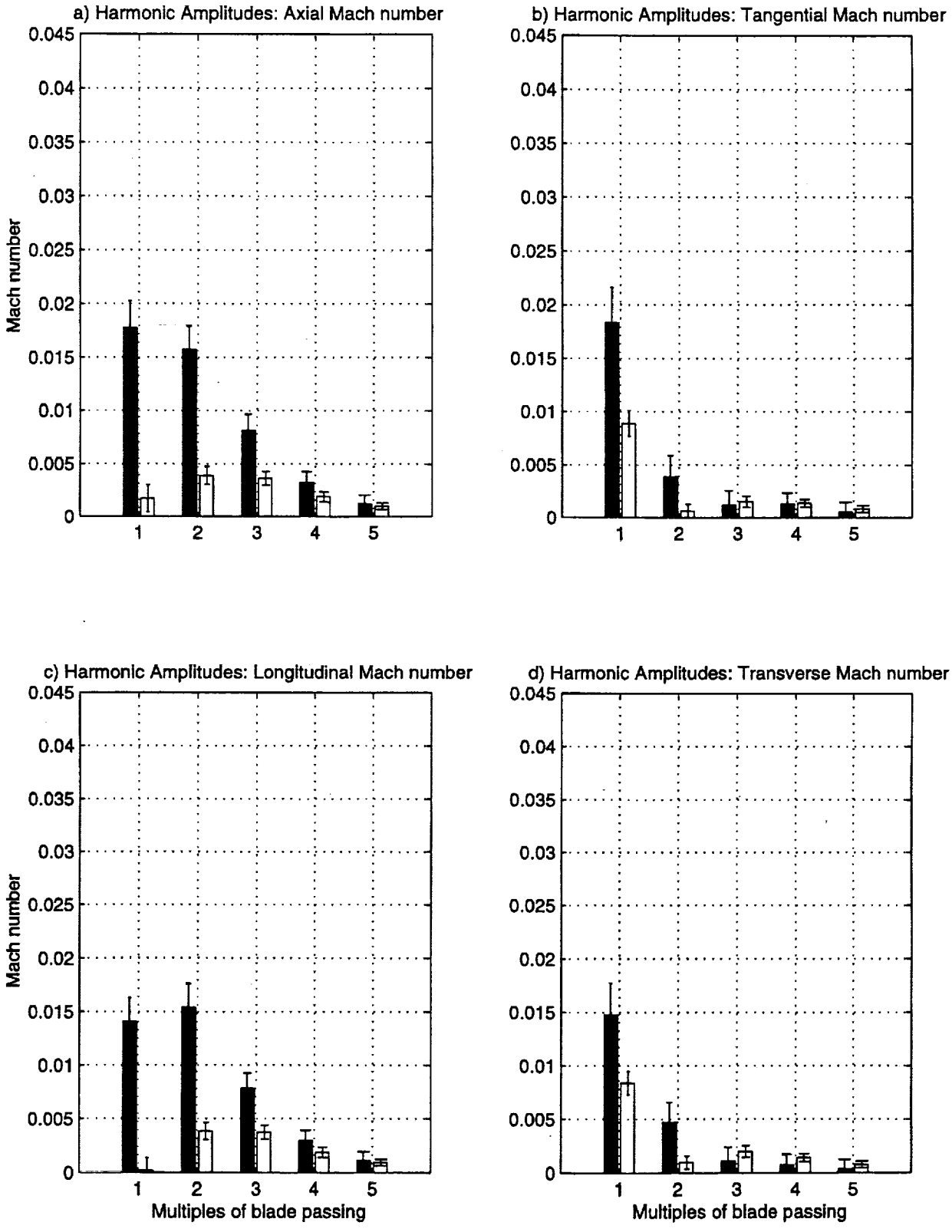

Figure 4-8: Wake harmonic data at 1.5c, 75% span (shaded)w/o blowing, (open)w/ blowing

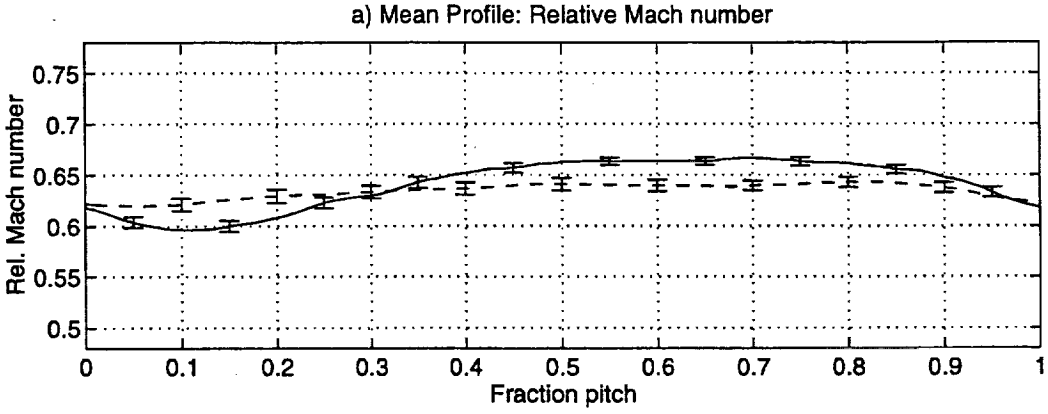

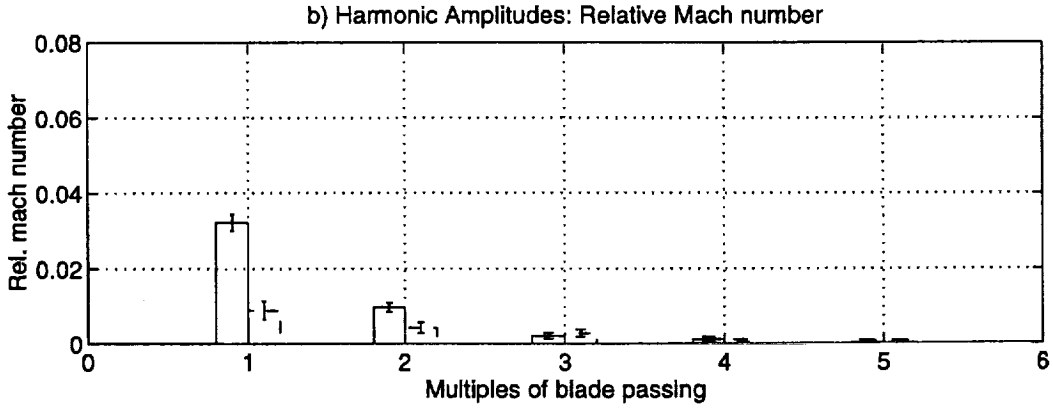

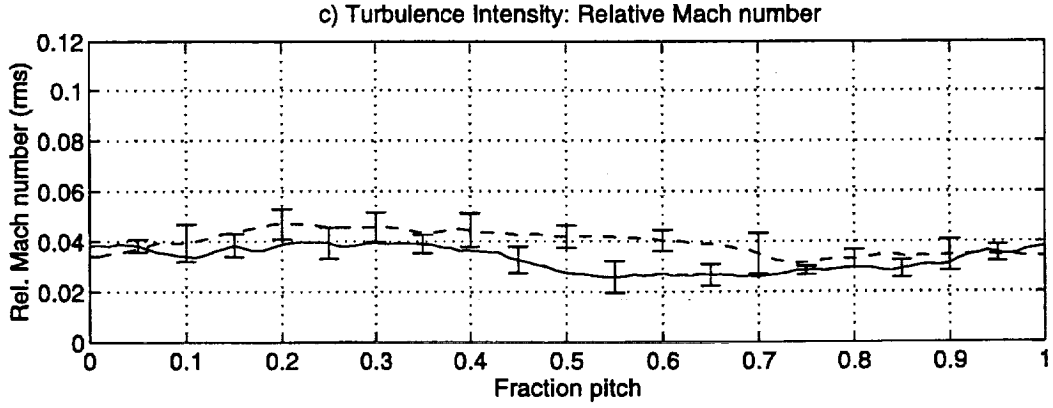

Figure 4-9: Relative Mach number data at 1.5c, 87.5% span. (—)w/o blowing, (- -)w/ blowing

Without Blowing	BPF	2*BPF	3*BPF	4*BPF	5*BPF
25% span	.0149	.0090	.0033	.0014	.0006
37.5% span	.0094	.0050	.0025	.0027	.0026
50% span	.0070	.0037	.0019	.0011	.0011
75% span	.0148	.0047	.0011	.0007	.0004
87.5% span	.0117	.0063	.0020	.0009	.0003
With Blowing	**BPF**	**2*BPF**	**3*BPF**	**4*BPF**	**5*BPF**
25% span	.0121	.0059	.0023	.0007	.0003
37.5% span	.0025	.0062	.0017	.0008	.0004
50% span	.0040	.0007	.0021	.0011	.0010
75% span	.0084	.0010	.0020	.0014	.0008
87.5% span	.0071	.0039	.0011	.0005	.0006

Table 4.1: Transverse Mach number harmonic amplitudes at 1.5 chord for cases with and without trailing edge blowing

35% is seen in the 3*BPF harmonic. For the longitudinal Mach number harmonics, the blowing case shows decreases of 89% and 63% for the first two multiples of BPF. The transverse Mach number harmonics show reductions in the first five multiples of BPF. In particular, the 1*BPF and 2*BPF harmonics are reduced by about 40% and 38% respectively.

Summary of Wake Harmonics

The transverse and longitudinal harmonic amplitudes are tabulated in Tables 4.1 and 4.3. Additionally, the harmonic amplitudes with trailing edge blowing are shown as fractions of the amplitudes without blowing in Tables 4.2 and 4.4. The first four multiples of BPF are also plotted versus span in Figures 4-11 and 4-12. Note that with blowing the 1*BPF harmonic is lower at all radial locations for both the transverse and the longitudinal Mach numbers. The 2*BPF harmonic was reduced at all spans for the longitudinal Mach number and at four out of five locations for the transverse Mach number. For completeness, the phases of the transverse and longitudinal Mach numbers are plotted versus span in Figures 4-13 and 4-14 for the first four multiples of BPF.

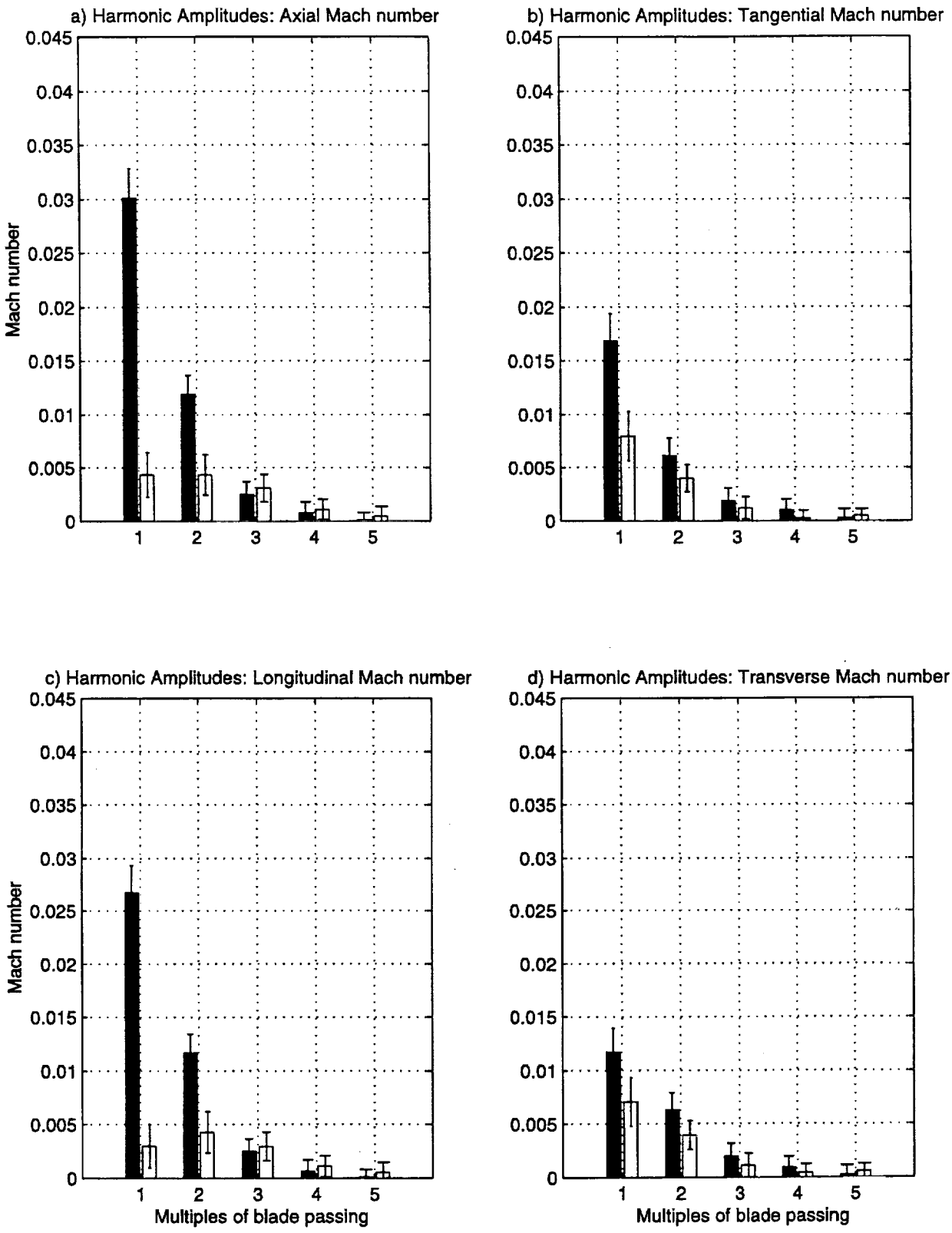

Figure 4-10: Wake harmonic data at 1.5c, 87.5% span (shaded)w/o blowing, (open)w/ blowing

	BPF	2*BPF	3*BPF	4*BPF	5*BPF
25% span	.81	.66	.68	.48	.57
37.5% span	.27	1.24	.66	.29	.16
50% span	.56	.19	1.13	1.06	.89
75% span	.57	.21	1.78	1.89	2.19
87.5% span	.60	.62	.58	.49	2.17

Table 4.2: Transverse Mach number harmonic amplitudes with blowing as fractions of harmonics without blowing

Without Blowing	BPF	2*BPF	3*BPF	4*BPF	5*BPF
25% span	.0347	.0061	.0015	.0012	.0005
37.5% span	.0227	.0074	.0028	.0017	.0015
50% span	.0158	.0075	.0067	.0033	.0014
75% span	.0141	.0154	.0079	.0030	.0011
87.5% span	.0267	.0117	.0025	.0007	.0001
With Blowing	**BPF**	**2*BPF**	**3*BPF**	**4*BPF**	**5*BPF**
25% span	.0147	.0055	.0020	.0015	.0008
37.5% span	.0024	.0004	.0032	.0012	.0008
50% span	.0031	.0018	.0020	.0015	.0011
75% span	.0002	.0038	.0037	.0019	.0009
87.5% span	.0030	.0043	.0030	.0011	.0005

Table 4.3: Longitudinal Mach number harmonic amplitudes at 1.5 chord for cases with and without trailing edge blowing

	BPF	2*BPF	3*BPF	4*BPF	5*BPF
25% span	.42	.89	1.31	1.24	1.77
37.5% span	.10	.05	1.16	.68	.56
50% span	.19	.24	.30	.45	.80
75% span	.13	.25	.48	.63	.84
87.5% span	.11	.37	1.18	1.66	5.83

Table 4.4: Longitudinal Mach number harmonic amplitudes with blowing as fraction of no blowing harmonics

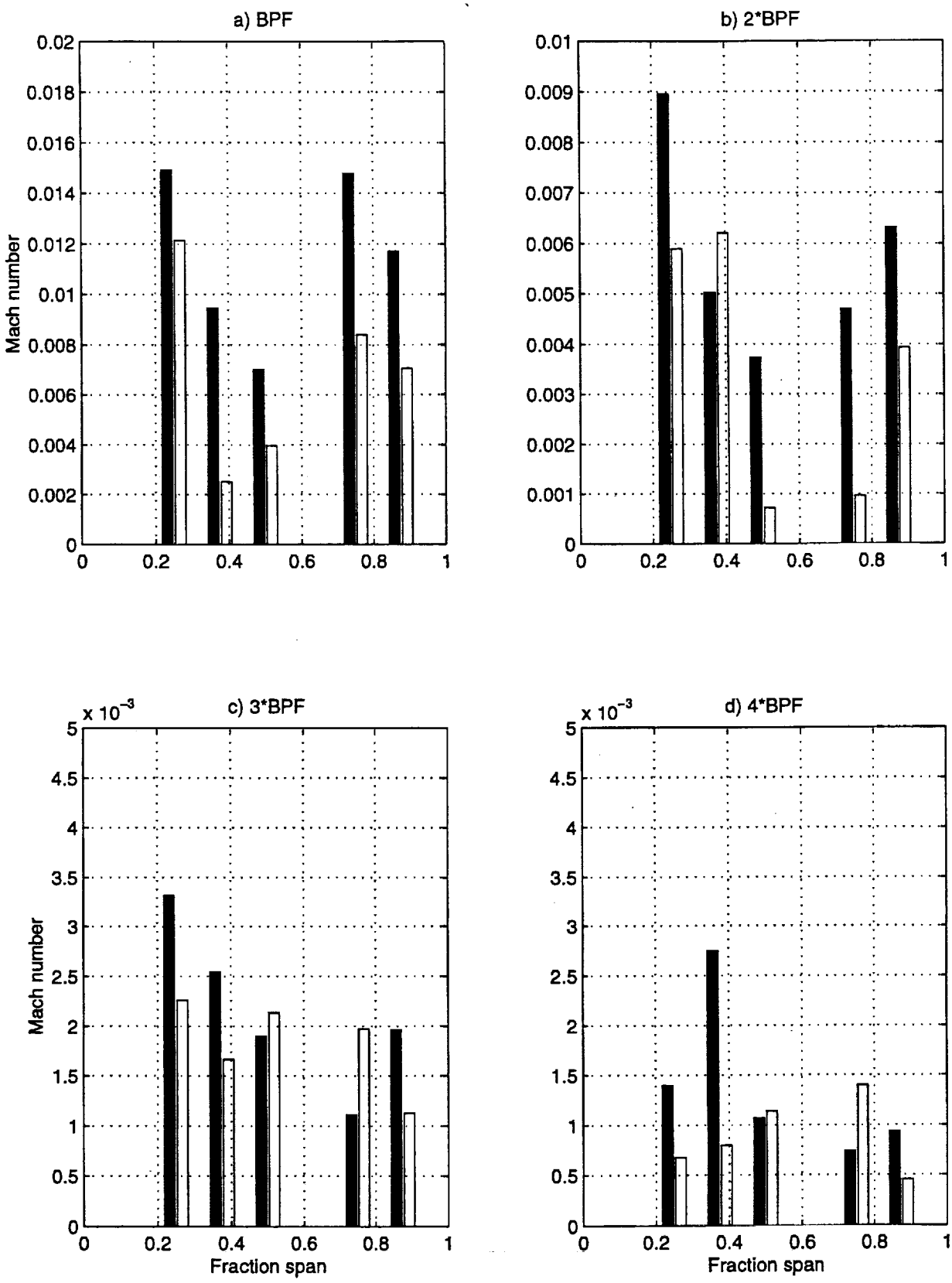

Figure 4-11: Transverse Mach number harmonic amplitudes vs. span, first four multiples of BPF. (shaded)w/o blowing, (open)w/ blowing

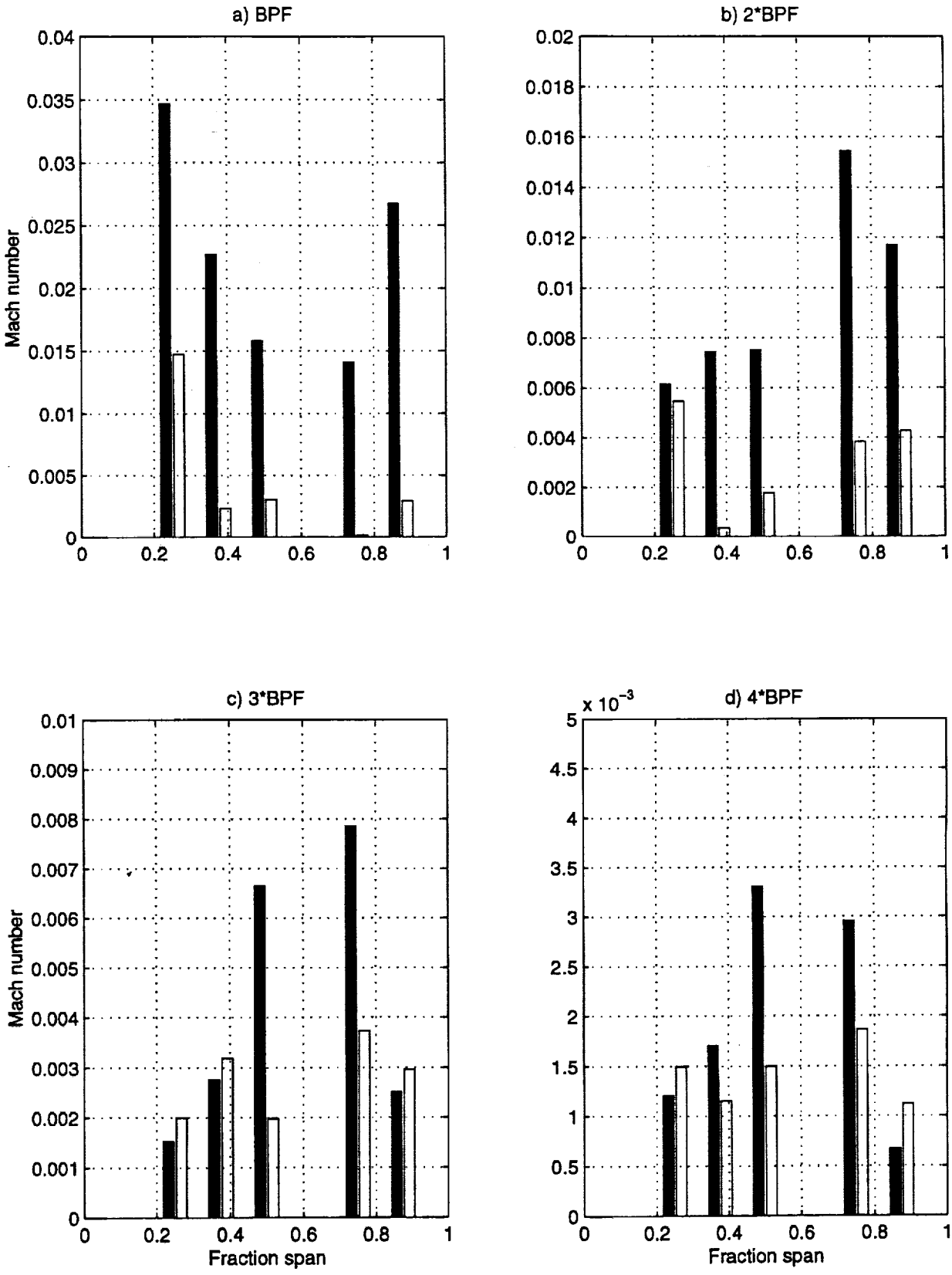

Figure 4-12: Longitudinal Mach number harmonic amplitudes vs. span, first four multiples of BPF. (shaded)w/o blowing, (open)w/ blowing

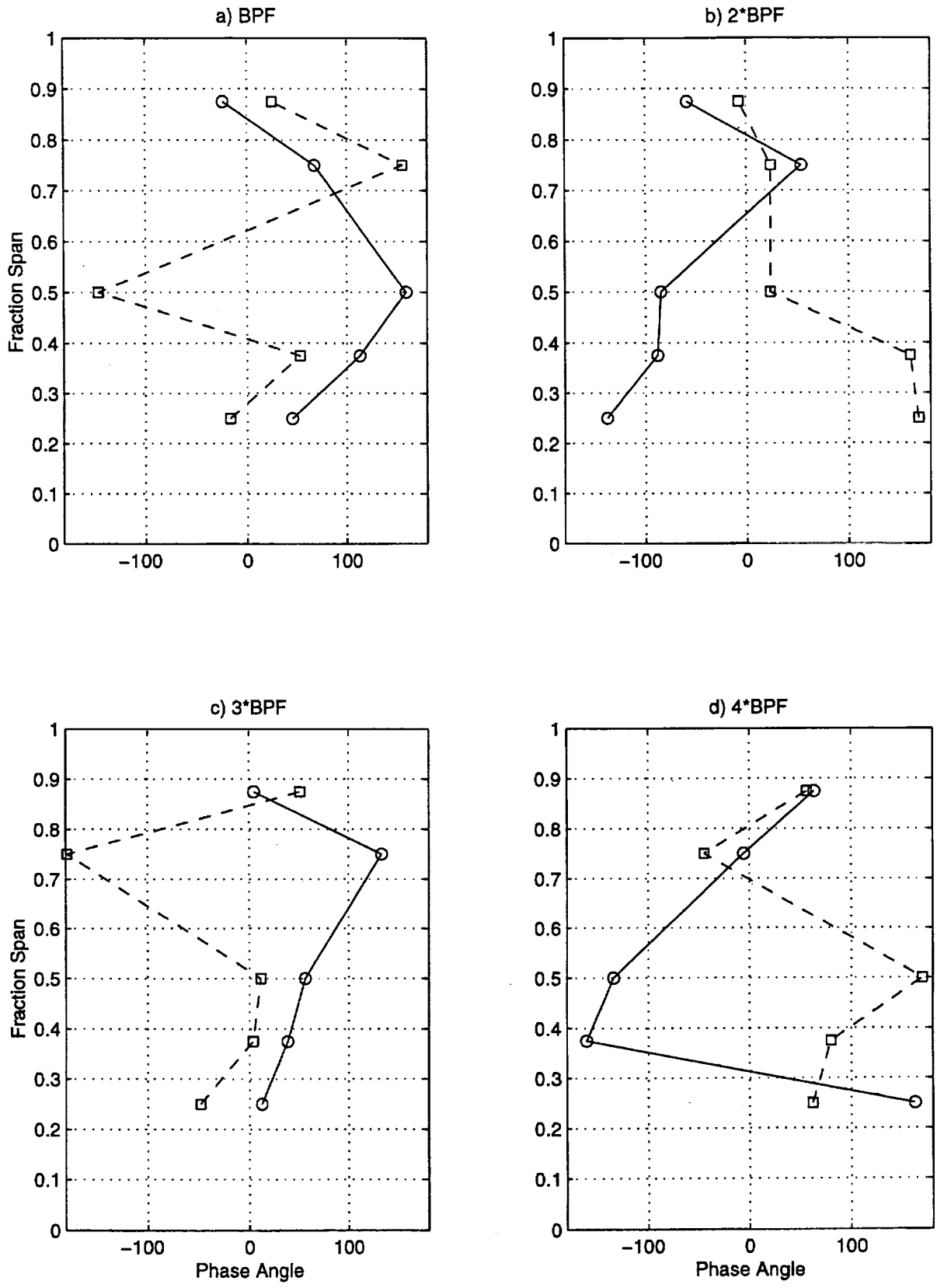

Figure 4-13: Transverse Mach number harmonic phases vs. span, first four multiples of BPF. (—)w/o blowing, (- -)w/ blowing

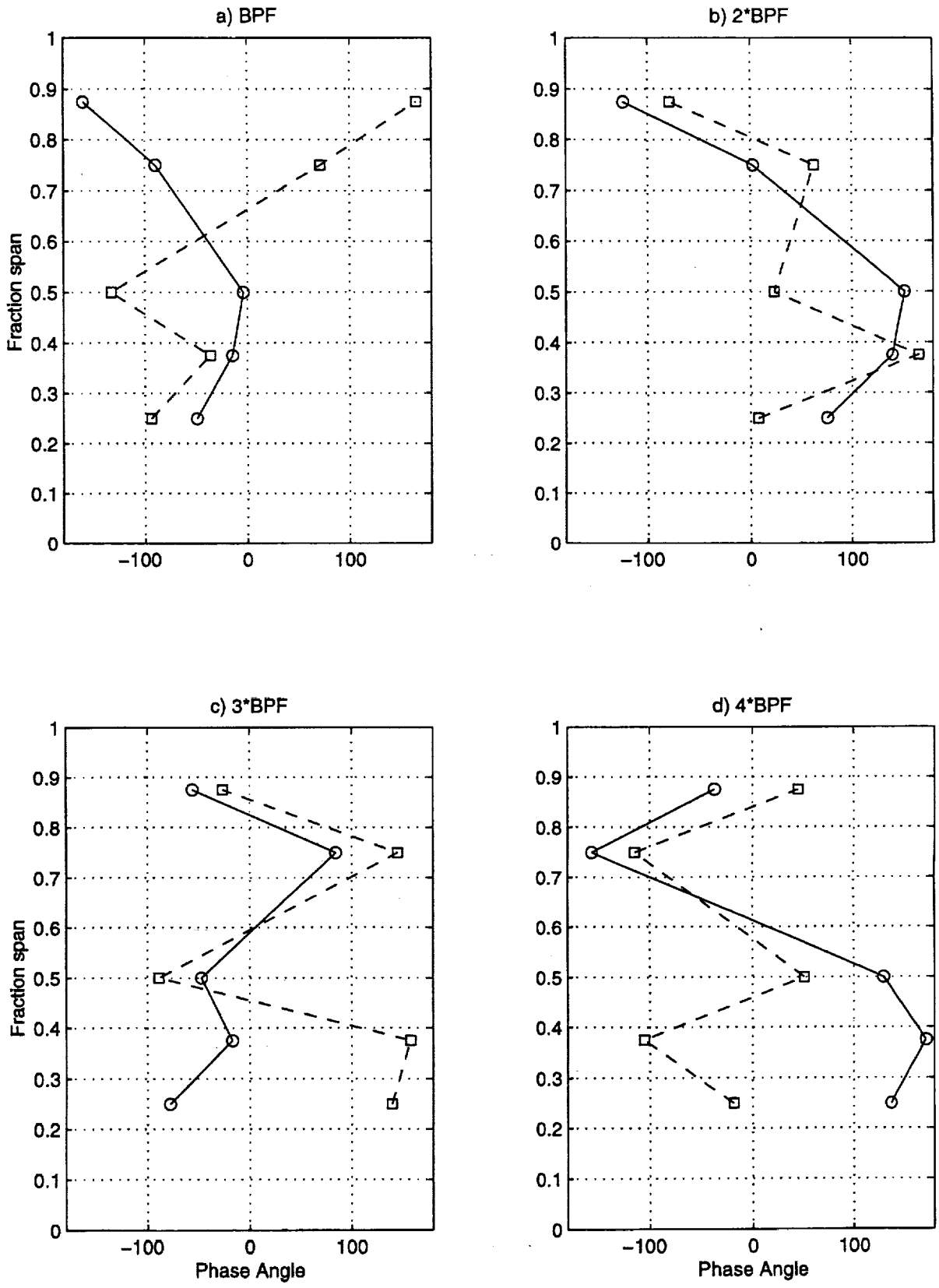

Figure 4-14: Longitudinal Mach number harmonic phases vs. span, first four multiples of BPF. (—)w/o blowing, (- -)w/ blowing

4.3 V072 Noise Prediction Code

The BBN/PW V072 rotor-stator interaction noise prediction program was developed by Pratt and Whitney under NASA funding. This code is a modification of two previously existing programs— the GE/NASA semi-empirical rotor wake/vortex model, and the BBN/NASA rotor-stator interaction noise prediction code. The V072 code can be broken down into two parts. In the first part, a model of the rotor wakes is calculated; in the second, the wake model is used to calculate stator noise response.

The rotor wake calculation section comes from a program originally developed by General Electric under NASA funding. It divides the annulus into strips and then unwraps those strips to form two-dimensional infinite cascades. This allows flow in the circumferential and axial directions but not in the radial direction. The flow across the rotor is assumed to be incompressible and the mean flow is analytically calculated along each streamline. The flow perturbations due to the rotor wake are calculated separately and superimposed on the mean flow. The perturbations are calculated using empirical data from existing fans. Once the wake velocity perturbations and mean flow are combined the upwash velocity at the stator leading edge is obtained. When obtaining the upwash velocity, it is assumed that the mean flow passes directly through the stator row producing no upwash. It is also assumed that the mean flow does not interact with the wake perturbations.

The noise calculation comes from a section originally developed by Bolt, Beranek, and Newman. Initially, the unsteady pressure distributions on the stator are found using two-dimensional strip theory. Once the chordwise pressure distributions have been found, the annulus is reformed. This results in an annular duct with spanwise and chordwise pressure distributions. Using the pressure distribution, the interaction with the duct acoustic modes is calculated and power levels for the circumferential and radial propagating modes can be found. Total noise power is given as a sum of these modes.

For the studies in this thesis, the majority of the rotor wake calculation section of

V072 was bypassed. Instead of using the wake calculated by the program, the upwash was calculated using experimental wake measurements at 25%, 37.5%, 50%, 75% and 87.5% span. The results were then interpolated to 41 spanwise locations and input into the noise calculation part of the program. The stator unsteady pressure distributions calculated in this second part of the program are presented in the following section.

4.4 Unsteady Stator Loading Predictions

The stator unsteady pressure distributions calculated using the V072 program are found in Figures 4-15 through 4-24. The amplitudes and phases are plotted against stator chord and are presented for the first three harmonics of BPF. The solid lines represent the no blowing case while the blowing case is represented by dashed lines.

Reductions in the amplitude of the first two harmonics of BPF are predicted at every spanwise location. For the 1*BPF harmonic, reductions of about 10dB are seen at the 50%, 75% and 87.5% span locations. A 15dB reduction is seen at 37% span while a 5dB reduction is seen at 25% span. Reductions of 2-3dB for the 2*BPF harmonic are seen at 25% and 37.5% span. The 87.5% span location shows a reduction of about 5dB, and reductions of 10-15dB are seen for the 50% and 75% locations. For the most part, the harmonic reductions follow the trend set by the reductions in the transverse harmonics. Slight discrepancies can most likely be attributed to interpolation of the data. The flow field measurements at the five measuring locations were interpolated to produce 41 sets of input for the V072 code. The predictions seen here were calculated using the interpolated upwash and not the actual measurements. Finally, note that at all of the locations the amplitude changes and the phase shifts are essentially uniform along the chord. It will be seen in Chapter 5 that the same does not hold true for the experimental measurements.

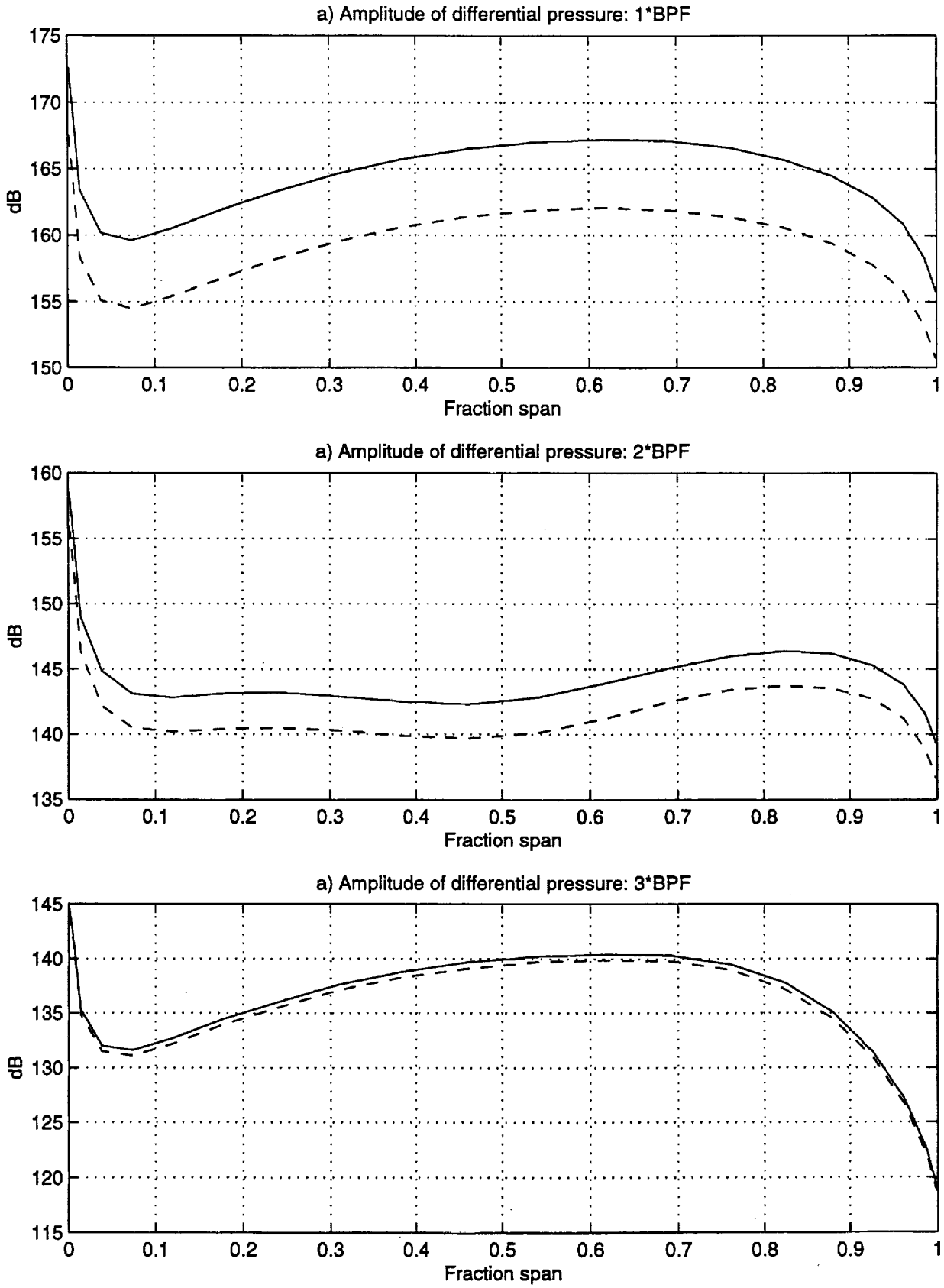

Figure 4-15: Stator unsteady loading predictions: harmonic amplitudes at 25% span. (—)w/o blowing, (- -)w/ blowing

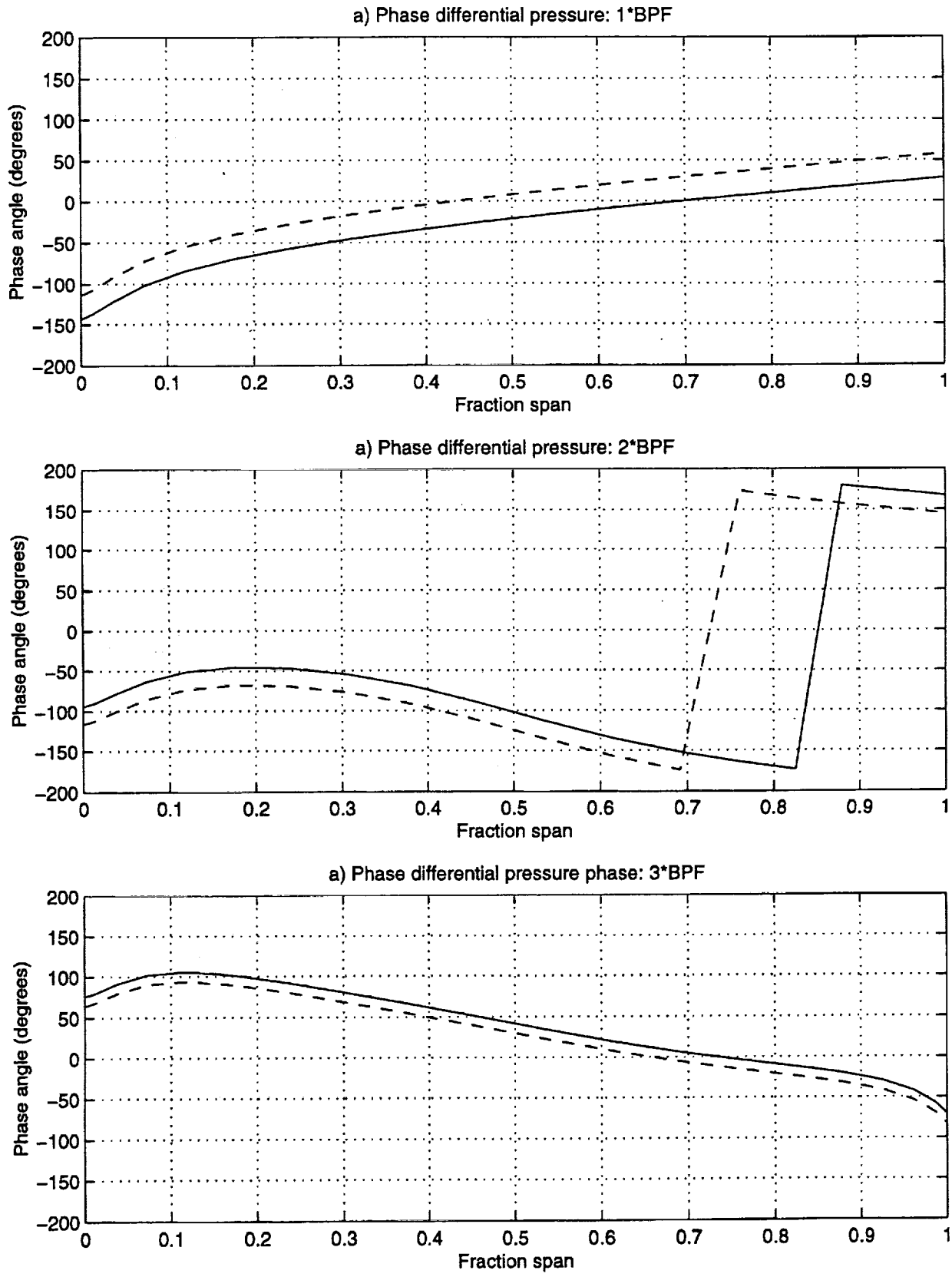

Figure 4-16: Stator unsteady loading predictions: harmonic phases at 25% span. (—)w/o blowing, (- -)w/ blowing

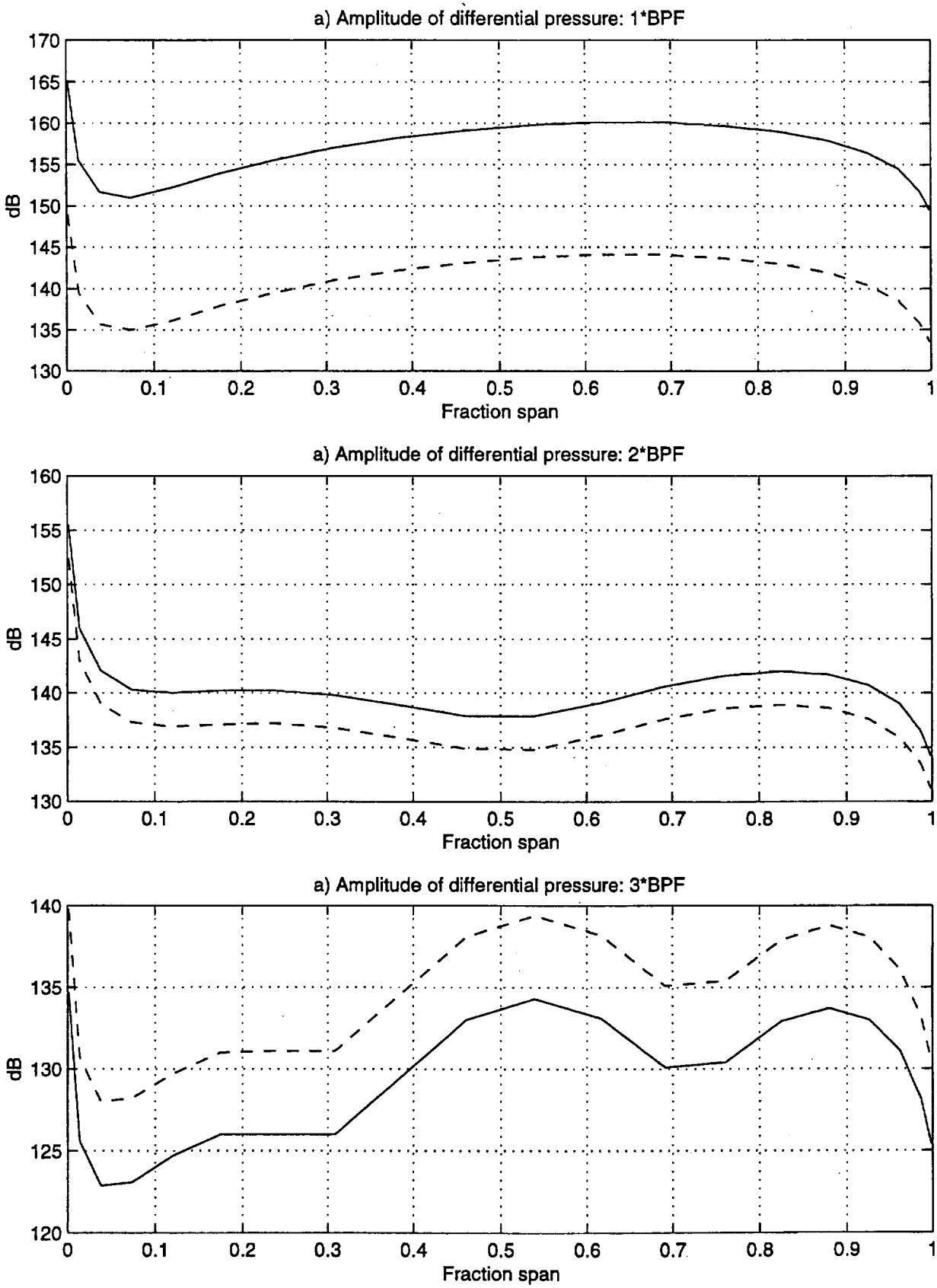

Figure 4-17: Stator unsteady loading predictions: harmonic amplitudes at 37.5% span. (—)w/o blowing, (- -)w/ blowing

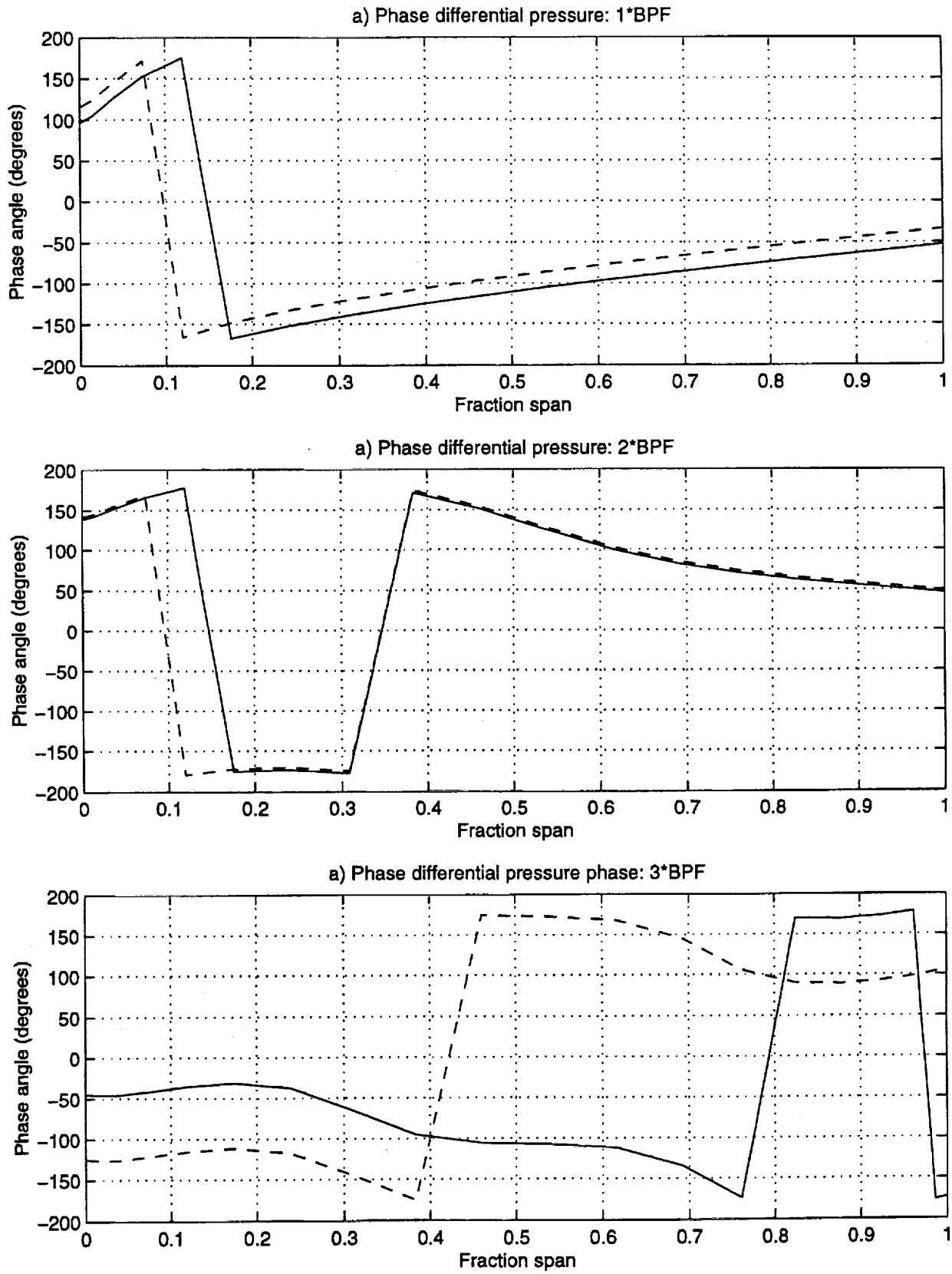

Figure 4-18: Stator unsteady loading predictions: harmonic phases at 37.5% span. (—)w/o blowing, (- -)w/ blowing

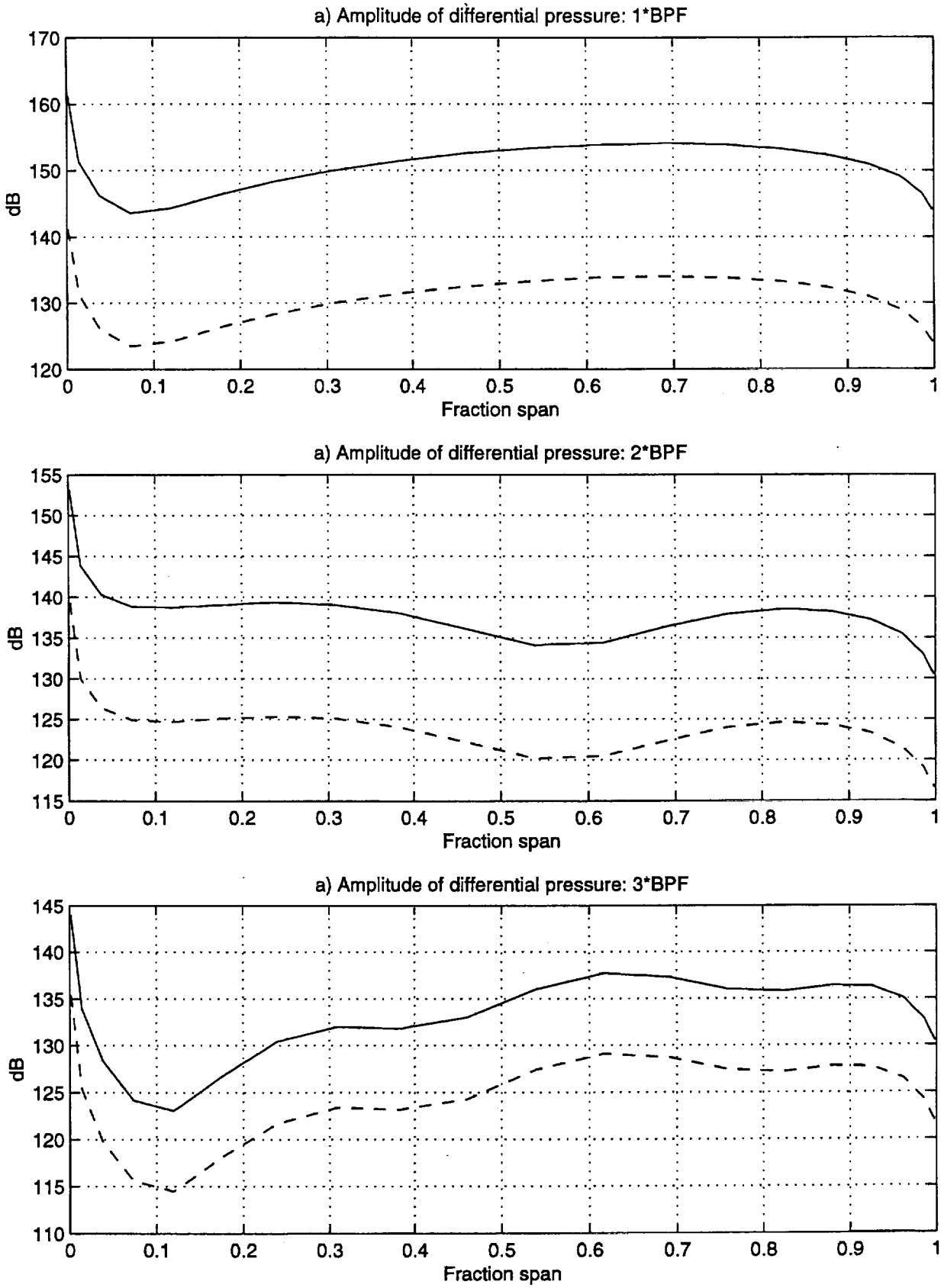

Figure 4-19: Stator unsteady loading predictions: harmonic amplitudes at 50% span. (—)w/o blowing, (- -)w/ blowing

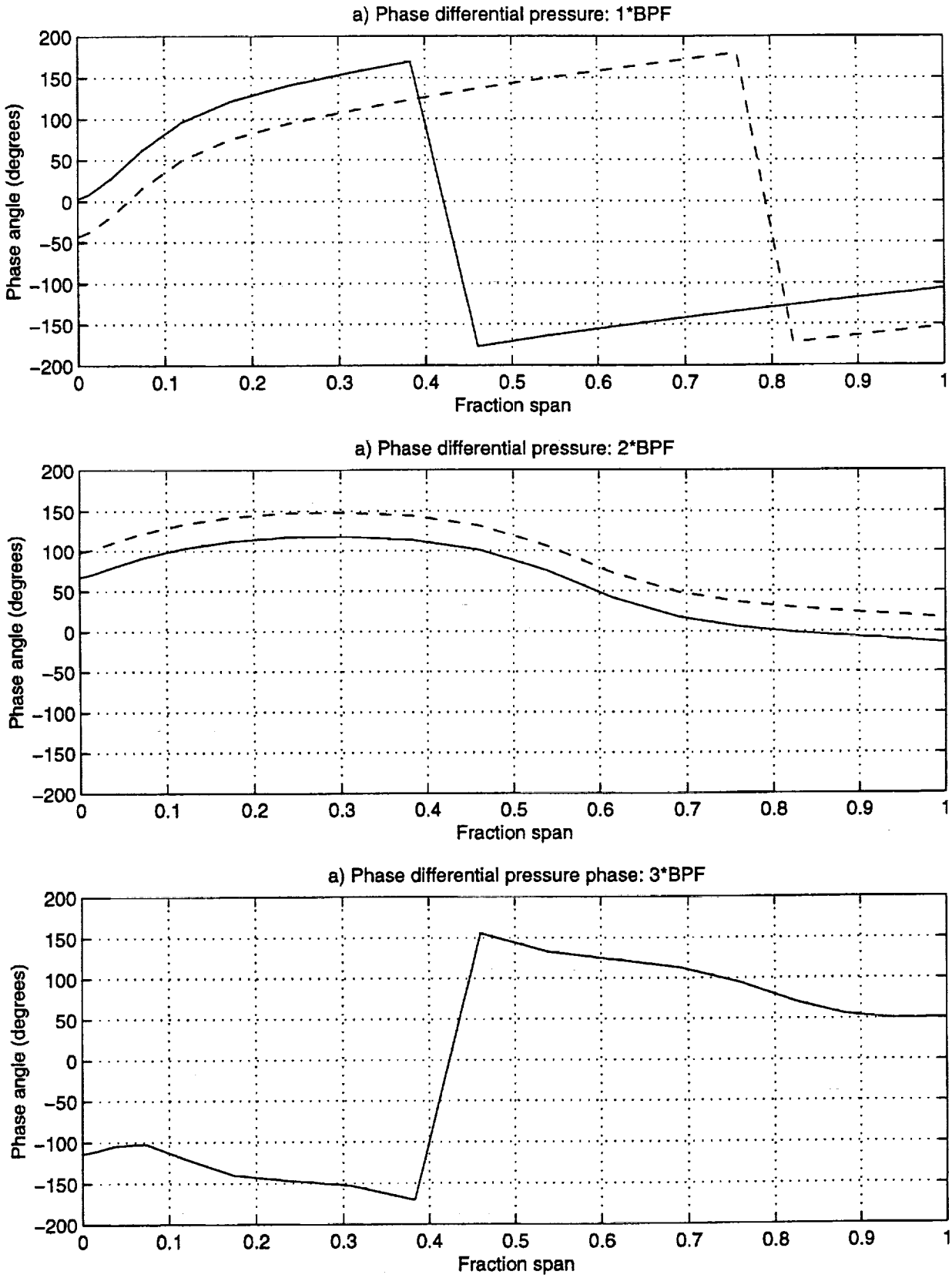

Figure 4-20: Stator unsteady loading predictions: harmonic phases at 50% span. (—)w/o blowing, (- -)w/ blowing

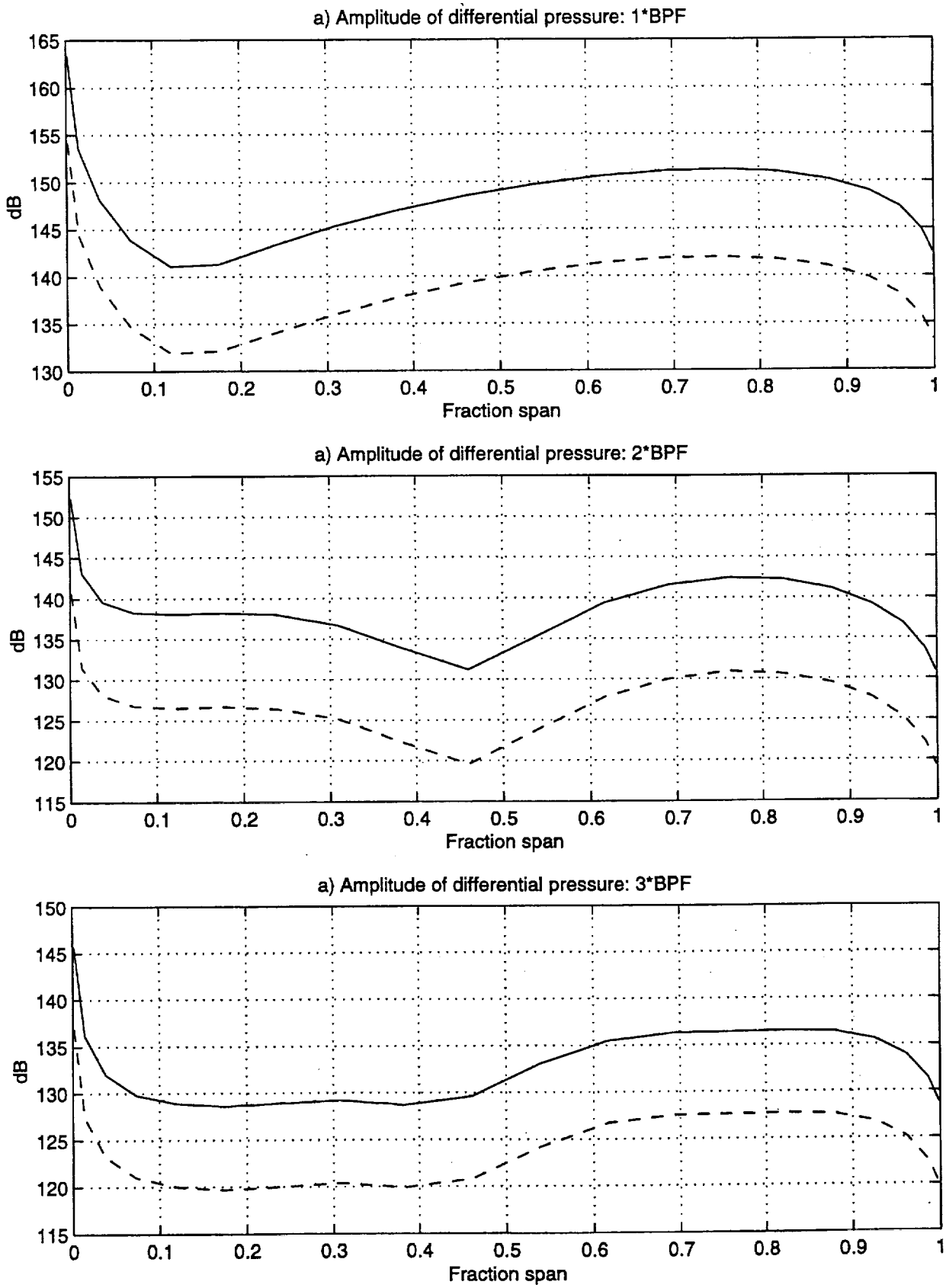

Figure 4-21: Stator unsteady loading predictions: harmonic amplitudes at 75% span. (—)w/o blowing, (- -)w/ blowing

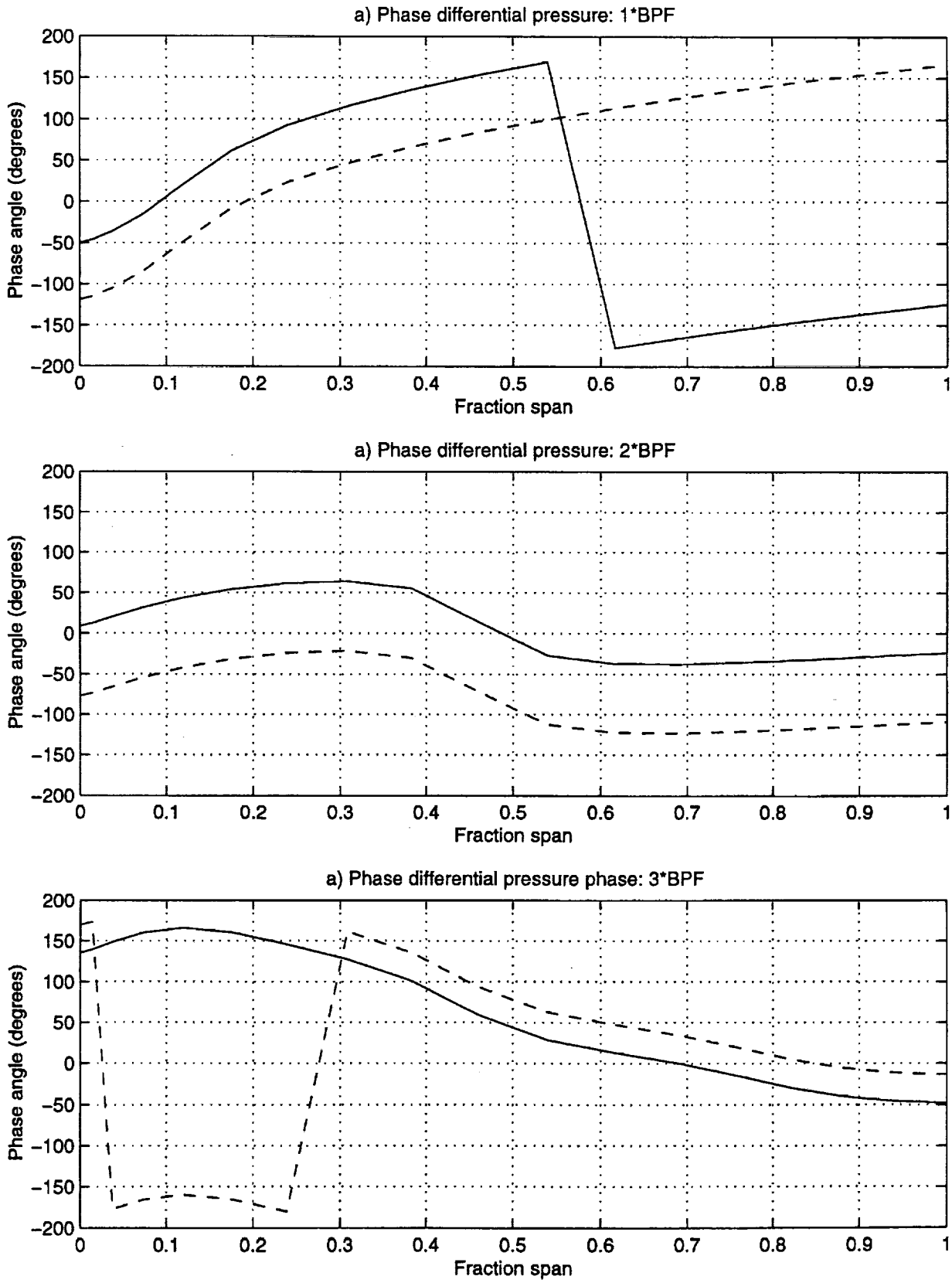

Figure 4-22: Stator unsteady loading predictions: harmonic phases at 75% span. (—)w/o blowing, (- -)w/ blowing

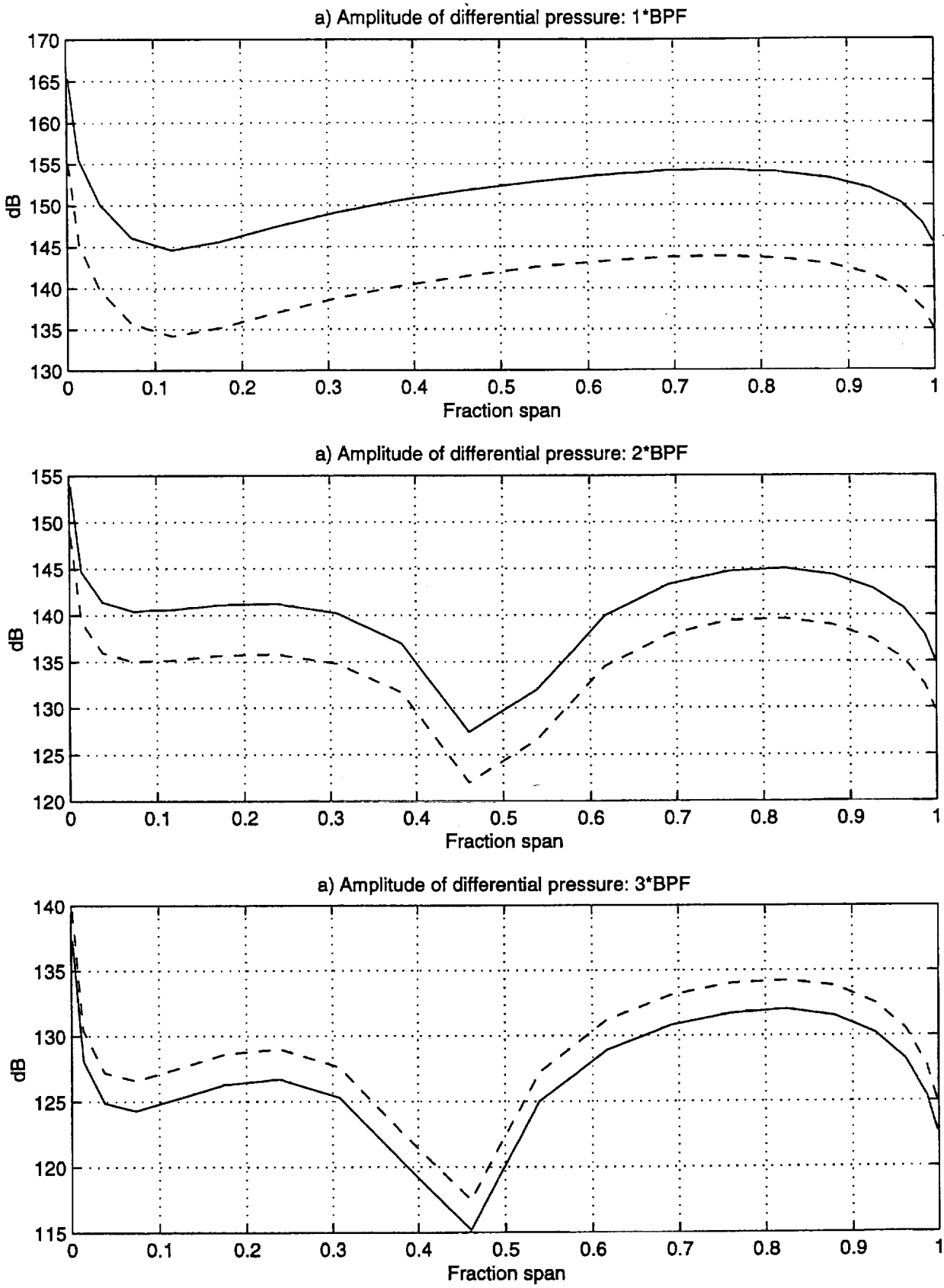

Figure 4-23: Stator unsteady loading predictions: harmonic amplitudes at 87.5% span. (—)w/o blowing, (- -)w/ blowing

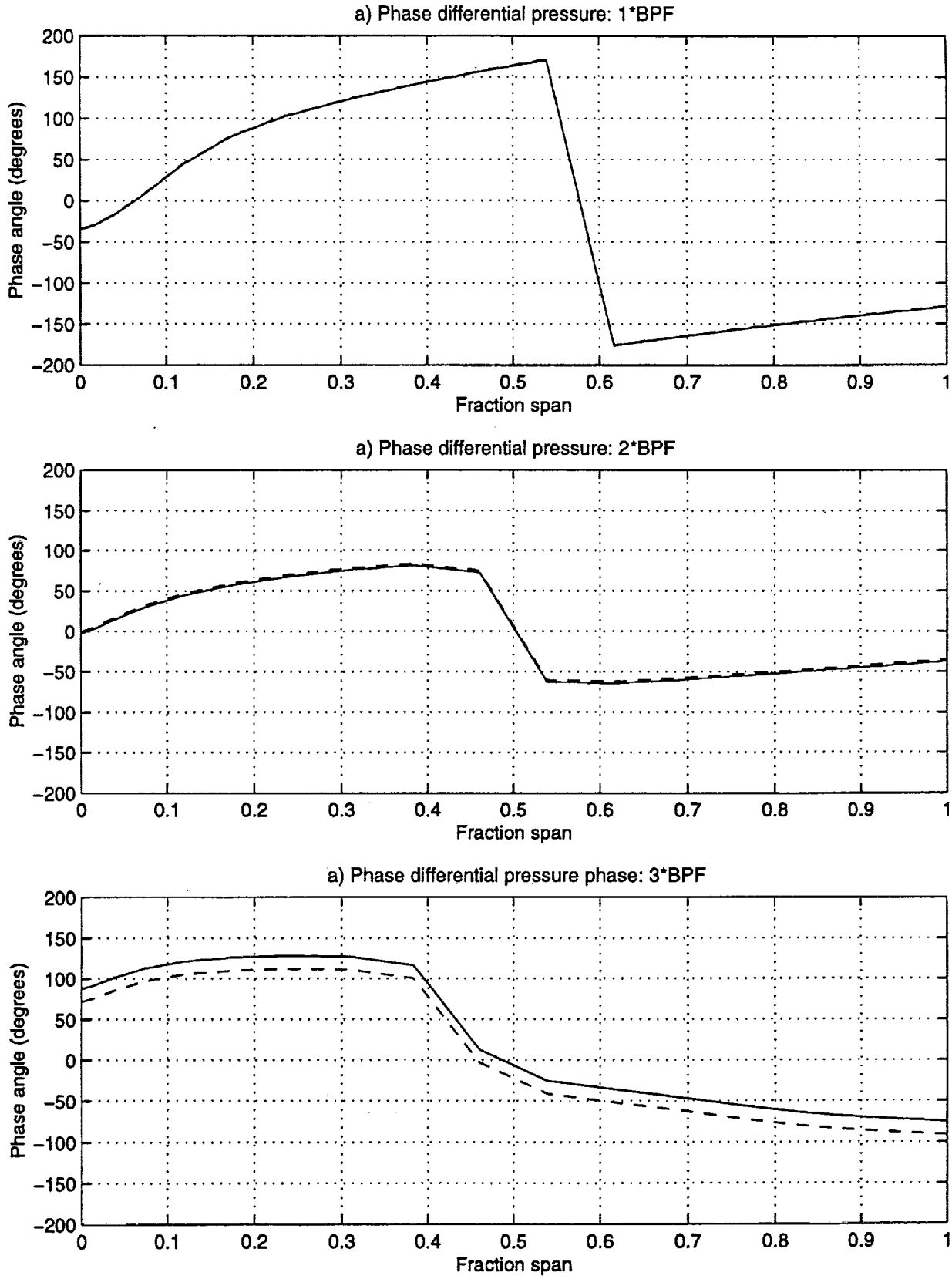

Figure 4-24: Stator unsteady loading predictions: harmonic phases at 87.5% span. (—)w/o blowing, (- -)w/ blowing

CHAPTER 5

STATOR LOADING MEASUREMENTS

This chapter presents stator loading measurements taken using the instrumented stator described in Chapter 2. Measurements were taken at the same five radial locations where flow field measurements were taken (i.e. 25%, 37.5% 50%, 75%, 87.5% span). As in Chapter 4, all data presented is an ensemble average on blade passing period and is shown along with 95% confidence intervals. At each radial location, the same number of runs were averaged in the blowing and the no blowing cases. For the 50%, 75% and 87.5% span locations 9 runs with 96 blade passing periods each were averaged. Due to time restrictions, the data presented for the 25% and 37.5% span locations is the average of 5 runs and 3 runs respectively.

The mean pressure envelopes are presented in Section 5.1. In Section 5.2, the amplitudes and phases of the differential pressure harmonics are presented. The amplitudes and phases of the stator pressure and suction side pressures can be found in Appendix C.

5.1 Mean Pressure Envelope

In order to show the general behavior of the flow field, the stator mean pressure envelopes are presented in Figures 5-1 through 5-5. The coefficient of pressure is defined as $C_p = (P_{local} - P_{upstream})/(P_t - P)_{upstream}$. Upstream values were obtained

from the four-way probe measurements in Appendix B. The case without blowing is shown as a solid line while the case with blowing is shown as a dashed line. The dashed-dot envelopes represent the minimum and maximum pressures seen over the ensemble-averaged period. Note that while the general shape of the curves does not change much with blowing, a slight increase in stator loading is seen. This increase is attributed to the changes in axial Mach number and tangential flow angle seen as a result of the blowing mass addition. This is a feature of the experimental facility, in which the throughflow is throttled by passing through a fixed area choke plate downstream of the test section.

5.2 Differential Pressures

The pressure difference across the stator was calculated from the pressures measured on the pressure side and suction side of the stator. The amplitudes and phases of the first three harmonics of the ensemble-averaged differential pressure are plotted along the stator chord for each spanwise location in Figures 5-6 through 5-15. The dashed and solid lines represent the blowing and no blowing cases respectively. Amplitudes are given in dB (dB = 20*$\log_{10}(P'_{rms}/2 * 10^{-5})$) while phases are given in degrees.

25% span

Figures 5-6 and 5-7 show the stator harmonic amplitudes and phases, respectively, at 25% span. The 1*BPF harmonic exhibits a significant reduction in amplitude ranging from about 5dB at the leading edge to about 15dB at the trailing edge and a fairly uniform phase shift of about -80 degrees along the entire chord. The 2*BPF harmonic amplitude is virtually unchanged, and although there appears to be a slight increase in the amplitude of the 3*BPF harmonic, it cannot be resolved within the 95% confidence intervals. A phase shift ranging from about -50 degrees at the leading and trailing edges to about -20 degrees at the midchord is seen for the 2*BPF harmonic. The 3*BPF harmonic phase has a shift ranging from about zero

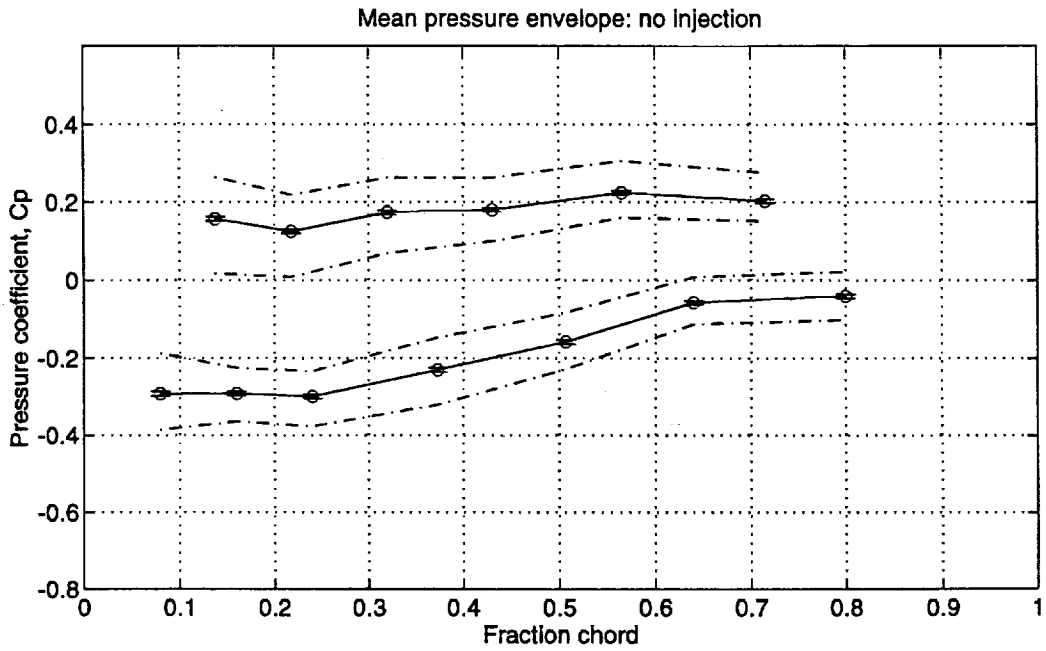

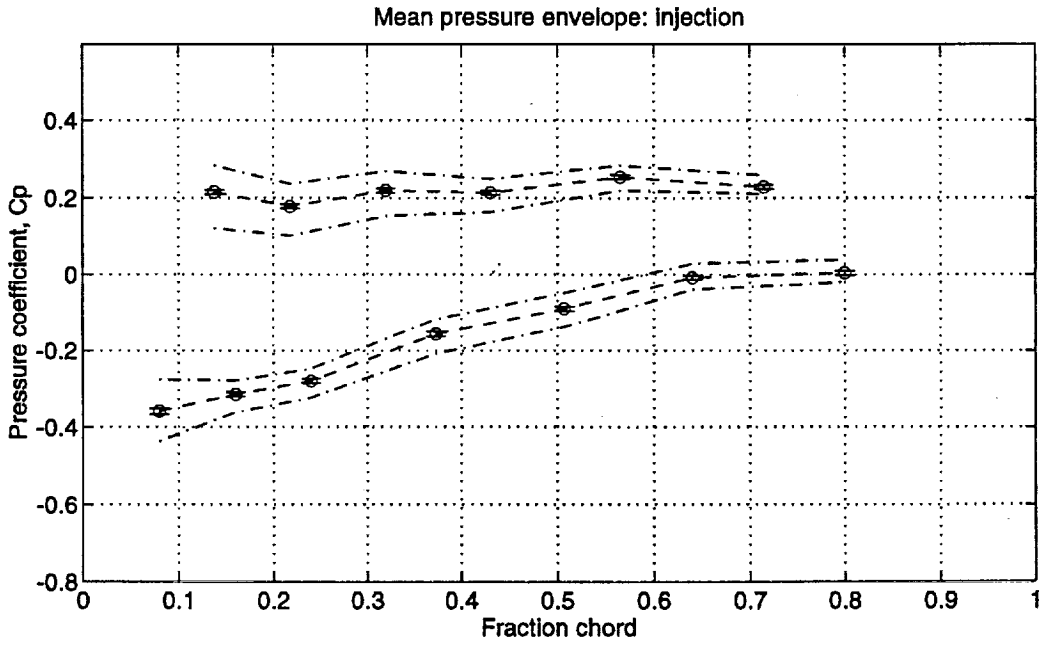

Figure 5-1: Stator mean pressure envelope at 25% span. (—)w/o blowing, (- -)w/ blowing

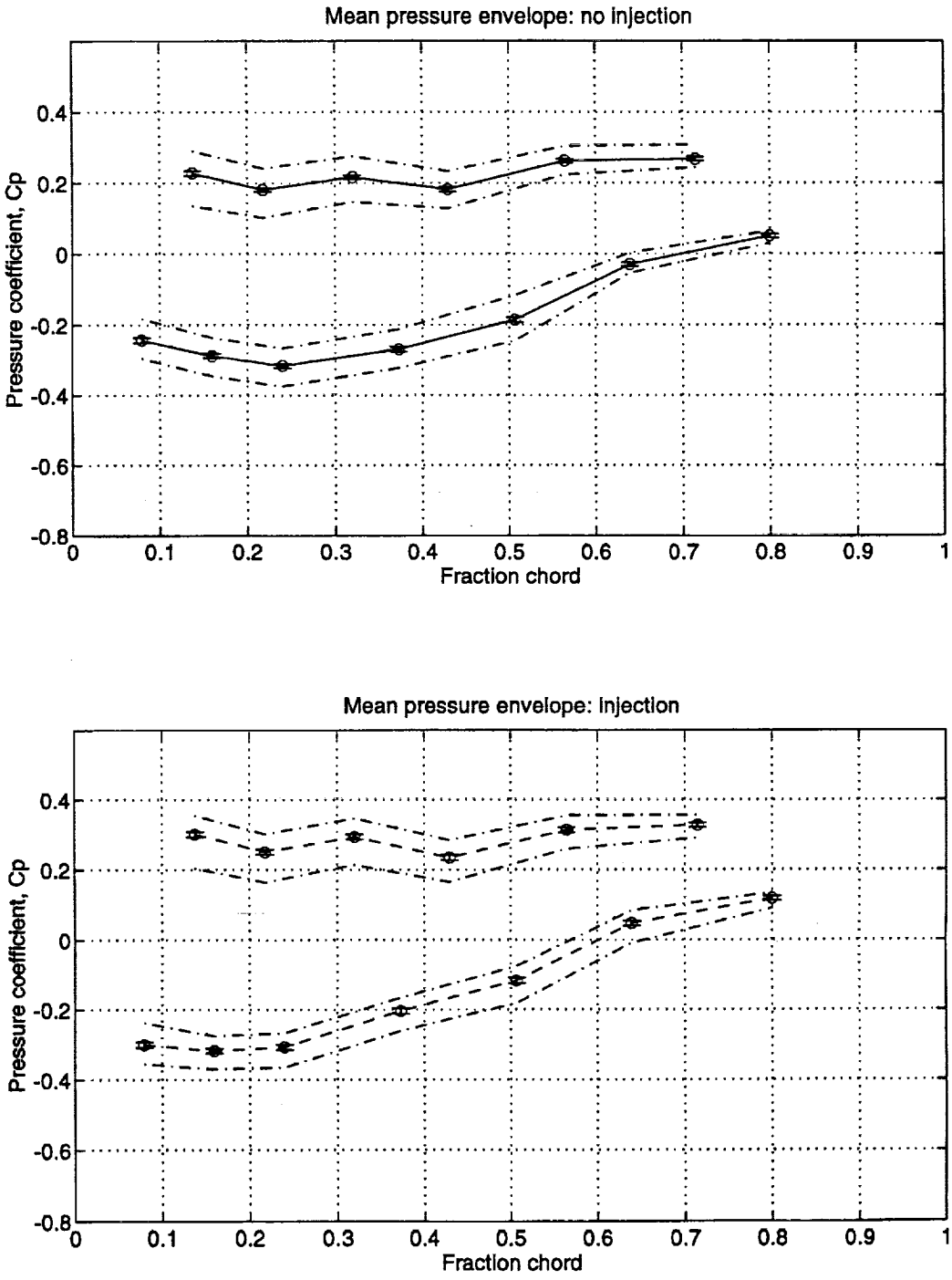

Figure 5-2: Stator mean pressure envelope at 37.5% span. (—)w/o blowing, (- -)w/ blowing

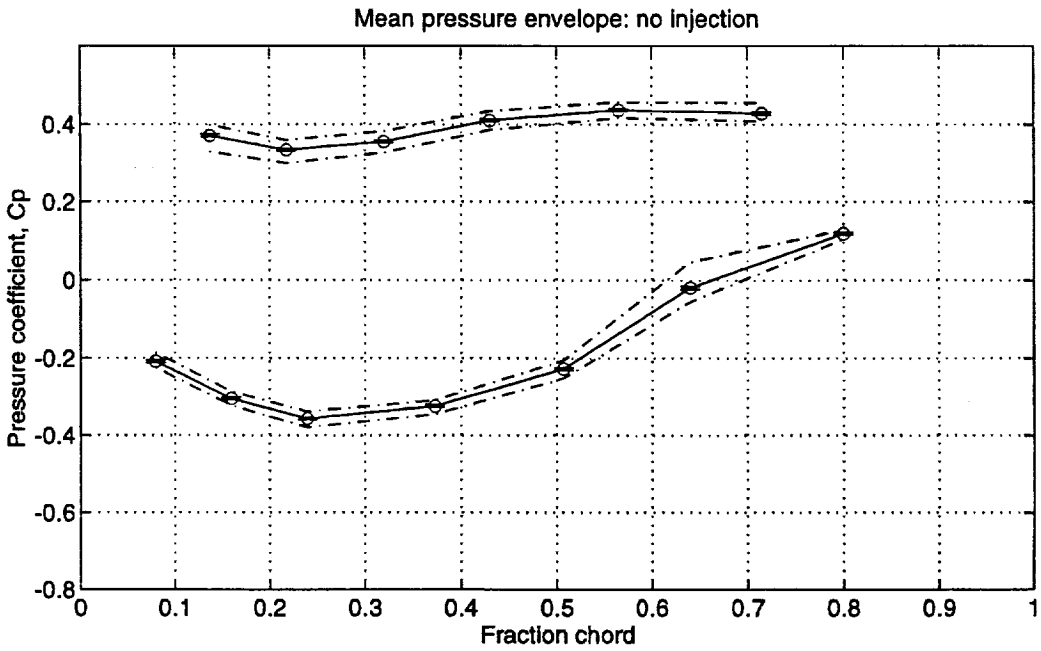

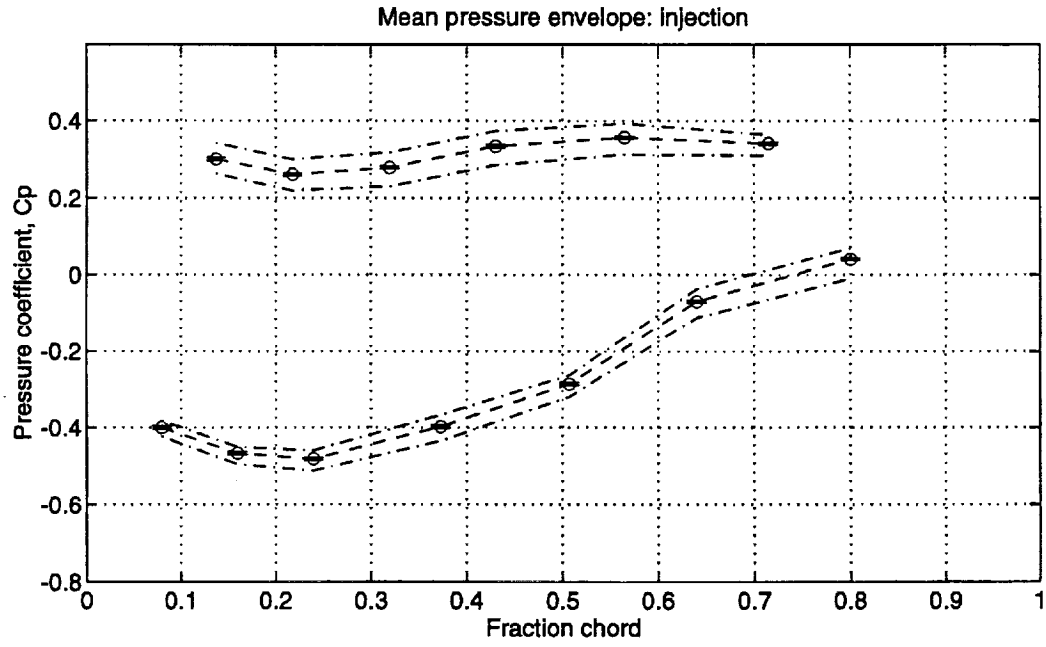

Figure 5-3: Stator mean pressure envelope at 50% span. (—)w/o blowing, (- -)w/ blowing

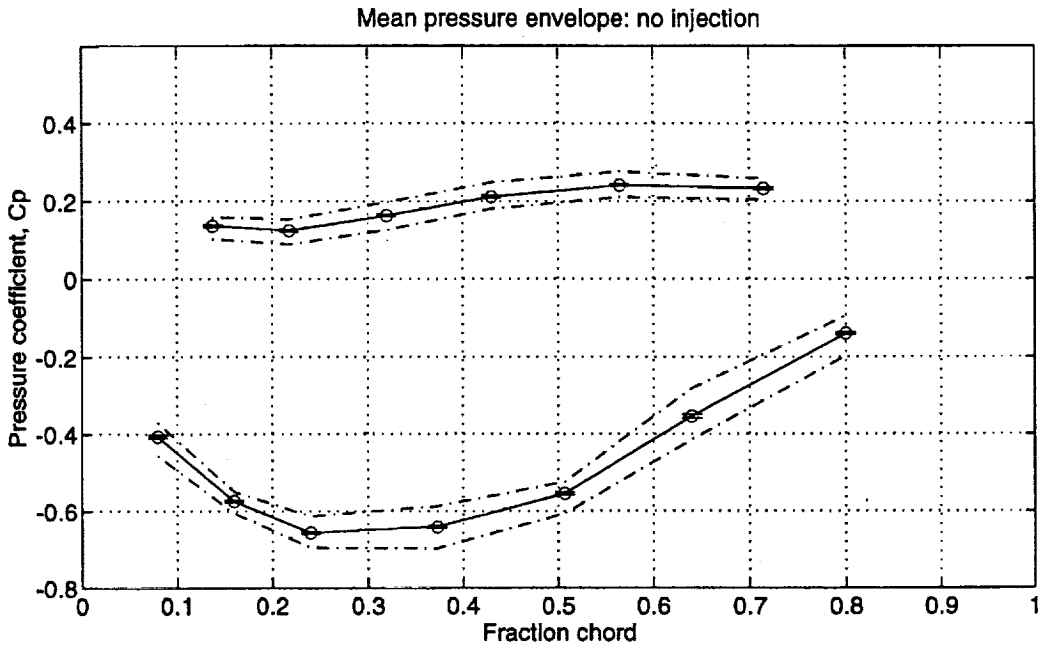

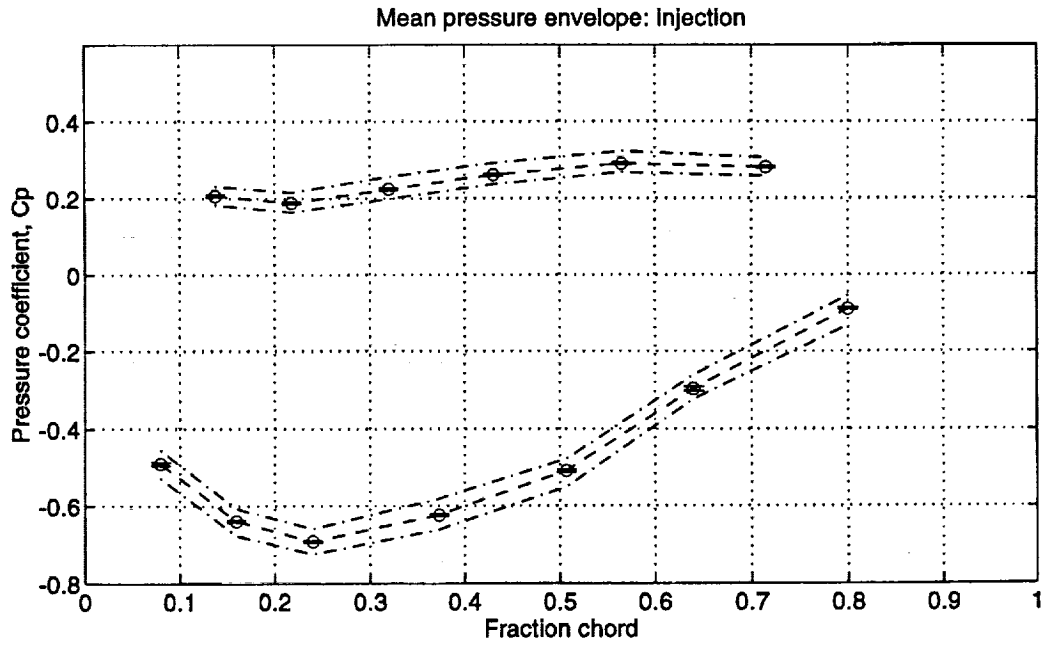

Figure 5-4: Stator mean pressure envelope at 75% span. (—)w/o blowing, (- -)w/ blowing

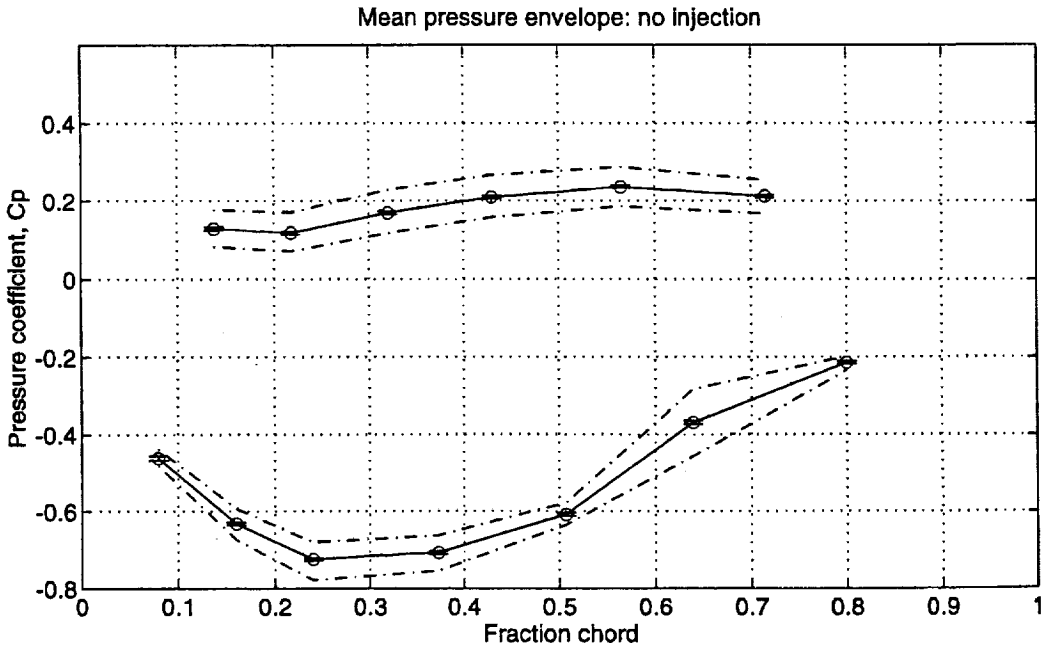

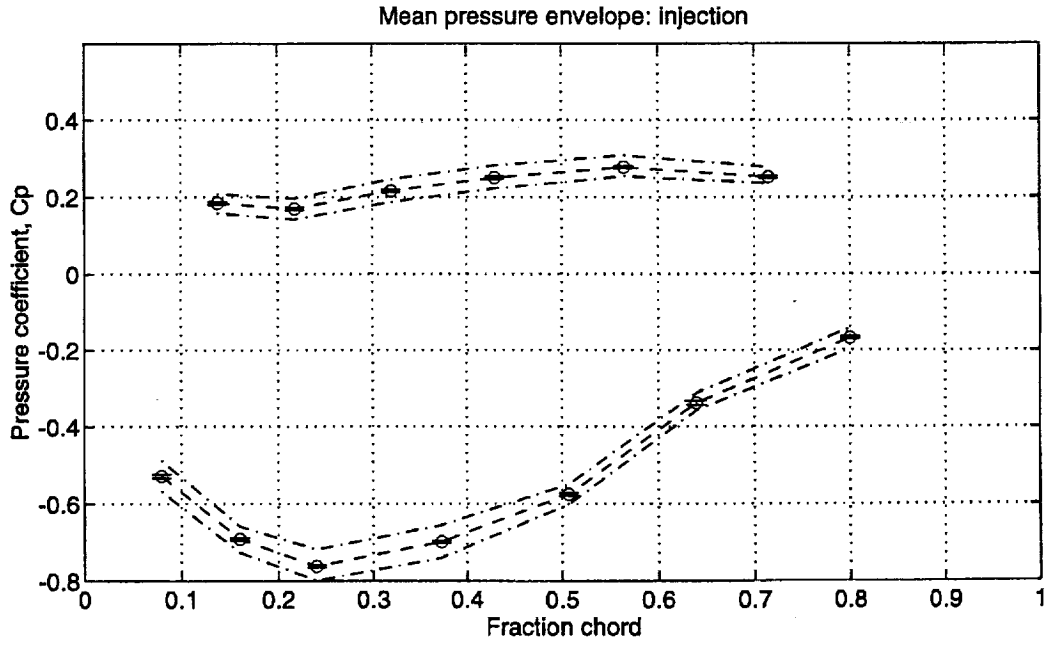

Figure 5-5: Stator mean pressure envelope at 87.5% span. (—)w/o blowing, (- -)w/ blowing

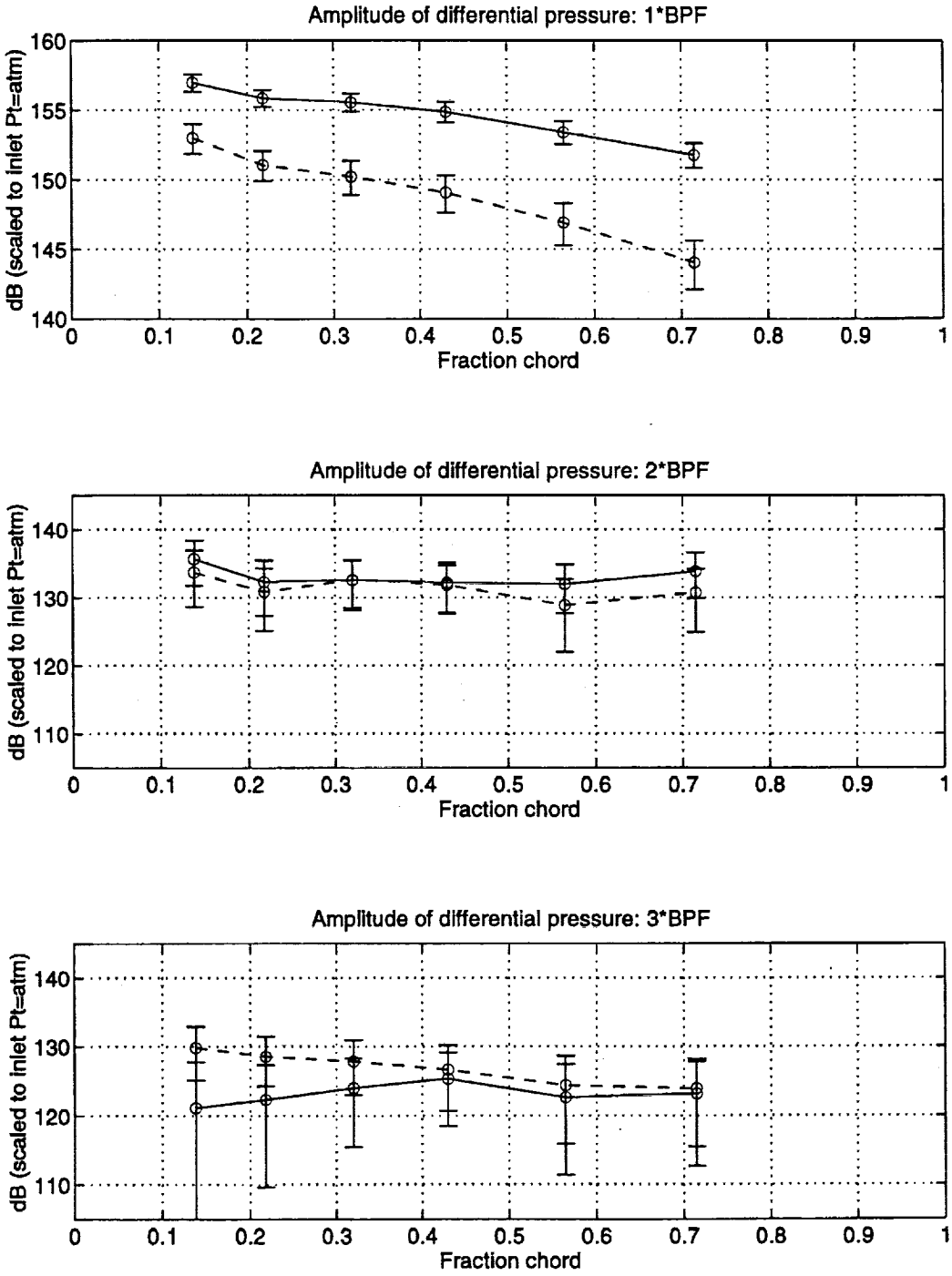

Figure 5-6: Harmonic amplitudes of stator differential pressure at 25% span. (—)w/o blowing, (- -)w/ blowing

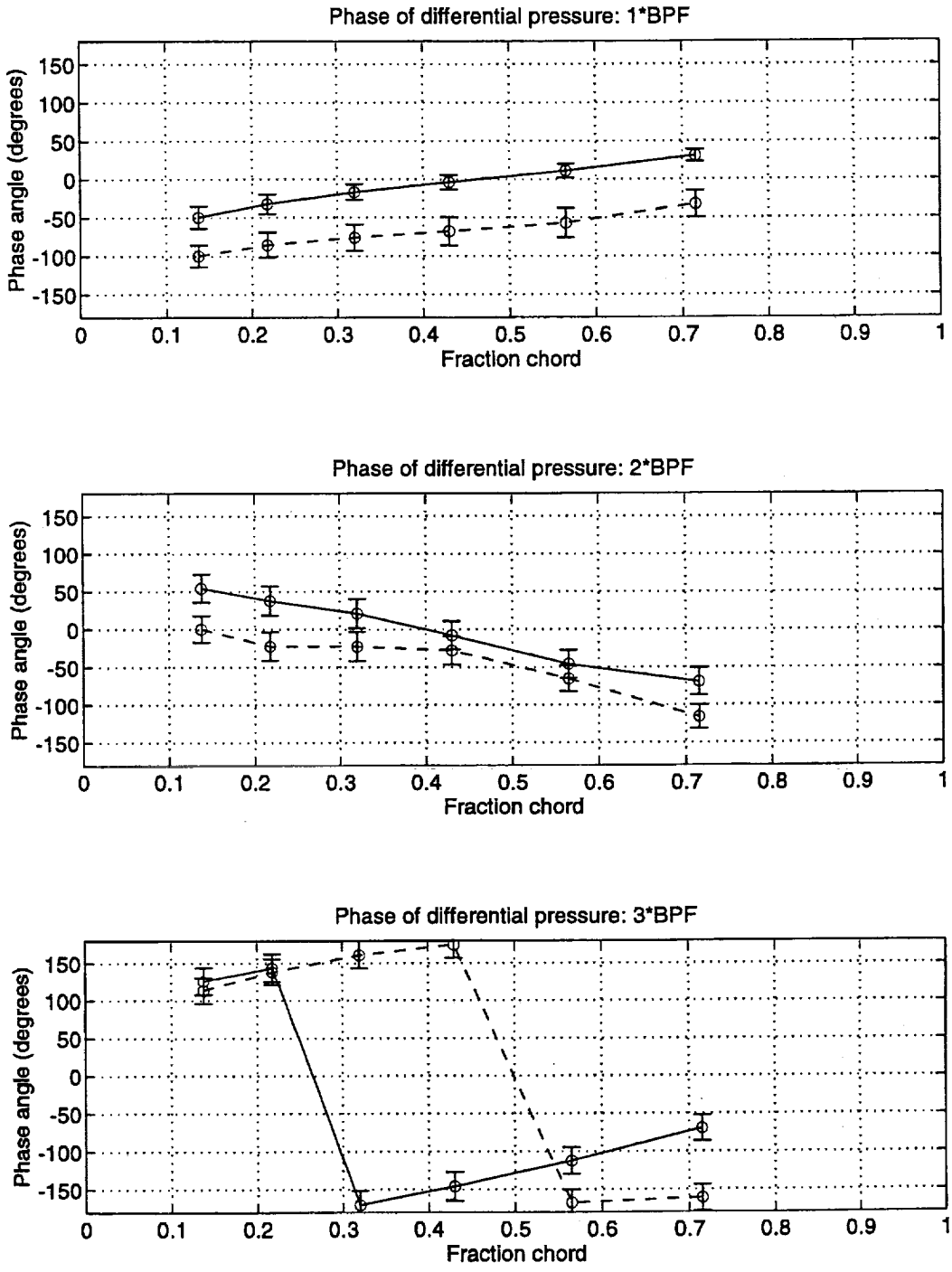

Figure 5-7: Harmonic phases of stator differential pressure at 25% span. (—)w/o blowing, (- -)w/ blowing

degrees at the leading edge to about -100 degrees at the trailing edge.

At this same spanwise location, reductions of about 5dB and 3dB were predicted for the 1*BPF and 2*BPF harmonic amplitudes (see Figure 4-15) and uniform shifts of about +30 degrees and -20 degrees (see Figure 4-16) were predicted for the phases of the 1*BPF and 2*BPF harmonics. While it may be said that there is rough agreement between the predicted amplitude reductions and the experimental measurements, the same cannot be said for the phase shifts.

37.5% span

In contrast to a predicted reduction of about 15dB in the 1*BPF harmonic amplitude at 37.5% span (see Figure 4-17), measurements show a slight decrease at the stator leading edge and a slight increase at the trailing edge but these changes are not discernible within the 95% confidence intervals (see Figure 5-8). Likewise, there seems to be little agreement between the predicted phase shifts and the phase shifts in the experimental measurements (see Figures 4-18 and 5-9).

50% span

The stator harmonic amplitudes at 50% span are shown in Figure 5-10. An increase in amplitude, ranging from about 2dB to about 7dB, is seen along the entire chord. The largest increase occurs in the midchord section. At 2*BPF and 3*BPF no significant changes are seen. For the harmonic phases, shifts ranging between -50 and -120 degrees are seen for the first three harmonics of BPF, (see Figure 5-11).

The changes in the stator harmonics at 50% span do not agree with the data presented in Chapter 4. At 50% span the longitudinal and transverse Mach number 1*BPF harmonic were reduced by about 80% and 45% respectively and a reduction of about 10dB was predicted for the stator 1*BPF harmonic. A possible reason for this inconsistency will be presented in Chapter 6.

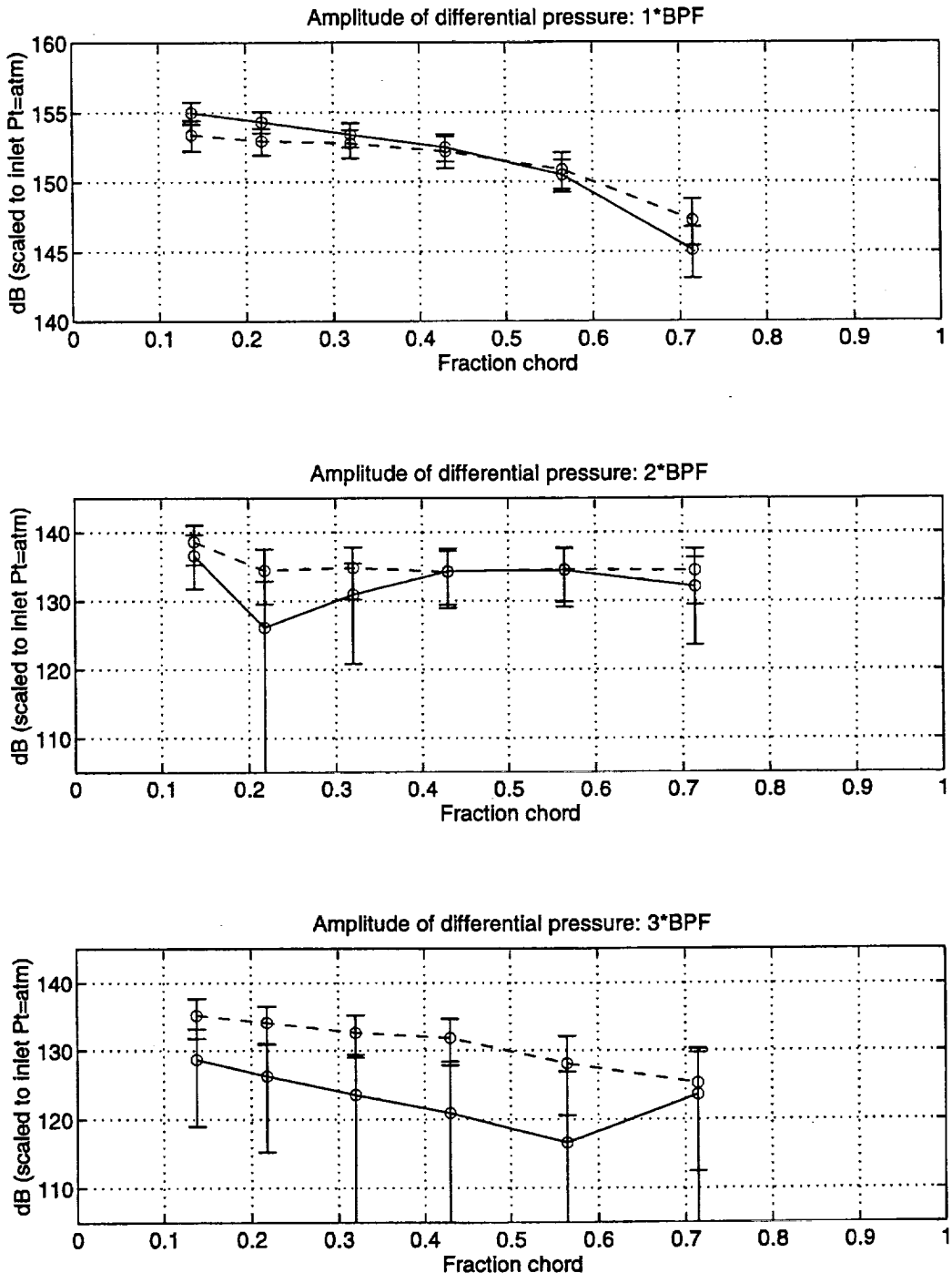

Figure 5-8: Harmonic amplitudes of stator differential pressure at 37.5% span. (—)w/o blowing, (- -)w/ blowing

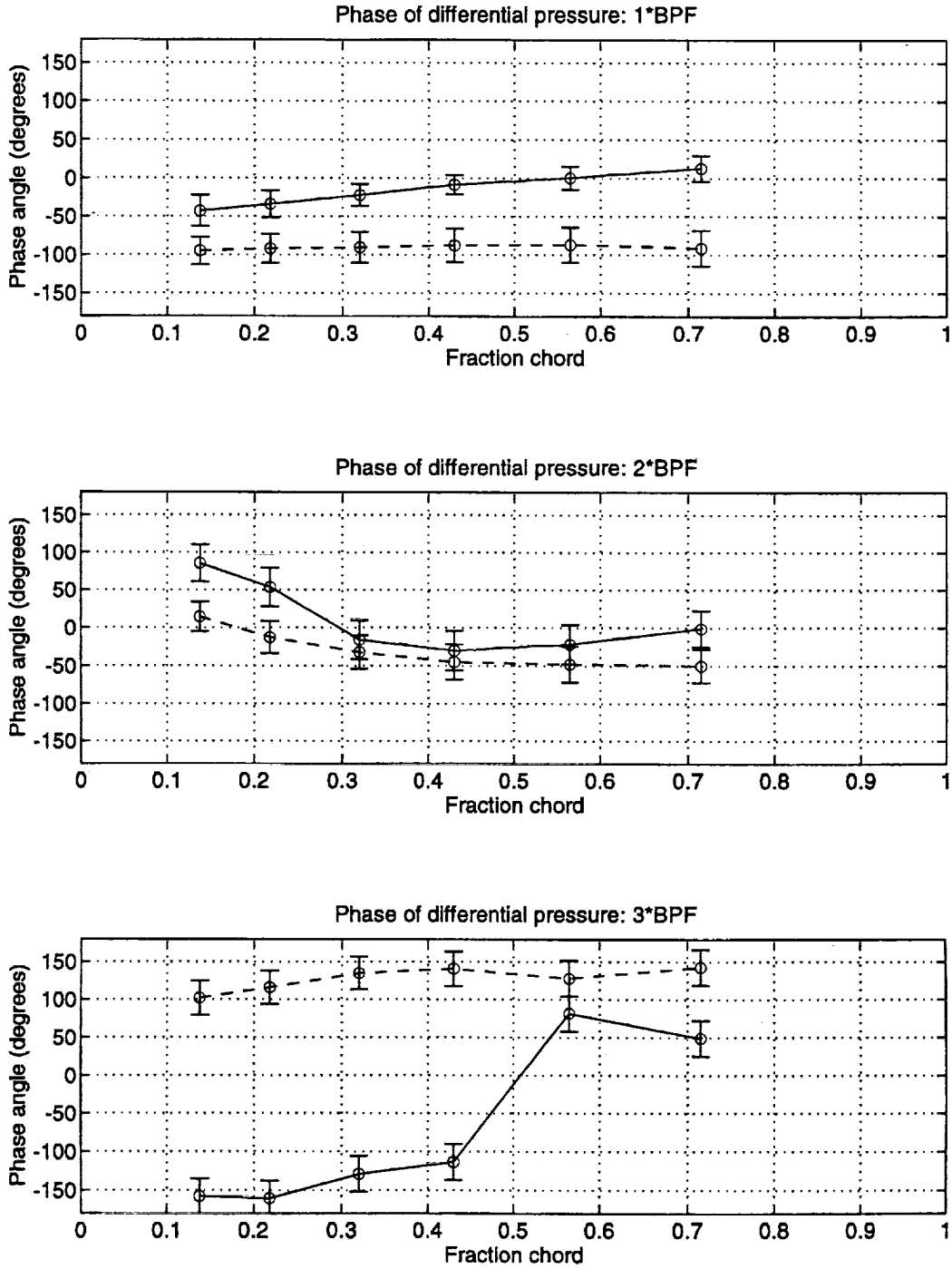

Figure 5-9: Harmonic phases of stator differential pressure at 37.5% span. (—)w/o blowing, (- -)w/ blowing

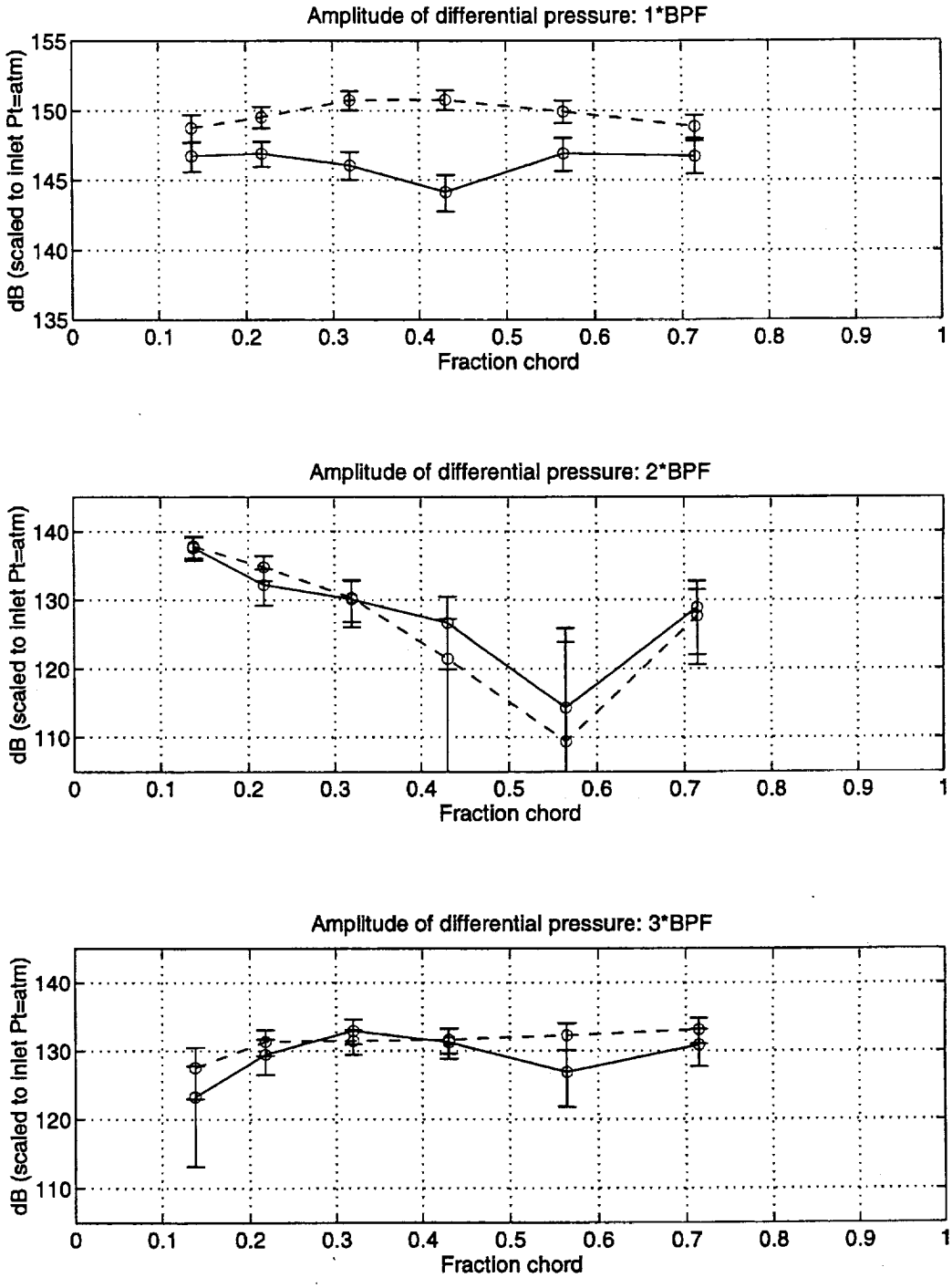

Figure 5-10: Harmonic amplitudes of stator differential pressure at 50% span. (—)w/o blowing, (- -)w/ blowing

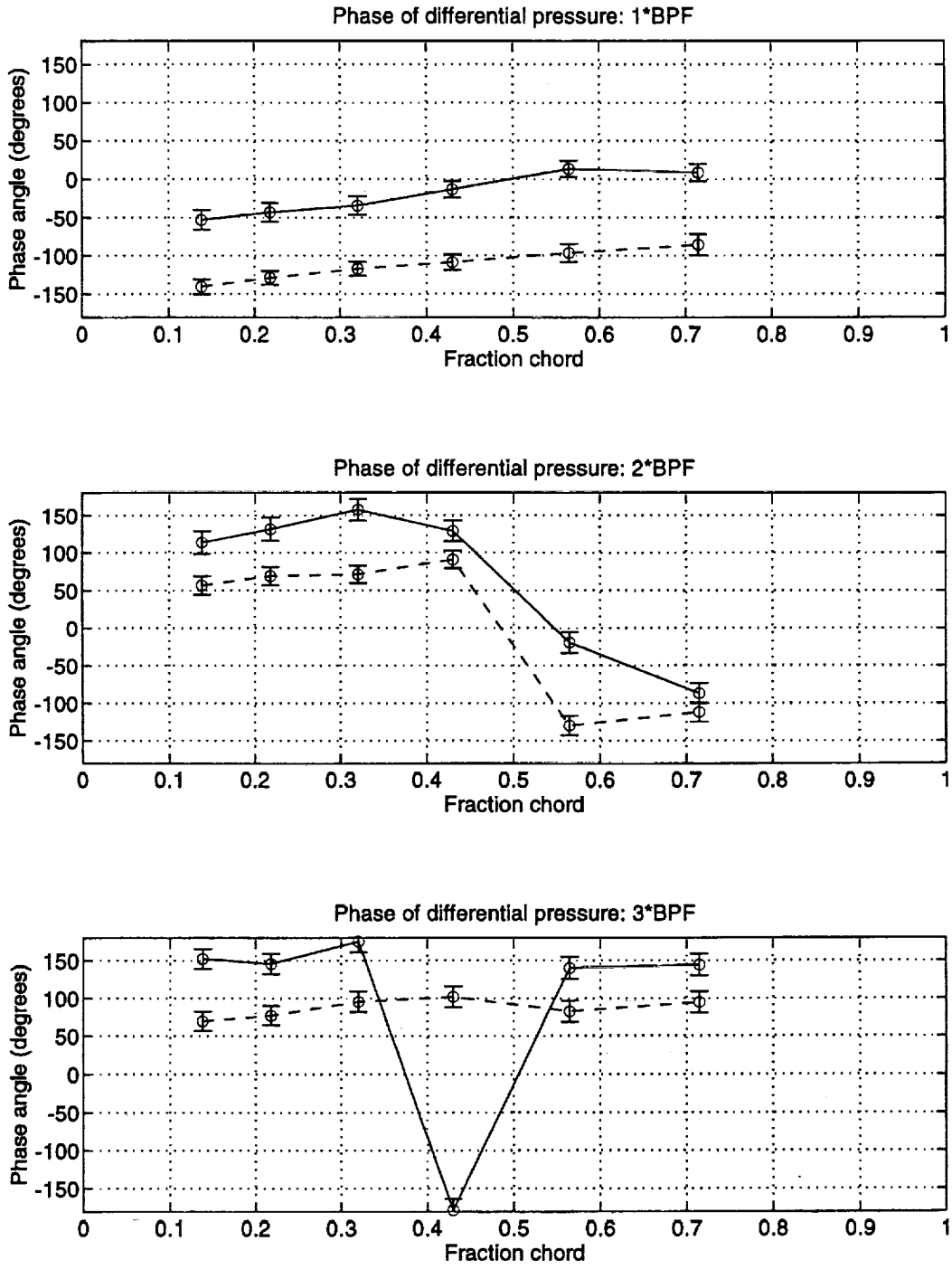

Figure 5-11: Harmonic phases of stator differential pressure at 50% span. (—)w/o blowing, (- -)w/ blowing

75% span

At 75% span the 1*BPF harmonic amplitude is reduced mostly at the midchord (by 3dB) and the trailing edge (by 5dB) while virtually no change is seen in the harmonic phase, (see Figures 5-12 and 5-13). Reductions along the entire chord are seen in the 2*BPF harmonic amplitude, although the reductions along the midchord are not altogether discernible within the 95% confidence levels. A reduction of about 15dB in the 3*BPF harmonic amplitude is seen at the leading edge of the stator, but no change is seen at the trailing edge. In contrast, the stator loading predictions presented in Chapter 4 show close to uniform reductions in amplitude along the entire chord for the first three harmonics of BPF. Reductions in amplitude of approximately 9dB are predicted for the first and third multiples of BPF, while a reduction of about 12 dB is predicted for the second harmonic. The predicted phase shifts are uniform along the chord, whereas in the stator measurements shifts in harmonic phase vary along the chord. Strong shifts in the 2*BPF harmonic phase are seen at the leading and trailing edges but shifts at the midchord section cannot be distinguished within the confidence intervals. The 3*BPF harmonic phase exhibits a shift of about +150 degrees at the leading edge and decreases along the chord to a shift of about -60 degrees at the trailing edge.

87.5% span

Figures 5-14 and 5-15 show the stator harmonic amplitudes and phases at 87.5% span. The 1*BPF harmonic amplitudes are reduced by about 2dB toward the leading edge and about 7 dB toward the trailing edge while a reduction of about 10 dB was predicted (see Figure 4-23). The front half of the stator shows reductions of about 7dB in the 2*BPF harmonic amplitudes, while the 3*BPF amplitudes remain virtually unchanged. Stator loading predictions showed a 5dB reduction and a 3dB increase in amplitude for the 2*BPF and 3*BPF harmonics respectively. Phase shifts of about -50, +50 and -100 degrees are seen along the entire chord for the 1*BPF, 2*BPF and 3*BPF respectively. There is a strong disagreement with the predicted phase shifts

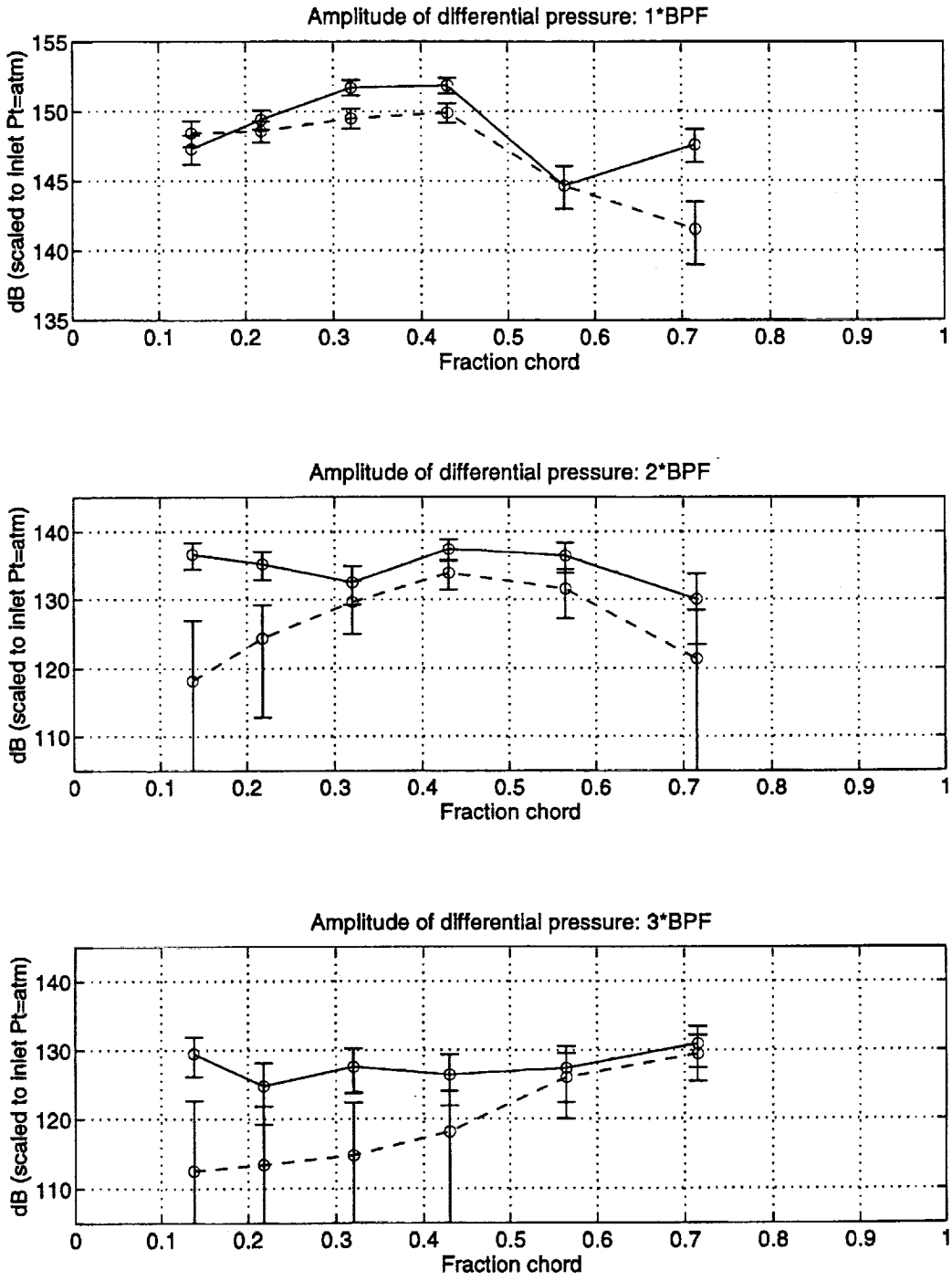

Figure 5-12: Harmonic amplitudes of stator differential pressure at 75% span. (—)w/o blowing, (- -)w/ blowing

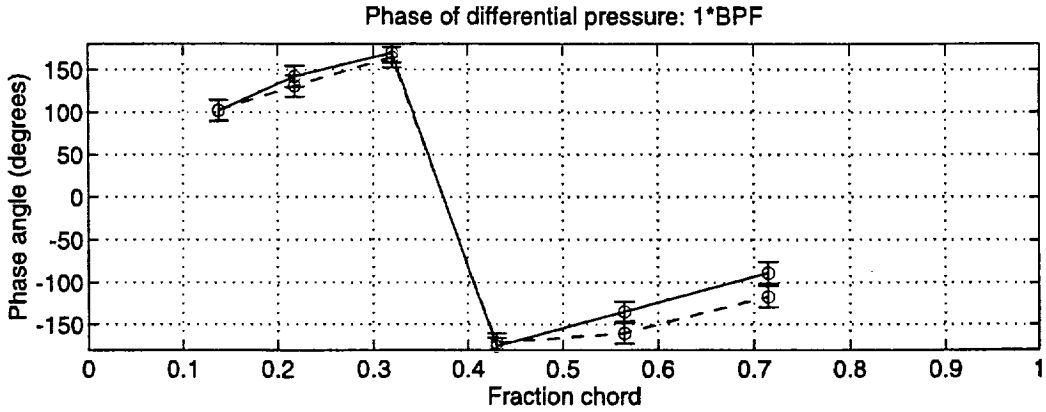

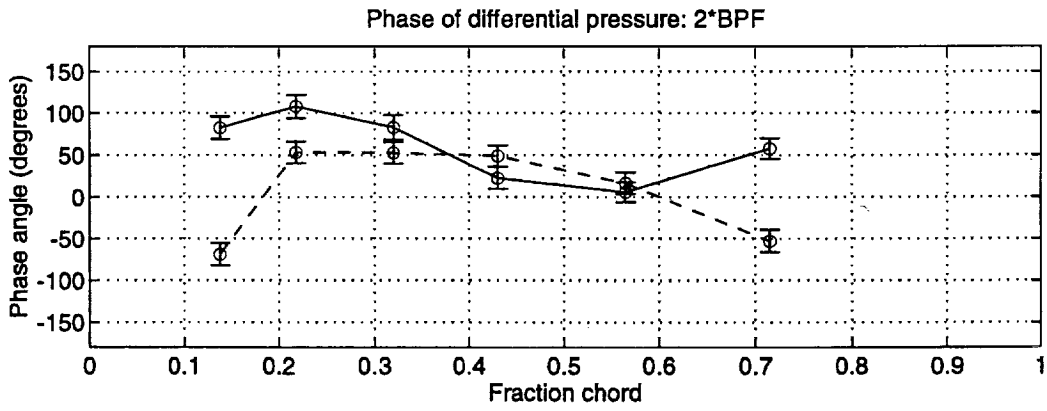

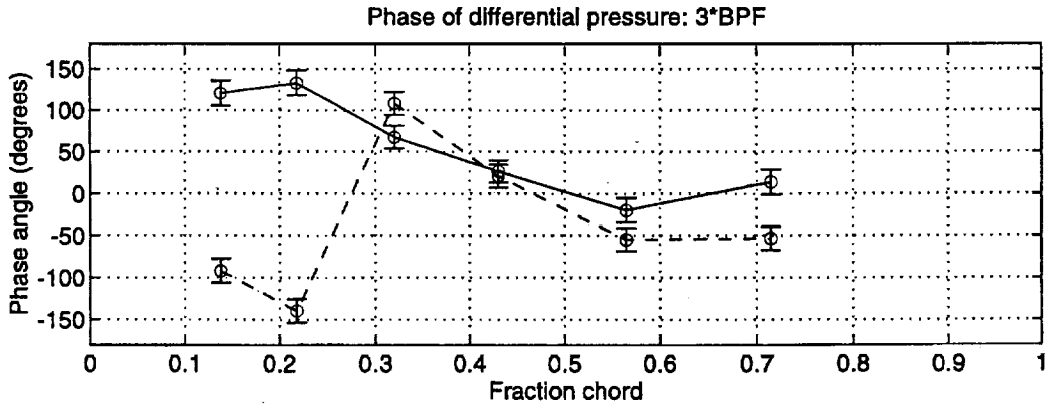

Figure 5-13: Harmonic phases of stator differential pressure at 75% span. (—)w/o blowing, (- -)w/ blowing

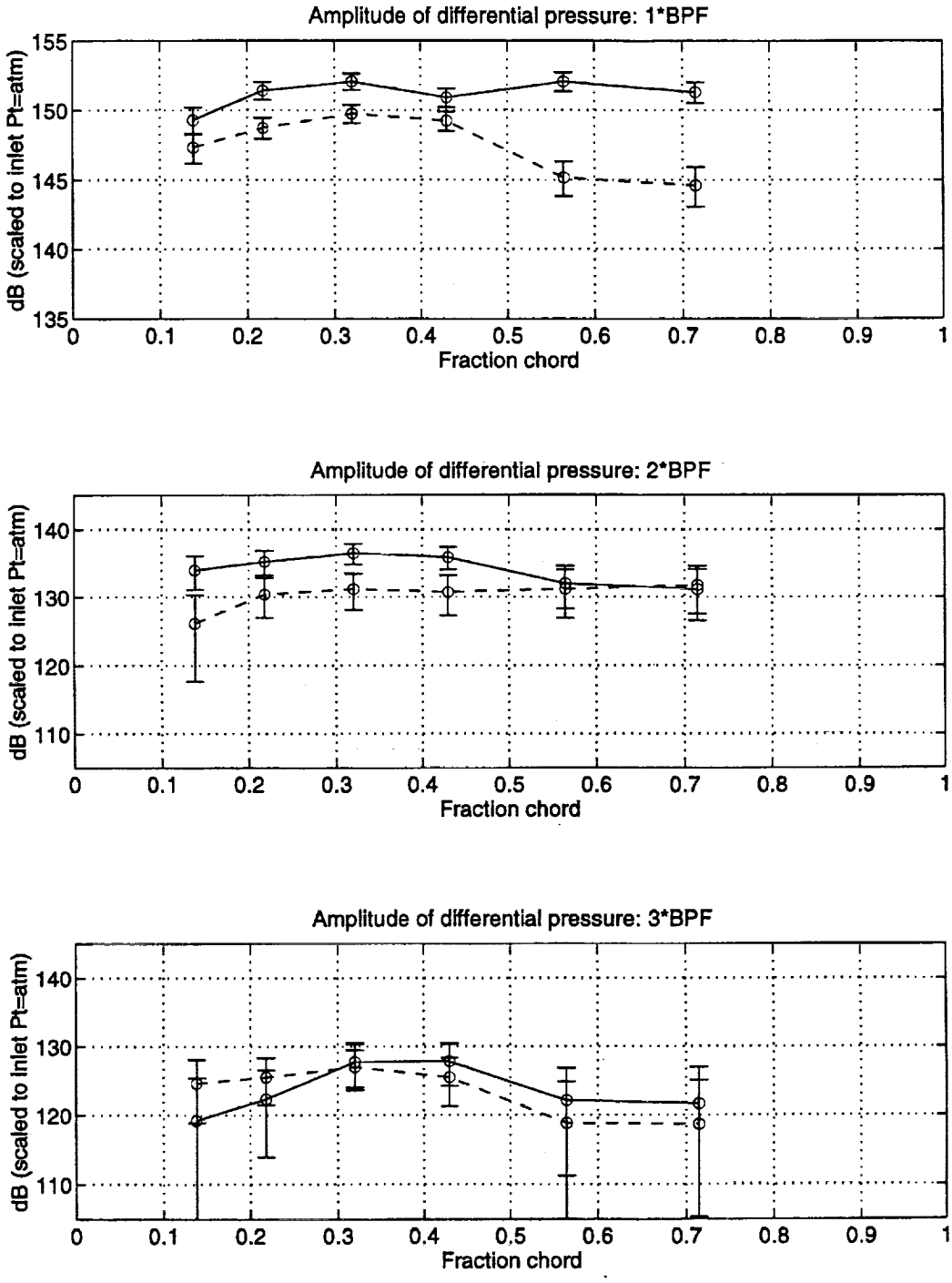

Figure 5-14: Harmonic amplitudes of stator differential pressure at 87.5% span. (—)w/o blowing, (- -)w/ blowing

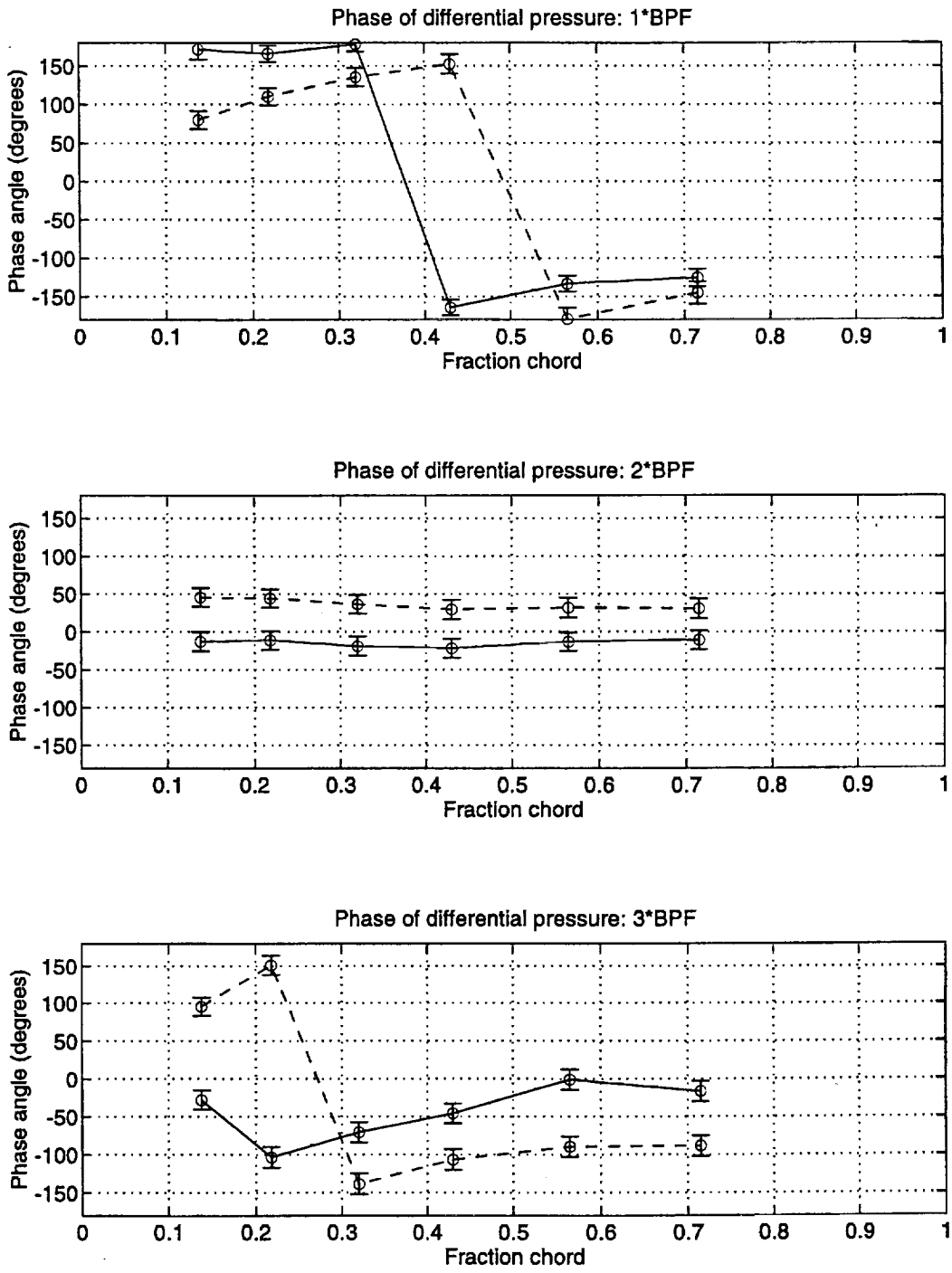

Figure 5-15: Harmonic phases of stator differential pressure at 87.5% span. (—)w/o blowing, (- -)w/ blowing

which ranged from about zero to 10 degrees, (see Figure 4-24).

Summary of stator loading measurements

There is some weak agreement between the harmonic amplitude reductions measured at the 25% and 87.5% span locations and the predicted changes. However, the same cannot be said for the other radial locations. For the first harmonic of BPF, amplitude reductions are seen at 25% span and 87.5% span. At 50% span, an increase in the amplitude is seen. Changes in the 2*BPF harmonic amplitude could not be distinguished at the 25%, 37.5% and 50% span locations. At 75% and 87.5% span amplitude reductions are seen, particularly for the front half of the stator chord.

CHAPTER 6

DISCUSSION

As seen in Chapter 5 there was a lack of correlation between changes in the stator harmonic amplitudes and changes in the wake harmonic amplitudes. Several possible hypotheses to explain the stator measurements were investigated and eliminated. These hypotheses are briefly discussed in Section 6.1. It was determined that wake cancellation may be responsible for the discrepancy between the stator measurements and the flow field measurements. This possibility is discussed in Section 6.2.

6.1 Discarded Hypotheses

Possible problems with the experimental facility, the data acquisition system, and the data reduction process were investigated first because the lack of correlation between the wake harmonic reductions and the changes in the stator harmonics was unexpected. The raw data traces of the instrumented stator transducers and the four-way probe pressure transducers were checked to ensure that the transducers were responding properly. To check the noise level in the data acquisition system, data was taken at constant conditions with all the instrumentation on. After the data was reduced, the noise level was found to be an order of magnitude less than the unsteady signals being measured. The manner in which the data was averaged and in which the wake harmonics were computed was investigated to ensure that the

results were not artificial. The data was averaged and the fourier transforms were computed with various methods and the end results were found to be in agreement with each other. A final concern was the possibility that the data was being affected by blade vibrations. To investigate this possibility, an accelerometer was attached to the instrumented stator blade and vibration tests were conducted. The natural frequency of the blade was found to be close to 2*BPF. The pressure transducers, however, were not in phase as would be expected if the blade was vibrating.

6.2 Wake Cancellation Hypothesis

As hypotheses were investigated, the focus was placed on the 50% span data because the stator and flow field measurements were in most obvious disagreement at that location. Figure 6-1 is a graphical representation of the gust impinging on the stator at 50% span. The solid line represents the freestream Mach number, the dashed line represents the wake (maximum deficit) Mach number, and the bold line represents the gust. Notice that in the no blowing case the wake is characterized by a drop in Mach number and an increase in angle of attack. Figure 6-1 suggests that the disturbance caused by the no blowing wake may be lower than would be expected due to the combination of Mach number and angle of attack changes. In other words, the increase in loading caused by the higher angle of attack is partially offset by the decrease in loading caused by a lower dynamic pressure. It would then be possible that when trailing edge blowing is applied the balance between the two effects could be diminished in such a way that although the gust is reduced the loading changes are increased. To determine the plausibility of this theory, a very simple analysis was conducted using MISES, a two-dimensional, steady, viscous cascade code [6].

At each radial location, the force coefficients were calculated for four different conditions using MISES. Cases were run at the free stream and the wake conditions for both blowing and no blowing. Once the force coefficients were obtained, the actual loads were calculated using the dynamic pressure at each condition. The unsteady

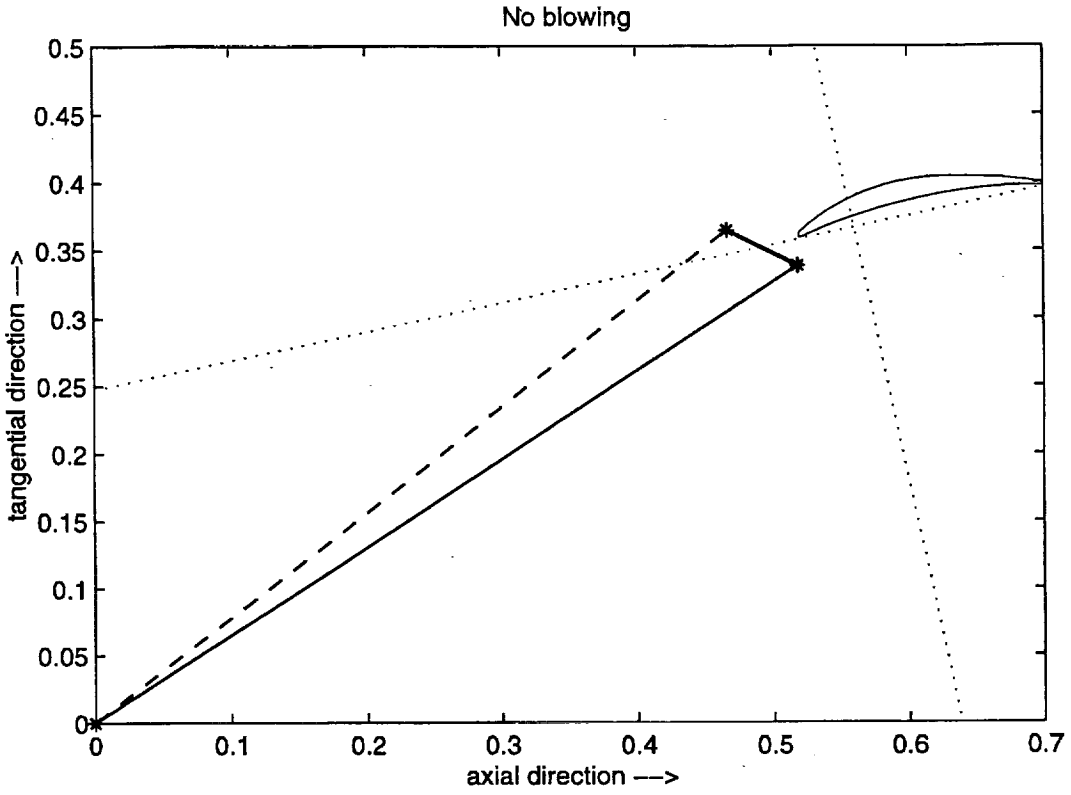

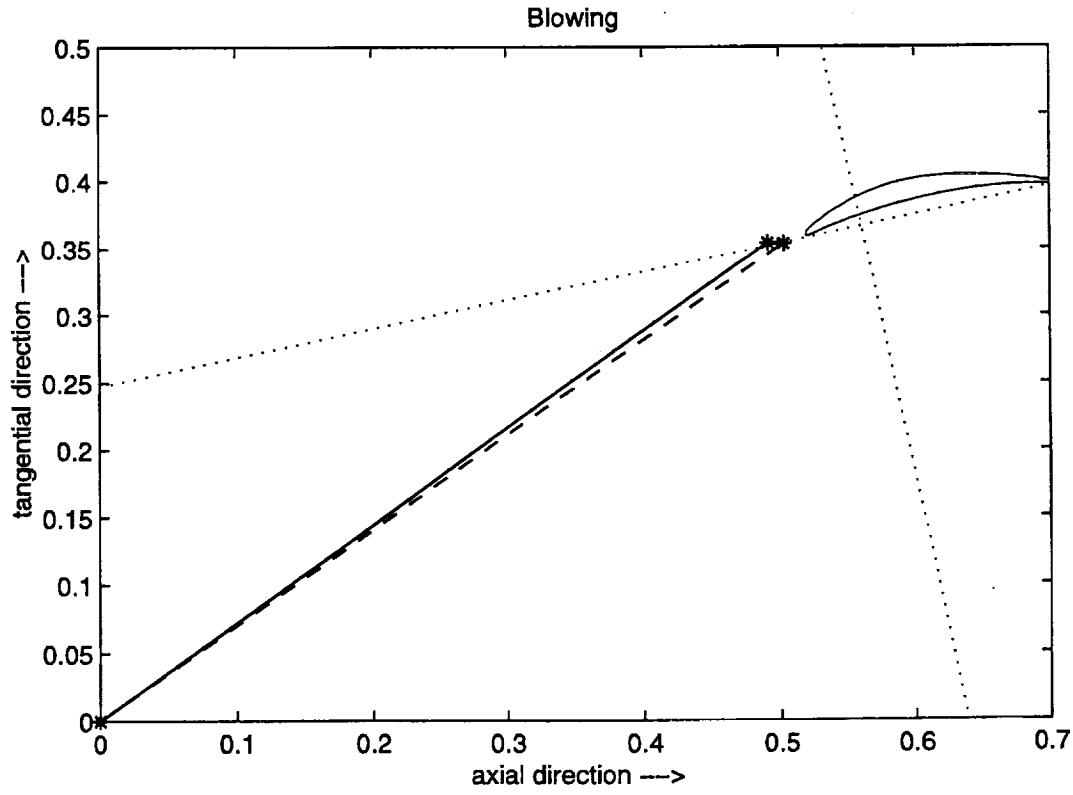

Figure 6-1: Gust impinging on stator at 50% span. (—)freestream, (- -)wake, (‾‾)gust

radial location	$\frac{\delta F_b}{\delta F_{nb}}$
25% span	7.46
37.5% span	2.34
50% span	1.58
75% span	0.60
87.5% span	0.52

Table 6.1: Loading difference with blowing as a fraction of loading difference without blowing

loading was then estimated by taking the difference between the freestream condition and the wake condition. At 50% span, the loading difference with blowing was 1.58 times that without blowing. The loading difference results for all radial locations are shown in Table 6.1. This simple analysis predicts the trend seen in the data for the three outer locations (50%, 75%, 87.5%) but not for the inner two locations (25%, 37.5%). However, it is important to note that the wakes at 25% and 37.5% have velocity excess and deficit components which are of roughly the same magnitude. Thus, a two point analysis such as the one being discussed cannot be expected to represent the situation accurately. For completeness, graphical representations of the points used in this analysis at the 25%, 37.5%, 75% and 87.5% span locations are shown in Figures 6-2 through 6-5.

The results from the above analysis clearly indicate that for this stage the stator unsteady response is dependent on both the transverse and longitudinal gust components. This dependence explains why the predicted stator loadings do not agree with the stator measurements. V072 only predicts the unsteady response caused by the upwash of the wake. Thus, the longitudinal component of the gust, first determined by Horlock [9] to have significant effects on the unsteady stator response, is completely ignored. Furthermore, because no interaction between the mean flow and the gust is allowed and because the mean flow is assumed to pass through the stator without producing any effect, the gust distortion effect determined by Goldstein and Atassi [7] to have important effects on the unsteady loading does not appear in the predictions.

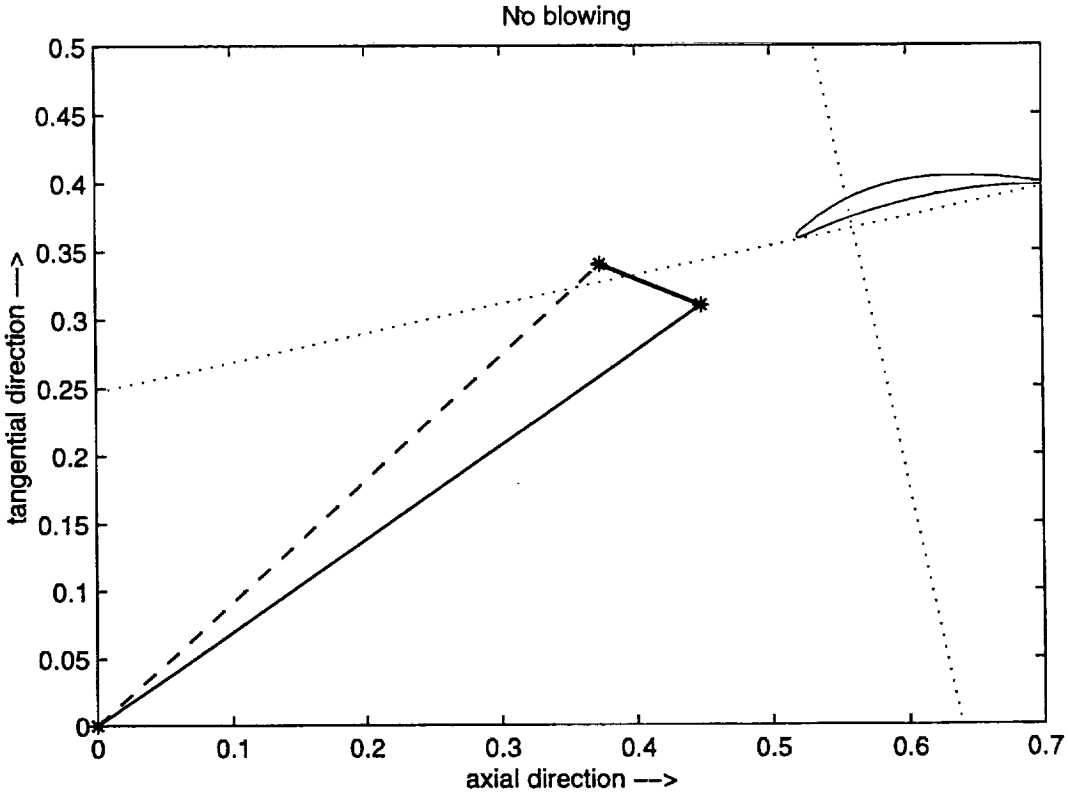

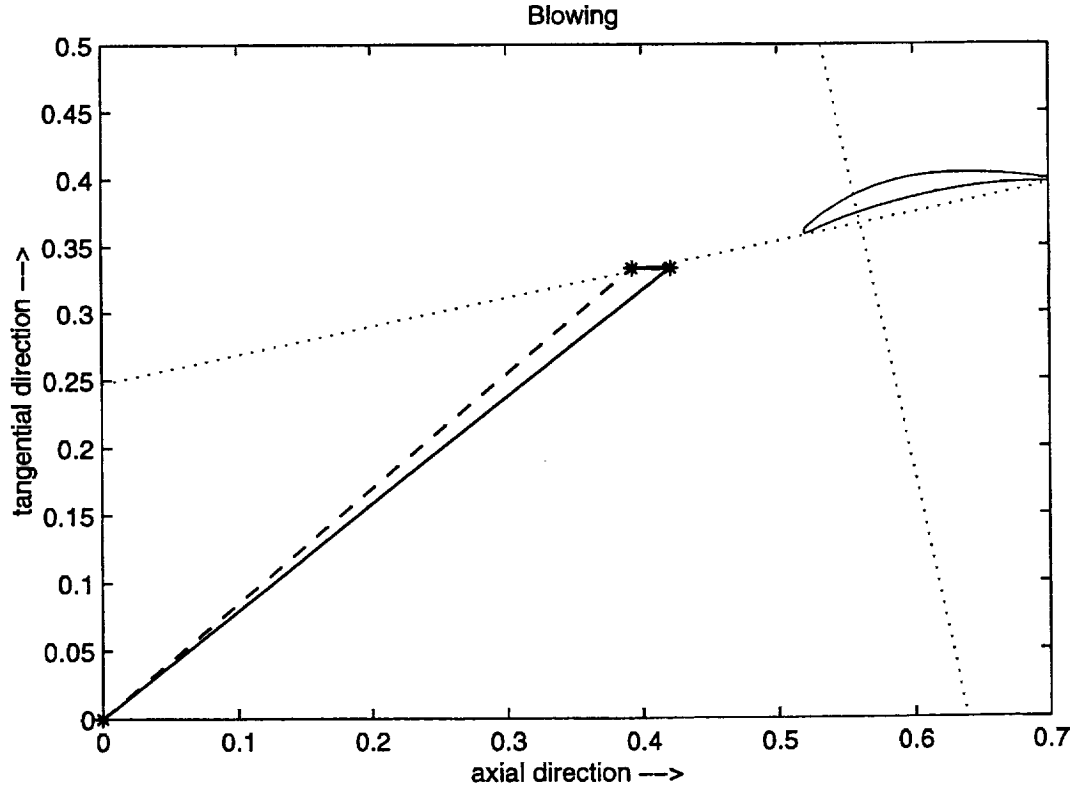

Figure 6-2: Gust impinging on stator at 25% span. (—)freestream, (- -)wake, (‾)gust

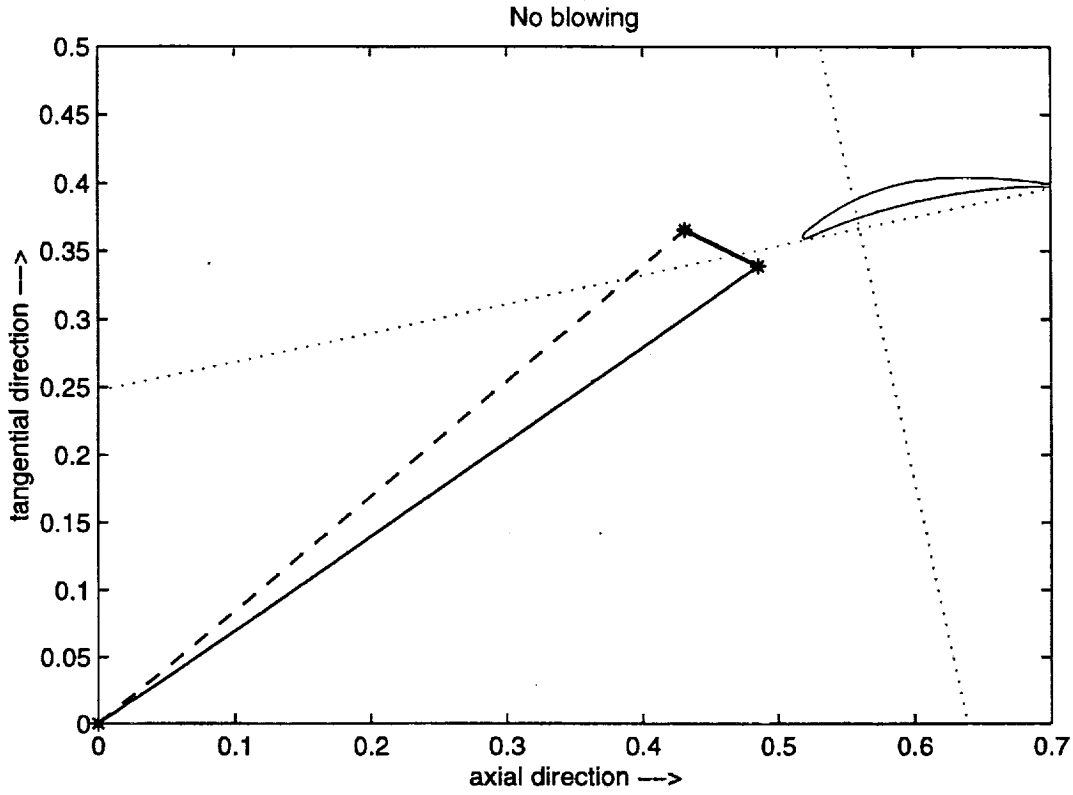

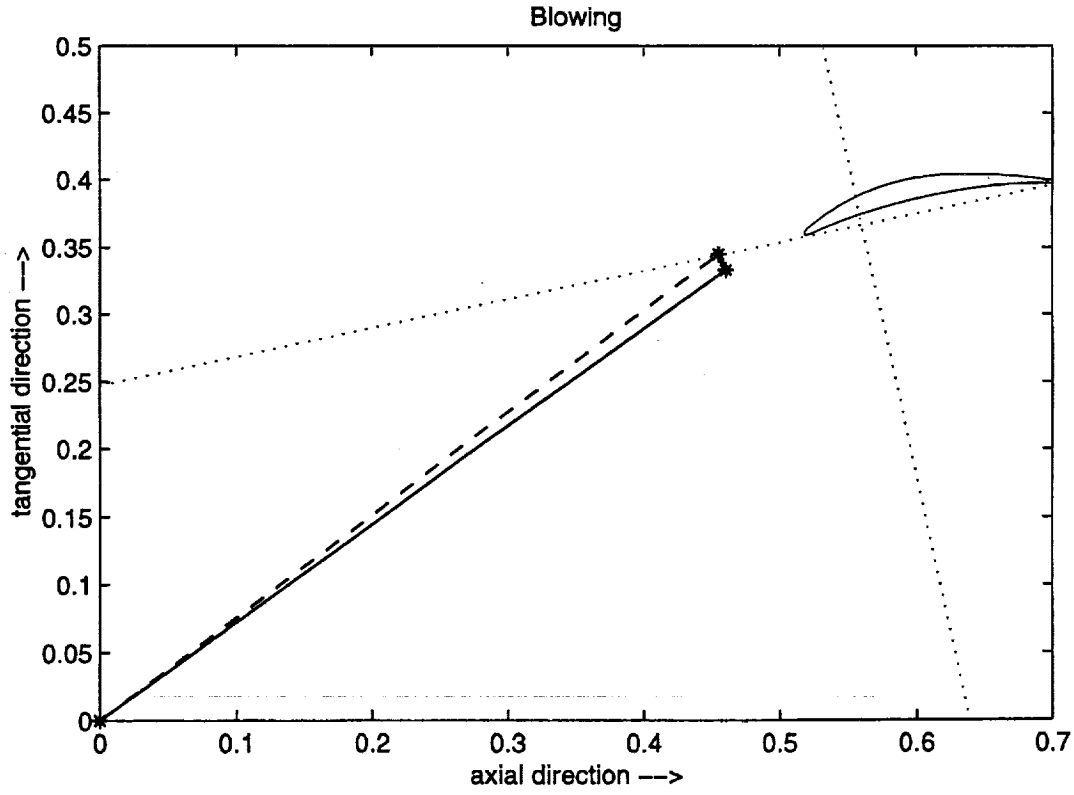

Figure 6-3: Gust impinging on stator at 37.5% span. (—)freestream, (- -)wake, (‾‾)gust

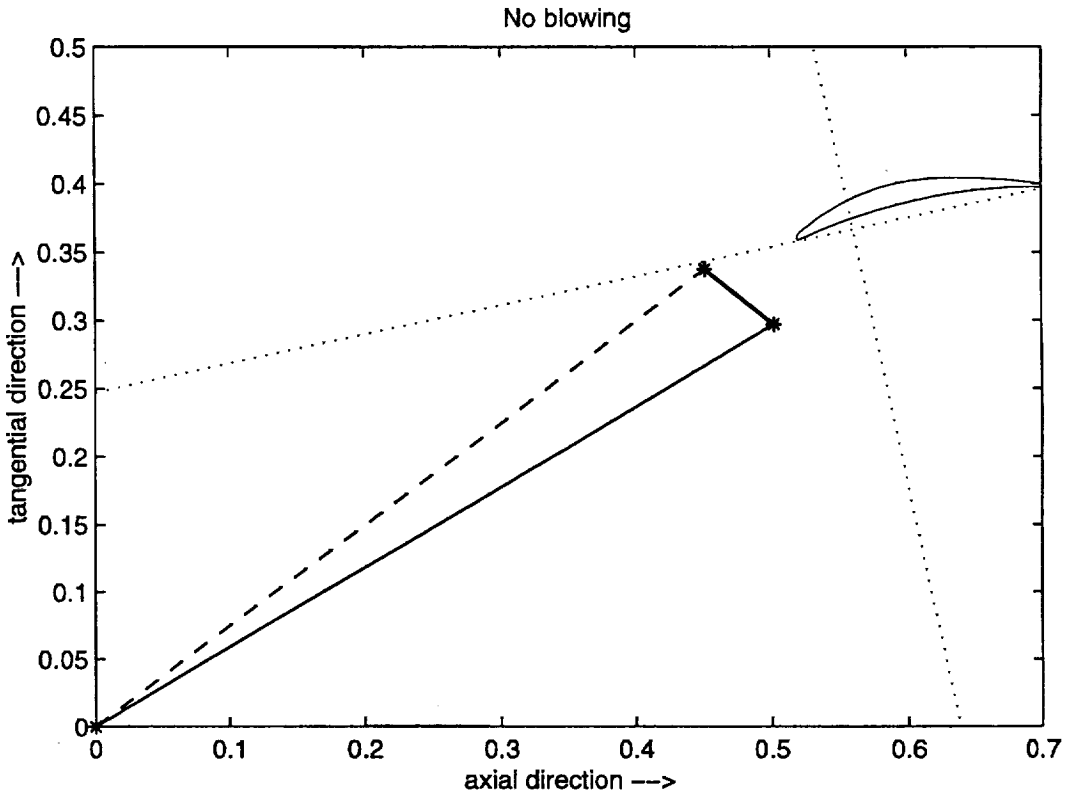

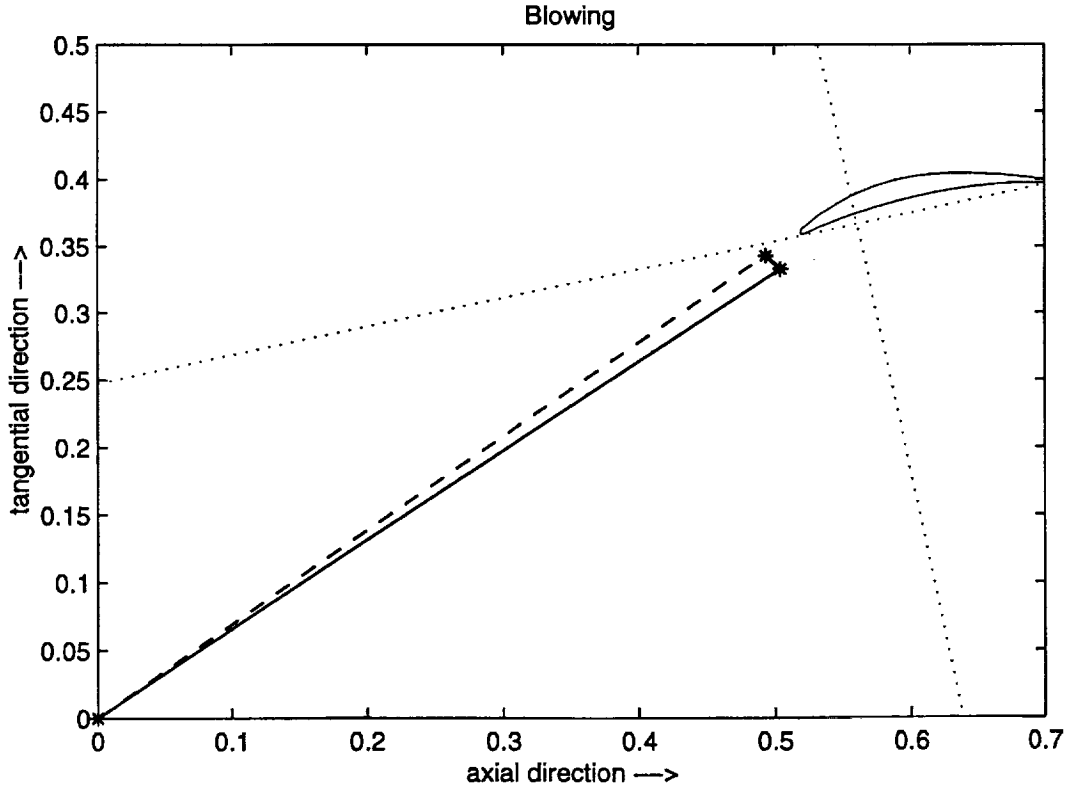

Figure 6-4: Gust impinging on stator at 75% span. (—)freestream, (- -)wake, (‾)gust

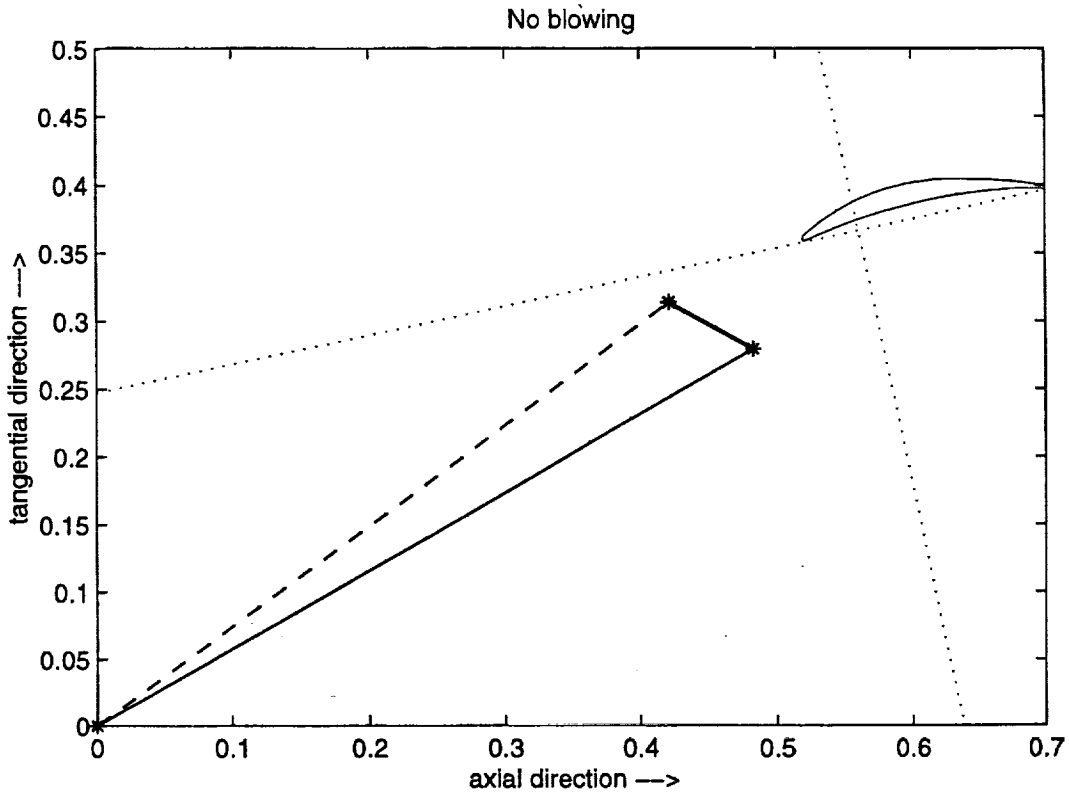

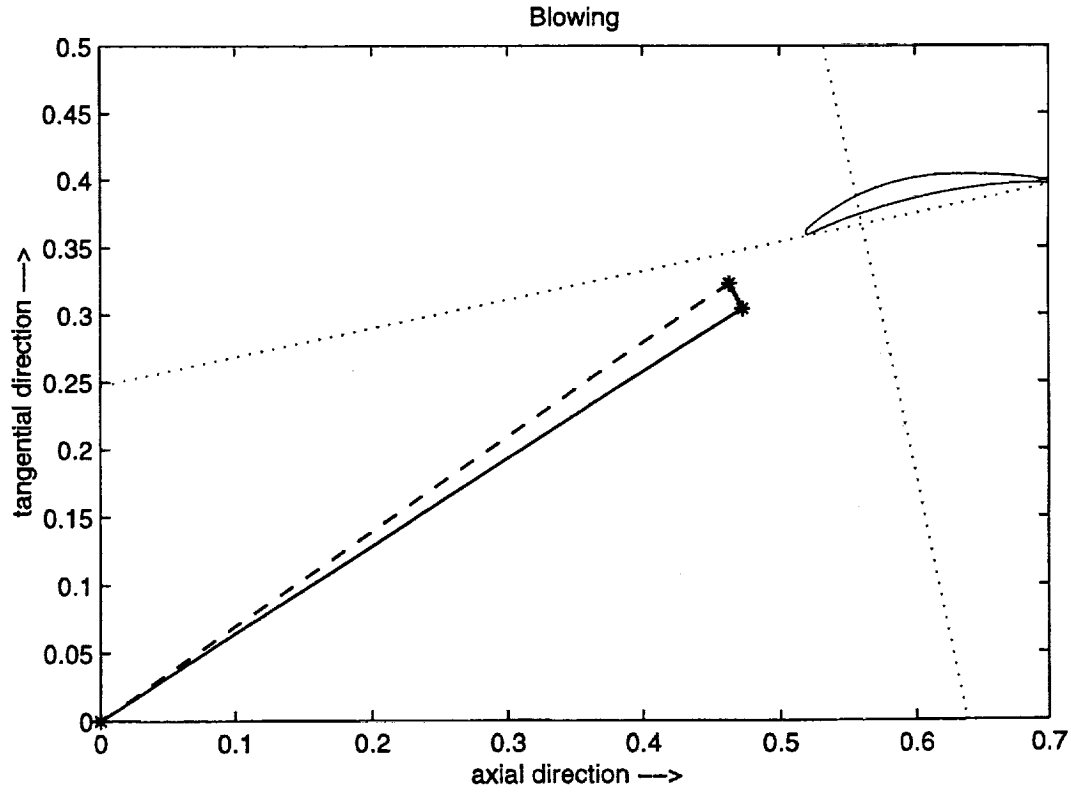

Figure 6-5: Gust impinging on stator at 87.5% span. (—)freestream, (- -)wake, (‾)gust

It is possible that analysis which incorporates all of the effects considered by Goldstein and Atassi [7] into a cascade setting could predict the experimental results. Unfortunately, time did not allow for such an analysis. However, the simple analysis performed does indicate that wake cancellation is a plausible explanation for the lack of correlation between the wake harmonics and the changes in the stator harmonics. Furthermore, the results highlight the importance of using prediction tools which include the effects of longitudinal and transverse gusts and the effects of the steady-state response when analyzing changes caused by trailing edge blowing.

CHAPTER 7

CONCLUSION

The effects of trailing edge blowing on the stator unsteady loading harmonics were investigated. Experiments using a new blowing distribution were conducted on Brookfield's [3] trailing edge blowing fan. Flow field and stator pressure measurements were taken with and without trailing edge blowing. Additionally, the experimental wake measurements were input into the BBN/PW V072 noise prediction code and stator unsteady loading predictions were computed.

The new blowing distribution filled the wake with less spanwise variation than previously tested distributions. A momentumless wake was produced at 50% span and was over 70% filled elsewhere. Reductions in the first two BPF harmonics of the relative Mach number were seen at all radial locations. However, it was seen that reductions in the relative harmonic amplitudes did not dictate reductions in the harmonic components parallel to and normal to the stator chord. For the 1*BPF harmonic, reductions ranging from 58% to 90% were seen for the longitudinal component, while reductions from 11% to 95% were seen for the transverse component. The 2*BPF harmonic underwent reductions ranging from 20% to 44% in the longitudinal component. The transverse component was reduced from 19% to 44% except at the 37.5% span location where an increase of 24% was seen. Correlating well with the wake harmonic reductions, the stator loading predictions showed reductions at all spans for the first 2 harmonics of BPF.

The stator unsteady loading measurements did not correlate well with the wake harmonic reductions. The strongest disagreement was seen at 50% span for the 1*BPF harmonic. At this location an increase in the harmonic amplitude of up to 7 dB was seen along the chord while the longitudinal and transverse wake harmonics were significantly reduced. Graphical representations of the gusts suggested that the effects of the longitudinal and transverse gust components could be partially cancelling each other. A simple two-dimensional analysis was done to determine the steady-state loading at the freestream and wake conditions. At 50% span, the difference in loading between the freestream and the wake was higher when trailing edge blowing was used. This result suggests that wake cancellation effects could account for the lack of correlation between the stator and wake harmonics.

The V072 stator loading predictions did not agree with the stator measurements. The discrepancy is most likely present because V072 only considers the effects due to transverse gusts. The wake measurements show that trailing edge blowing affected both the longitudinal and the transverse harmonics. Furthermore, in the set of experiments presented here, trailing edge blowing resulted in an increase of the steady-state stator loading. Because V072 models neither the effects of the longitudinal gusts nor the distortion effects of the steady-state loading, the unsteady loading changes caused by trailing edge blowing cannot be truly captured.

If trailing edge blowing is to be used to reduce noise, it is important to understand the effects it has on the unsteady stator loading. To increase this understanding, the experimental wakes should be used in a stator loading prediction tool which can accurately capture all the changes caused by the blowing. The results will not only help to understand the effects of trailing edge blowing but may also increase the understanding of the airfoil unsteady response to gusts.

APPENDIX A

WAKE IDENTIFICATION METHOD

The edges of the wakes were identified using the same method employed by Sell [21]. The rms profile was examined from both ends for the point at which the value of the next point was larger by a factor of k. The result was checked visually, against both the rms and the mean profiles. If the edges did not appear reasonable, k was adjusted. Some wakes, such as the one seen in Figure A-1, were easy to identify. Others, especially those with trailing edge blowing, proved more difficult to identify (see Figure A-2). In such cases, the best judgement of the author was used to determine the edges of the wake.

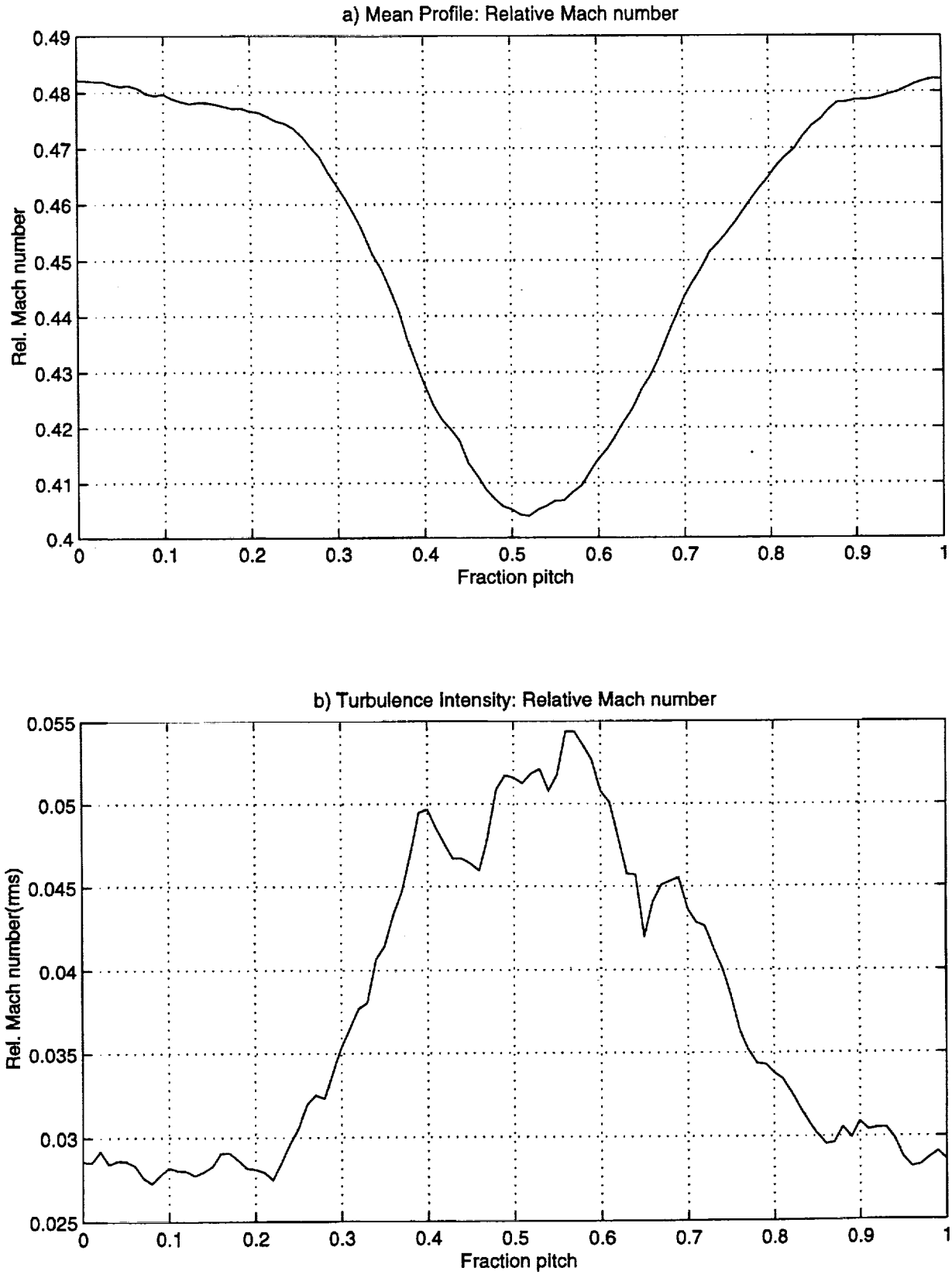

Figure A-1: Example of wake that is easy to identify

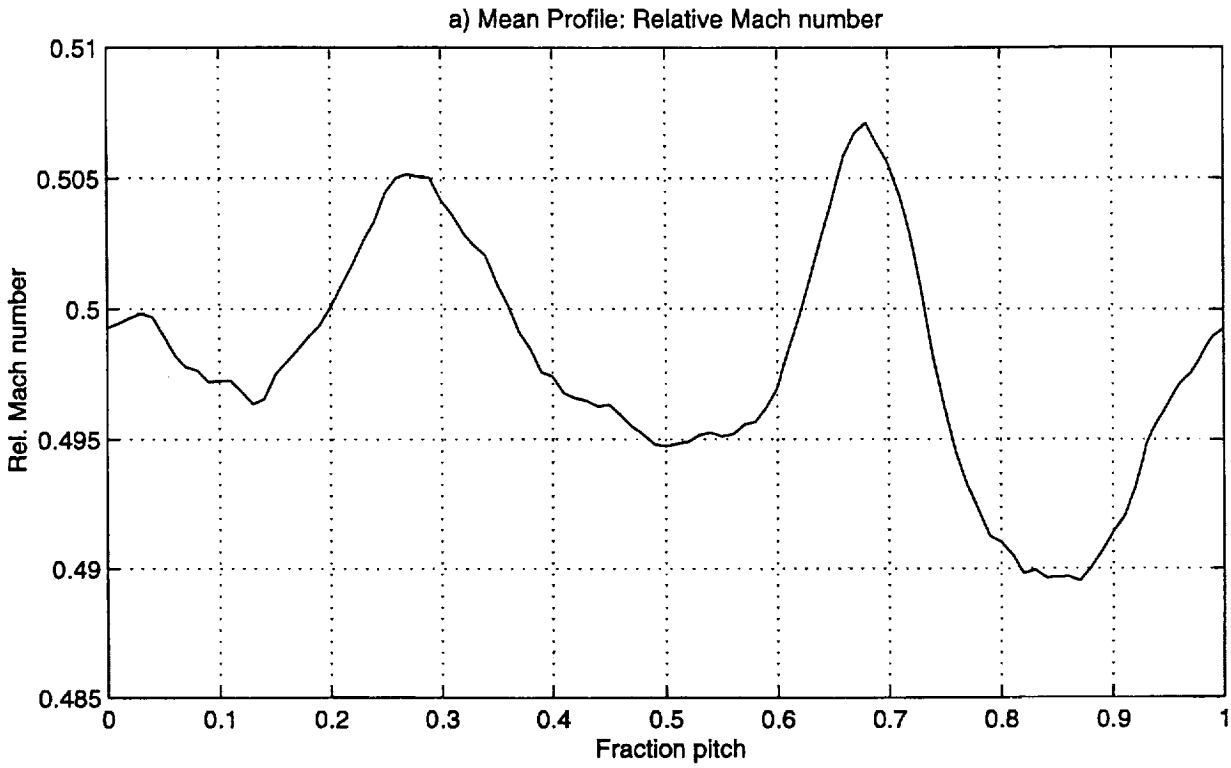

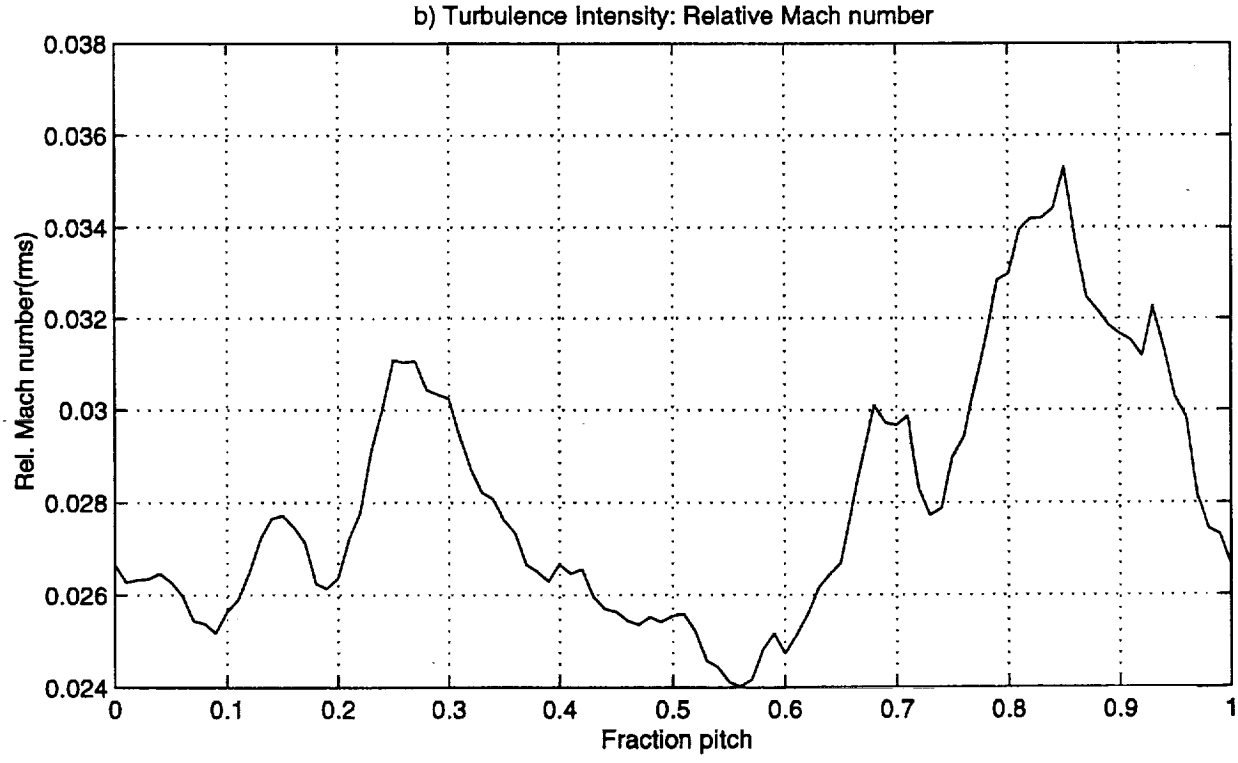

Figure A-2: Example of wake that is hard to identify

Appendix B

Four-way Probe Measurements

The flow field varaibles that are not presented in Chapter 4 are presented here. These include the components of Mach number, the flow angles, and the pressures. As in Chapter 4 the data presented consists of the an ensemble average of one or two runs with 96 blade passing periods. Data is shown along with 95

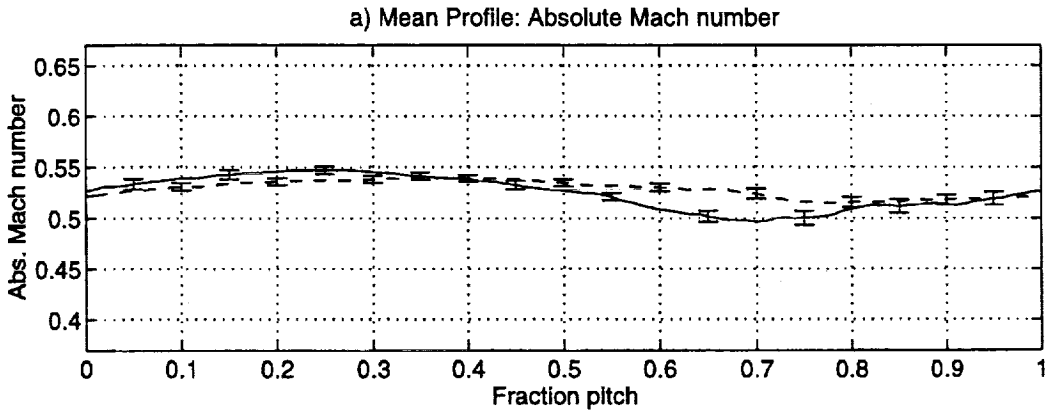

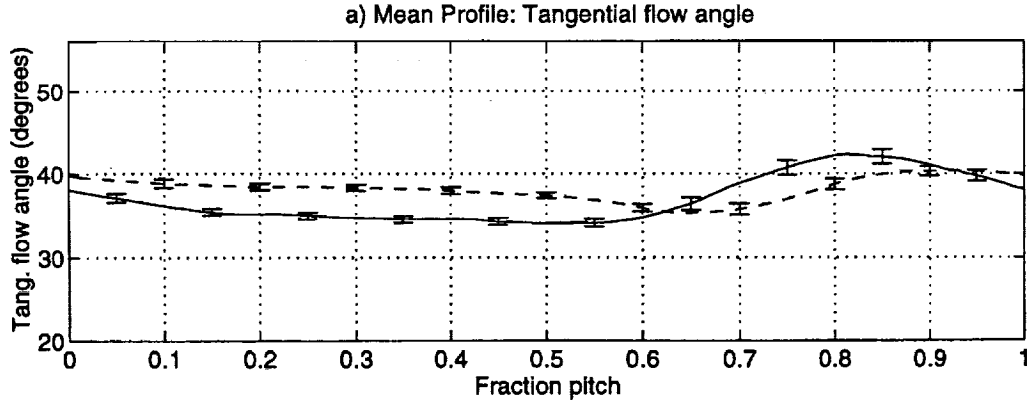

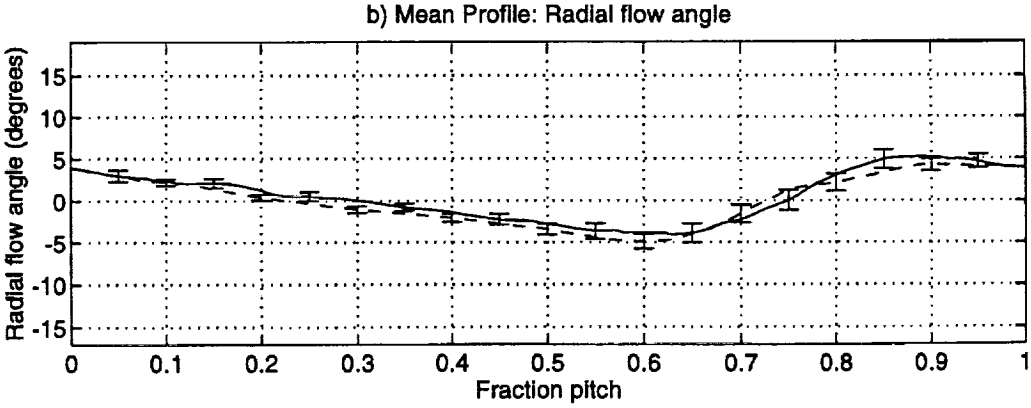

Figure B-1: Absolute Mach number and flow angles at 1.5c, 25% span. (—)w/o blowing, (- -)w/ blowing

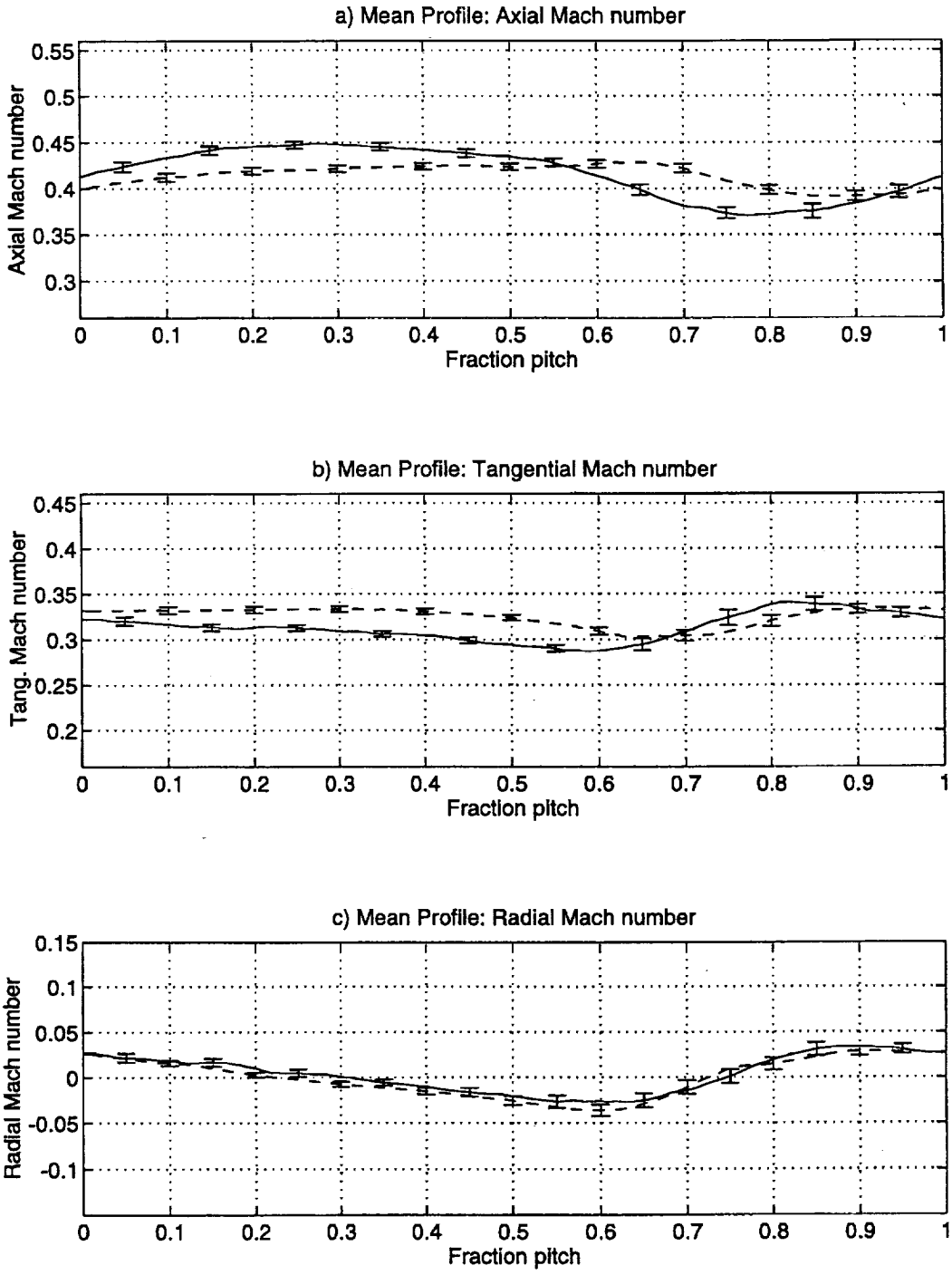

Figure B-2: Components of Mach number at 1.5c, 25% span. (—)w/o blowing, (- -)w/ blowing

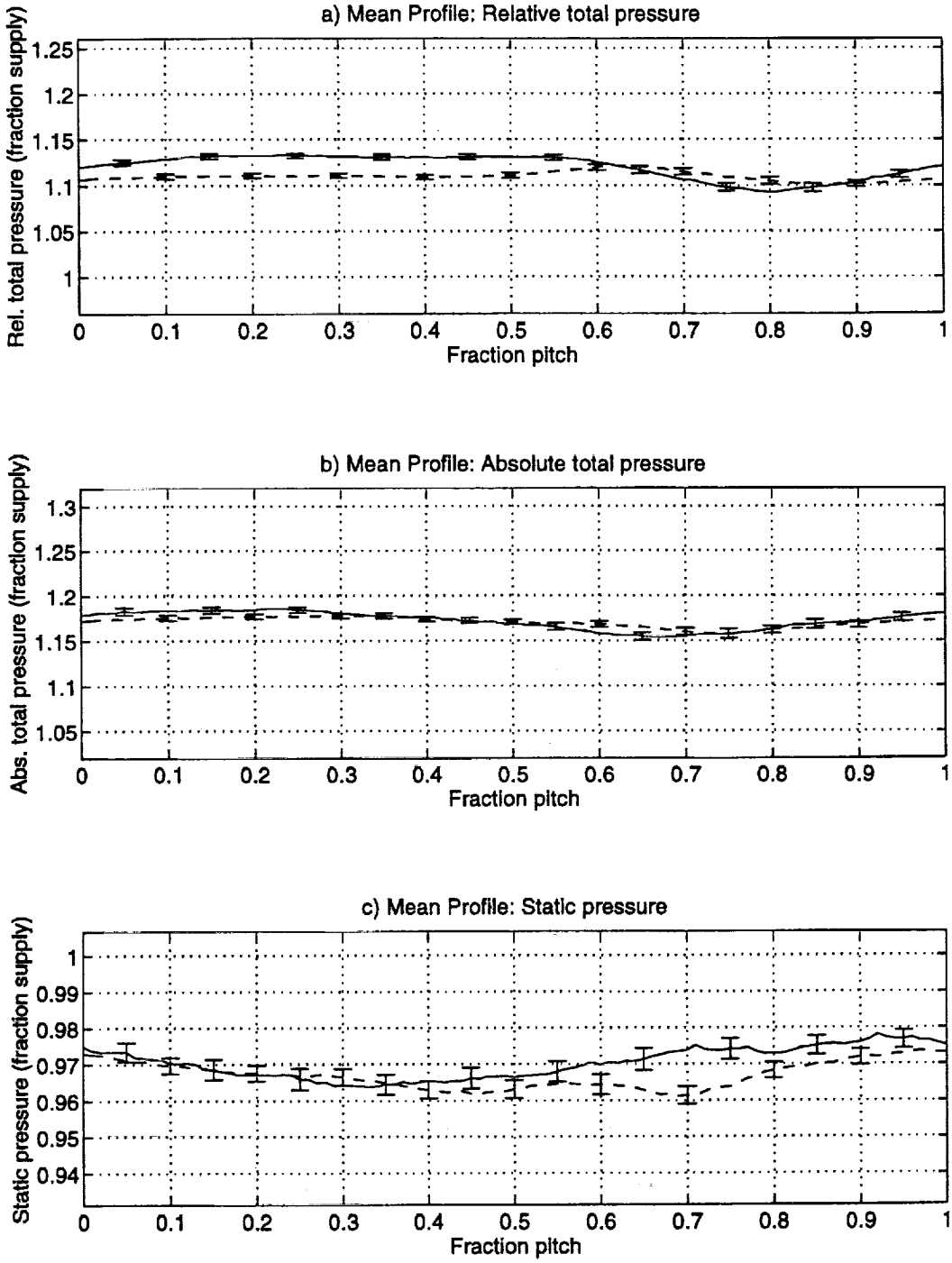

Figure B-3: Pressures at 1.5c, 25% span. (—)w/o blowing, (- -)w/ blowing

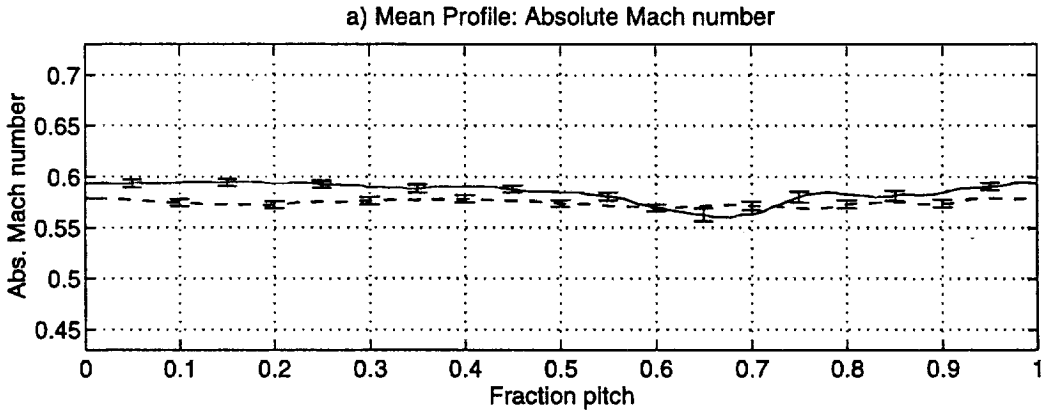

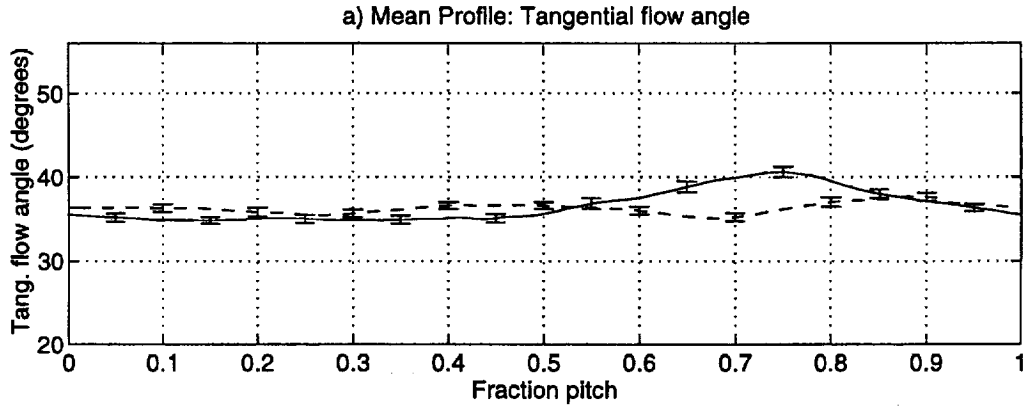

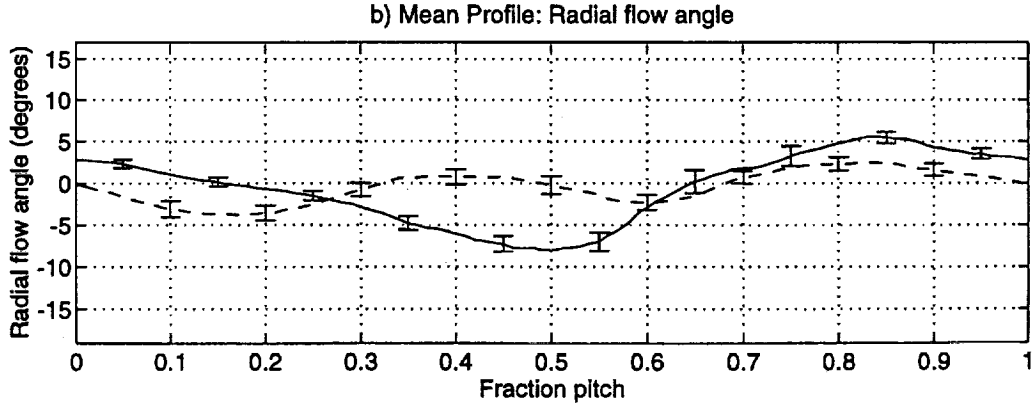

Figure B-4: Absolute Mach number and flow angles at 1.5c, 37.5% span. (—)w/o blowing, (- -)w/ blowing

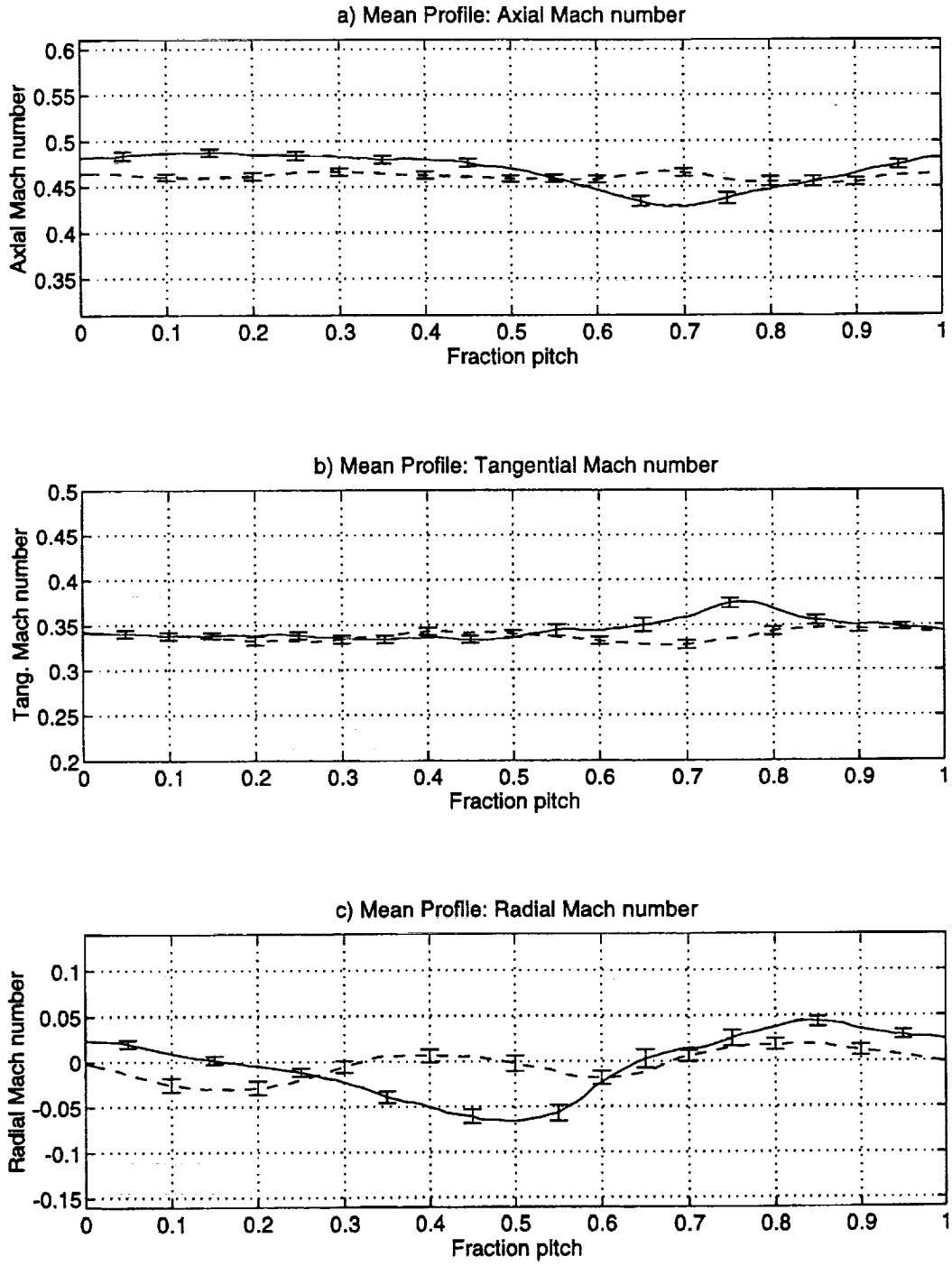

Figure B-5: Components of Mach number at 1.5c, 37.5% span. (—)w/o blowing, (- -)w/ blowing

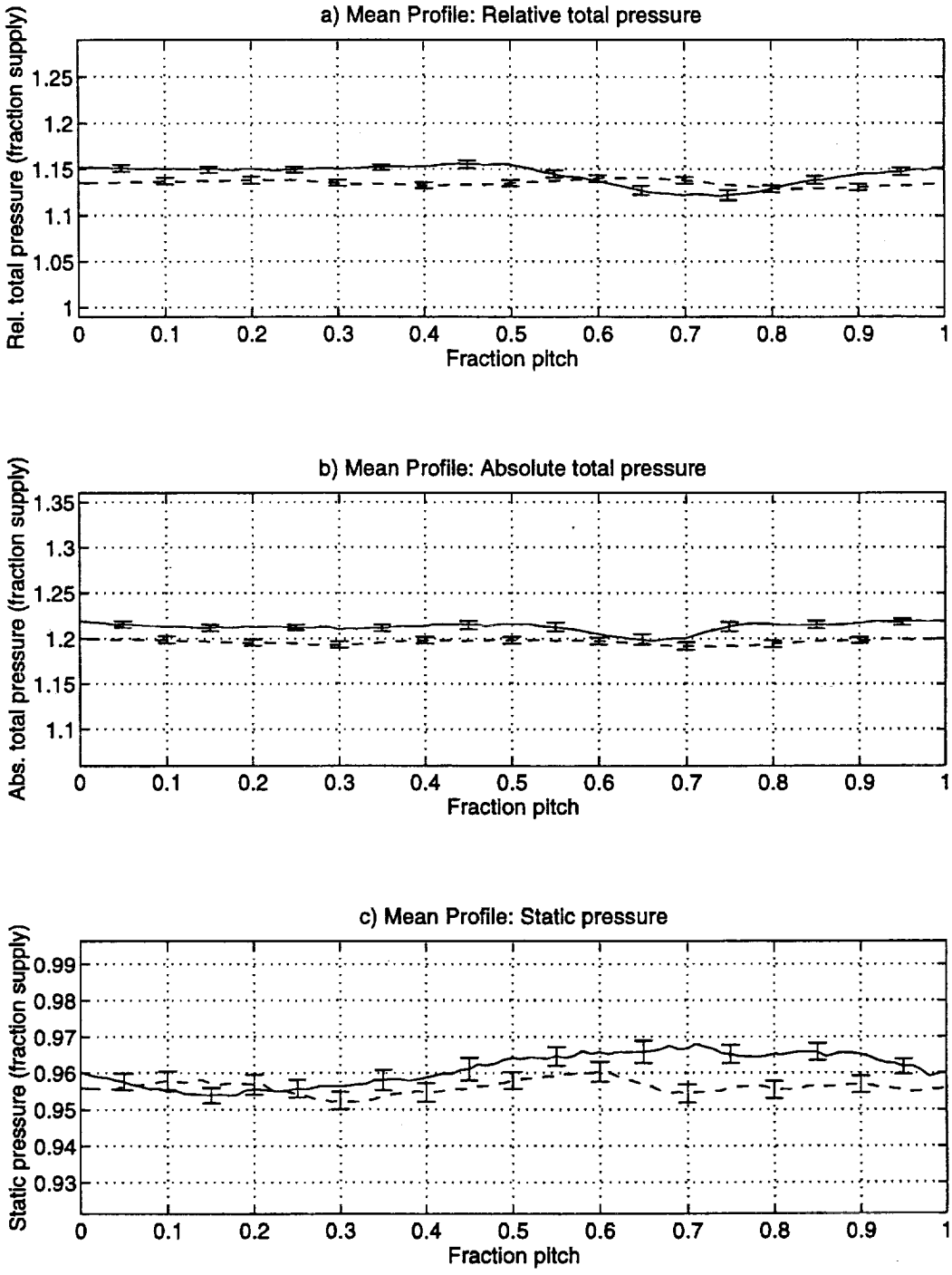

Figure B-6: Pressures at 1.5c, 37.5% span. (—)w/o blowing, (- -)w/ blowing

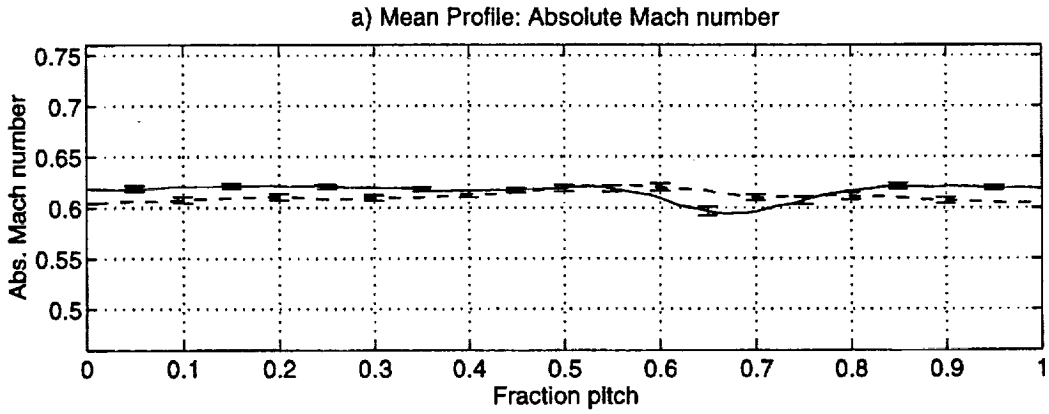

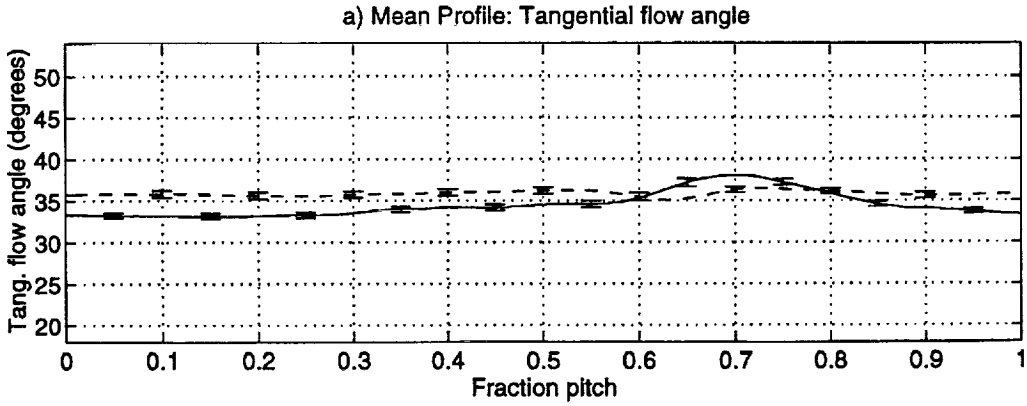

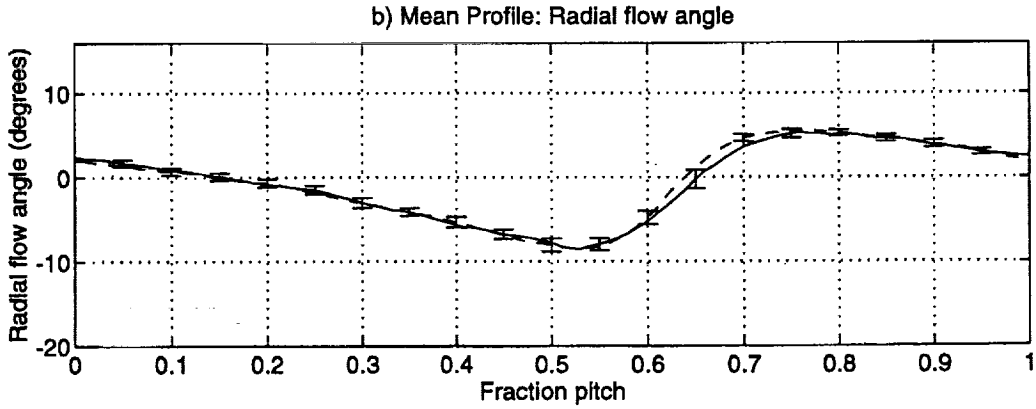

Figure B-7: Absolute Mach number and flow angles at 1.5c, 50% span. (—)w/o blowing, (- -)w/ blowing

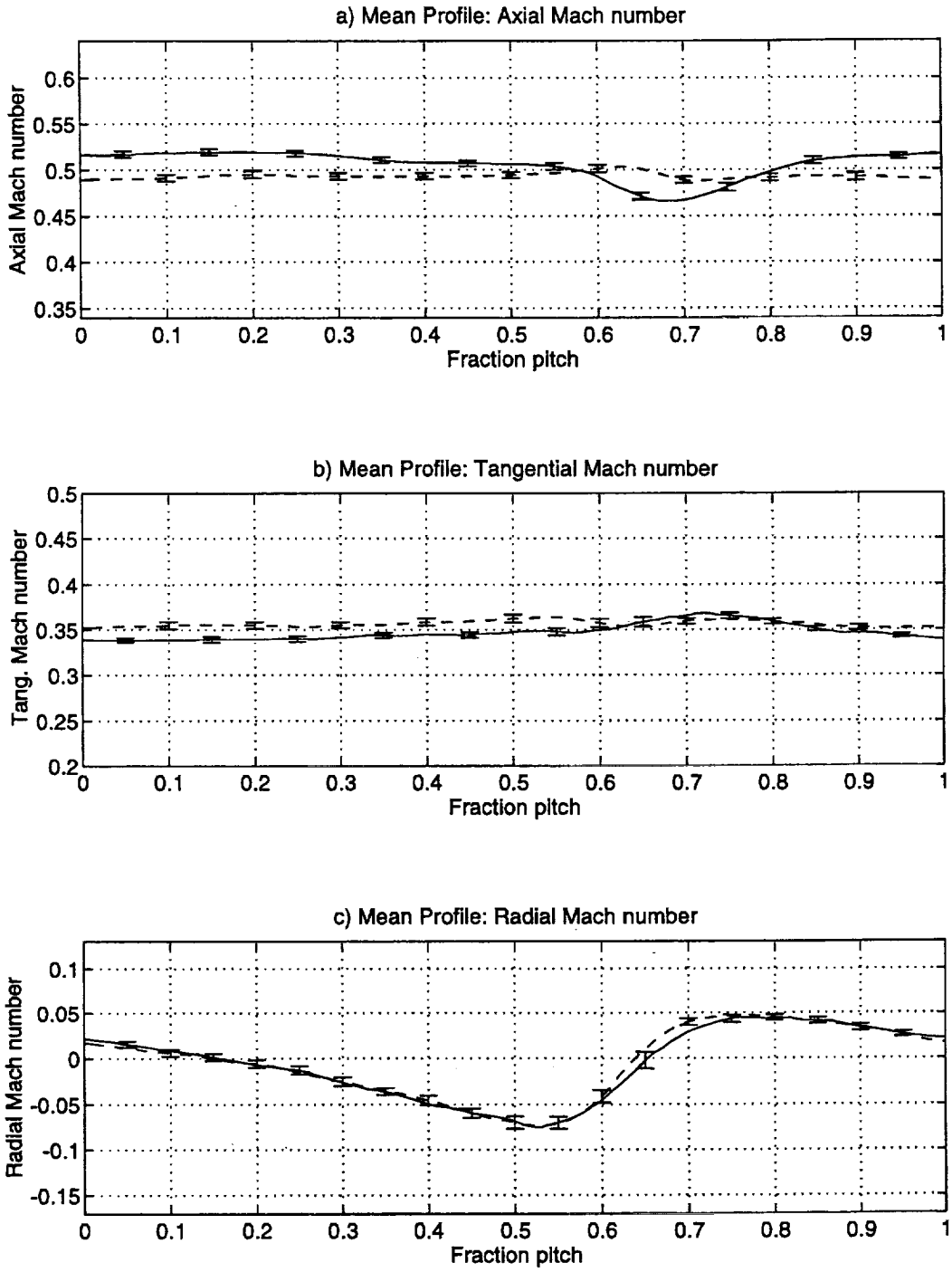

Figure B-8: Components of Mach number at 1.5c, 50% span. (—)w/o blowing, (- -)w/ blowing

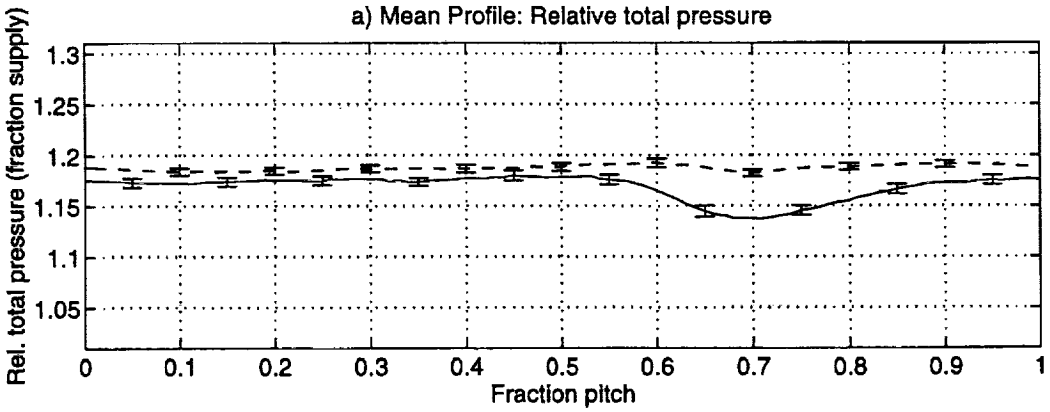

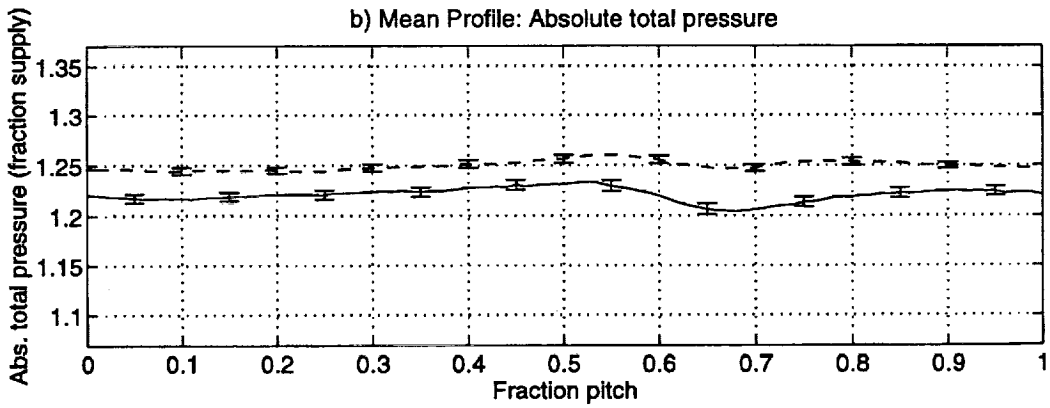

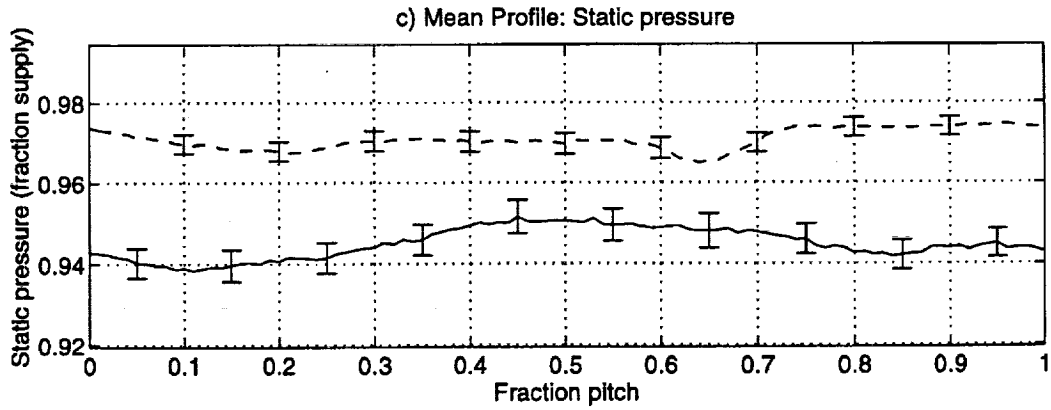

Figure B-9: Pressures at 1.5c, 50% span. (—)w/o blowing, (- -)w/ blowing

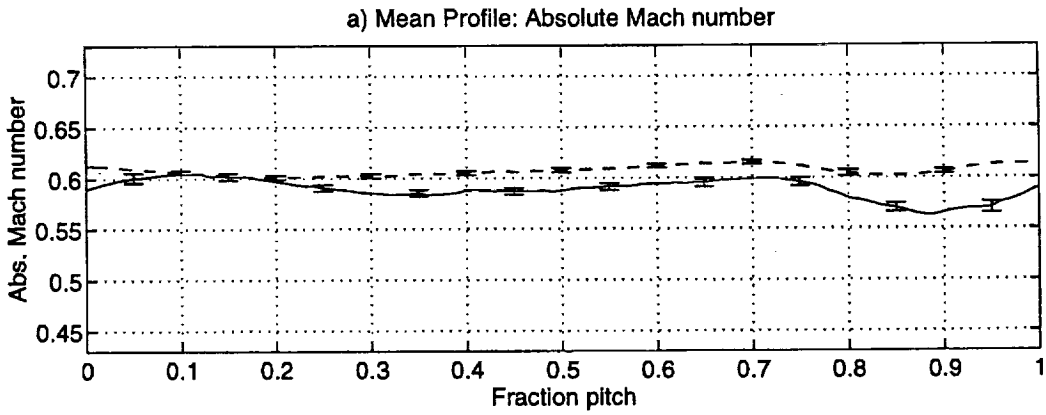

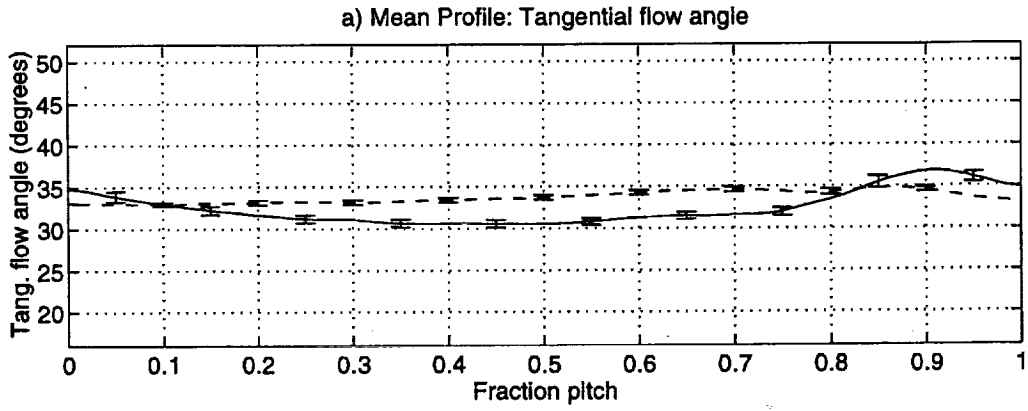

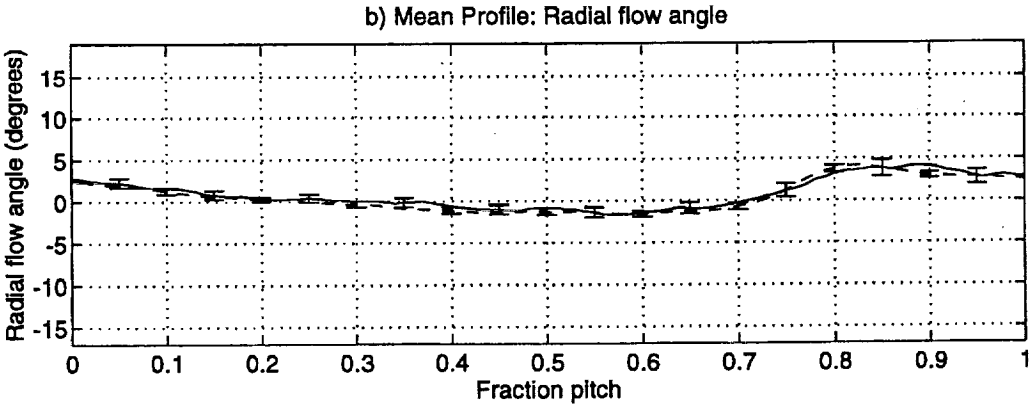

Figure B-10: Absolute Mach number and flow angles at 1.5c, 75% span. (—)w/o blowing, (- -)w/ blowing

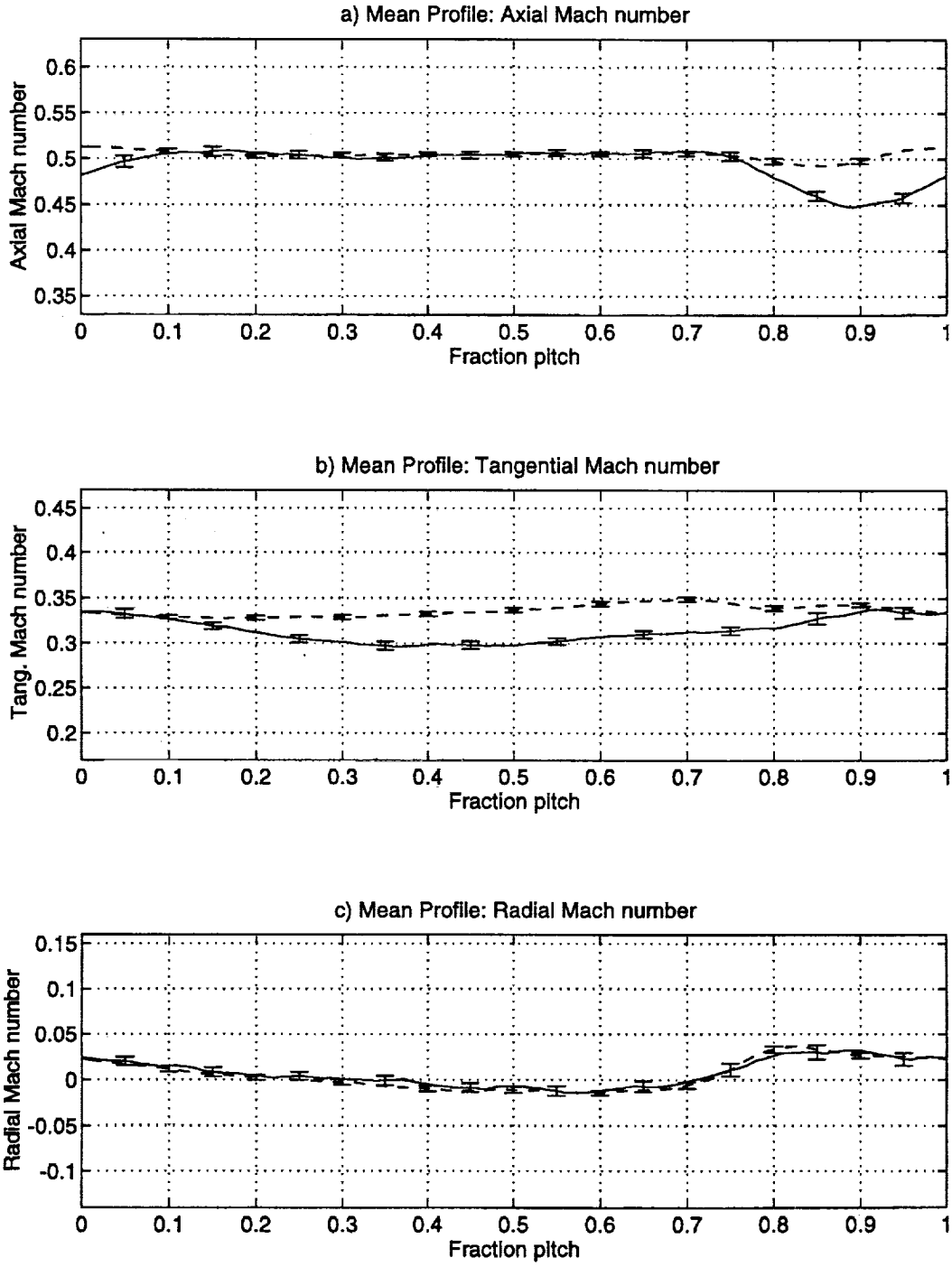

Figure B-11: Components of Mach number at 1.5c, 75% span. (—)w/o blowing, (- -)w/ blowing

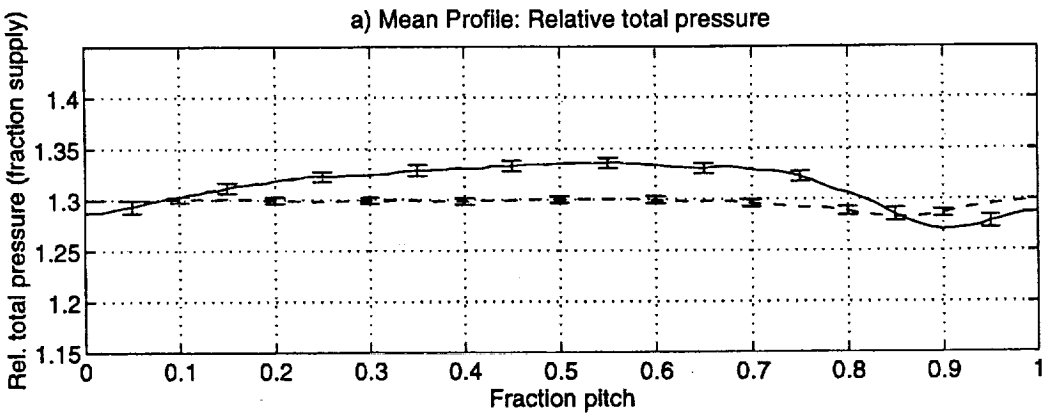

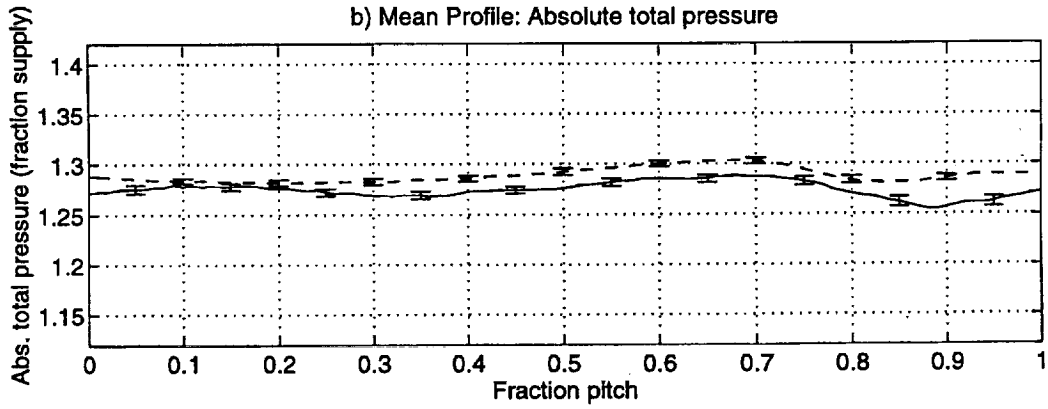

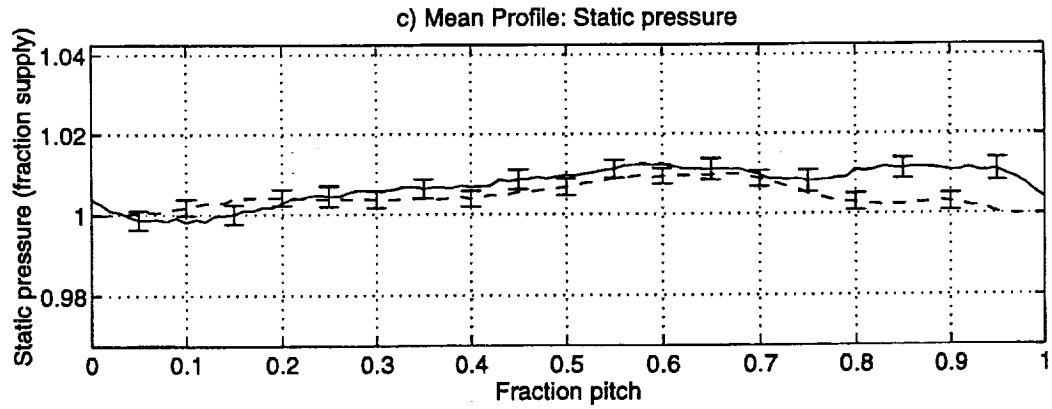

Figure B-12: Pressures at 1.5c, 75% span. (—)w/o blowing, (- -)w/ blowing

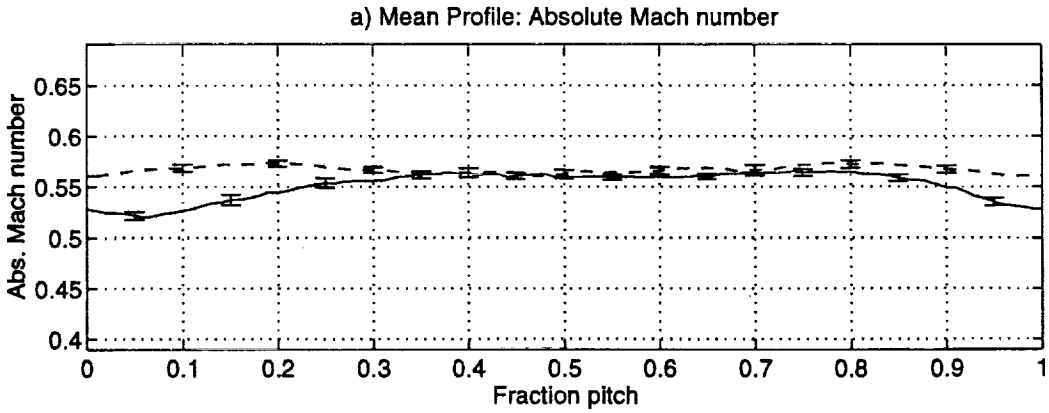

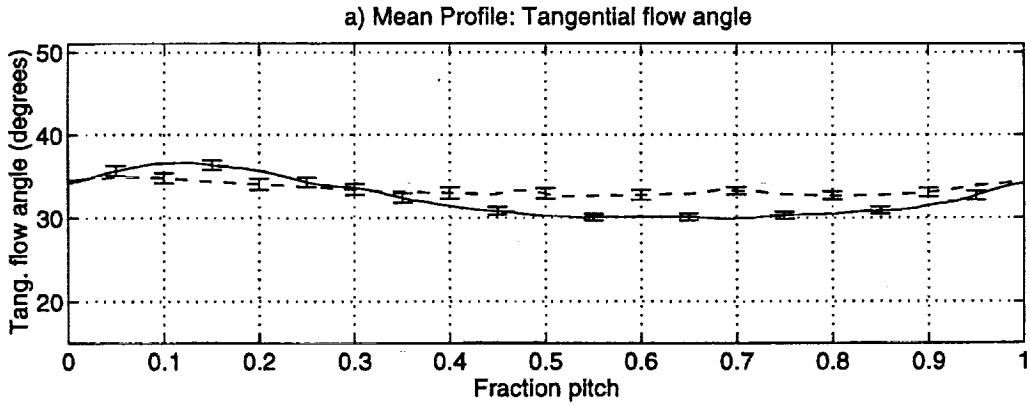

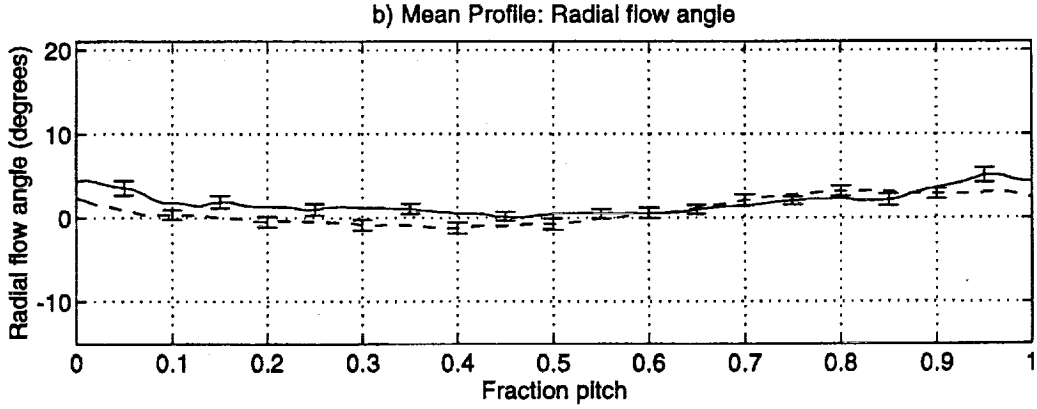

Figure B-13: Absolute Mach number and flow angles at 1.5c, 87.5% span. (—)w/o blowing, (- -)w/ blowing

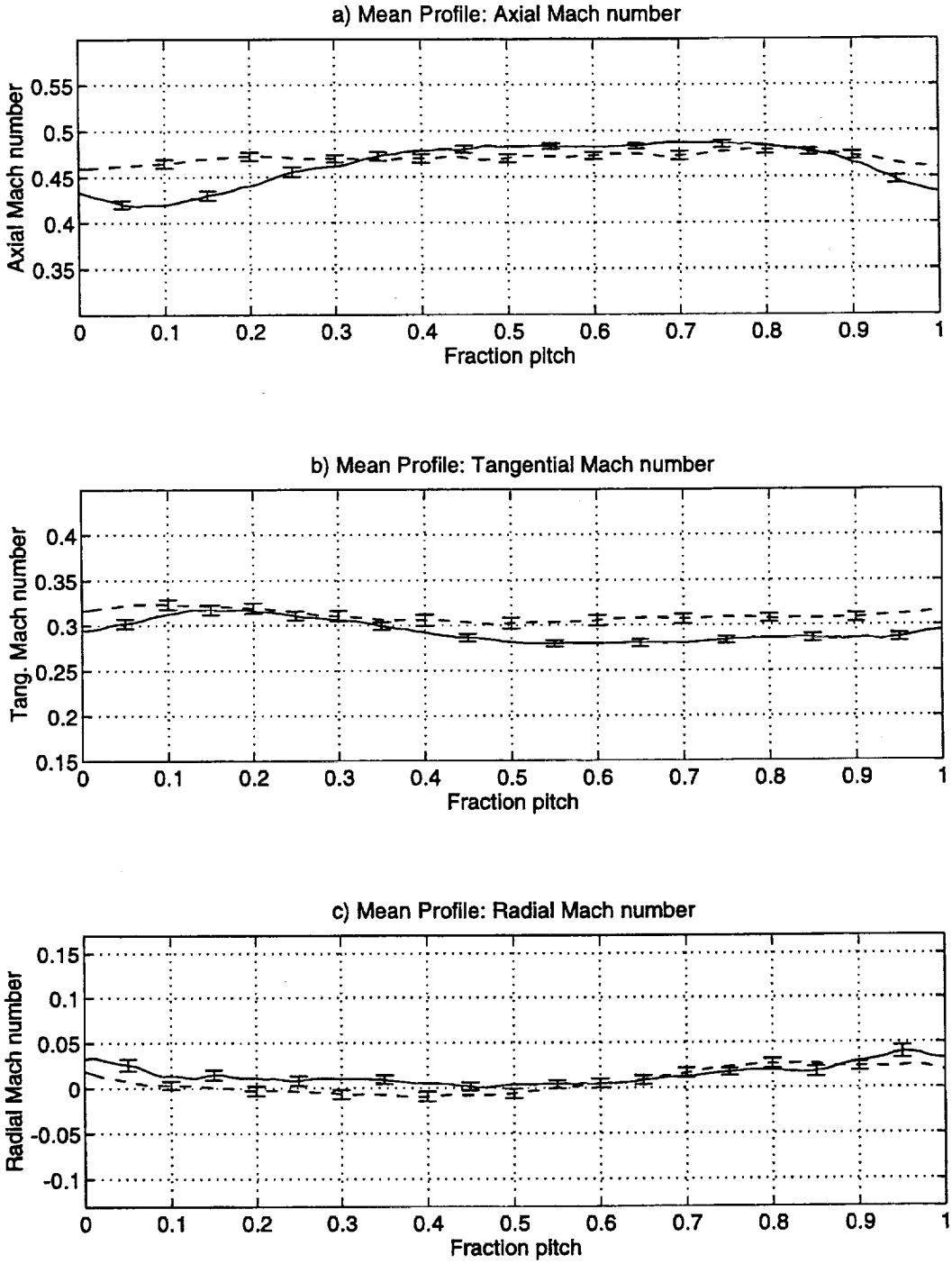

Figure B-14: Components of Mach number at 1.5c, 87.5% span. (—)w/o blowing, (- -)w/ blowing

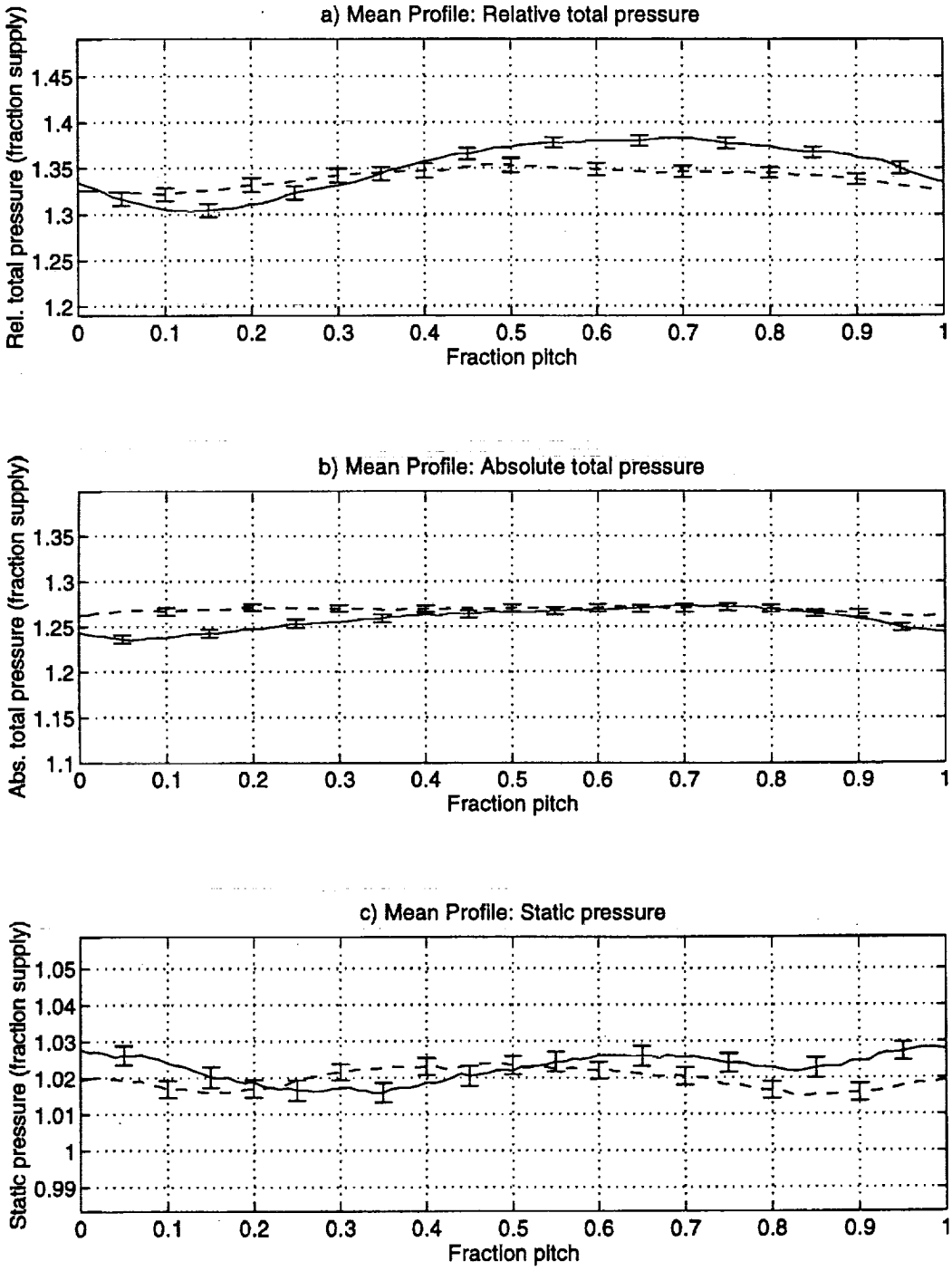

Figure B-15: Pressures at 1.5c, 87.5% span. (—)w/o blowing, (- -)w/ blowing

Appendix C

Instrumented Stator Measurements

The harmonic amplitudes and phases of the stator pressure side and suction side are presented here. All data presented consists of an ensemble average as detailed in Chapter 5 and is plotted along with 95% confidence intervals. The no blowing data is shown by solid lines while the blowing data is represented by dashed lines.

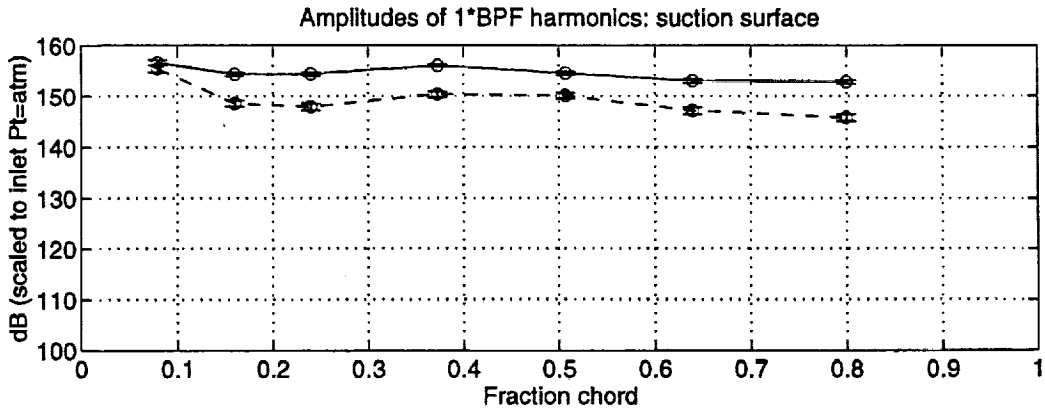

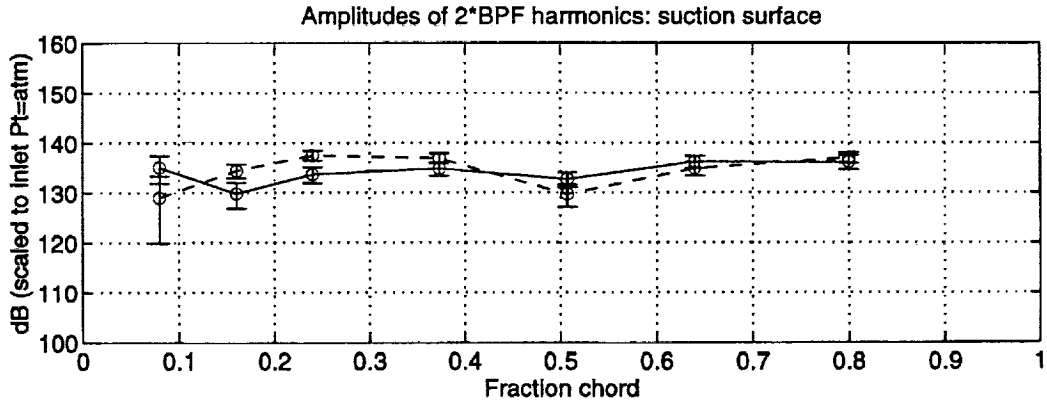

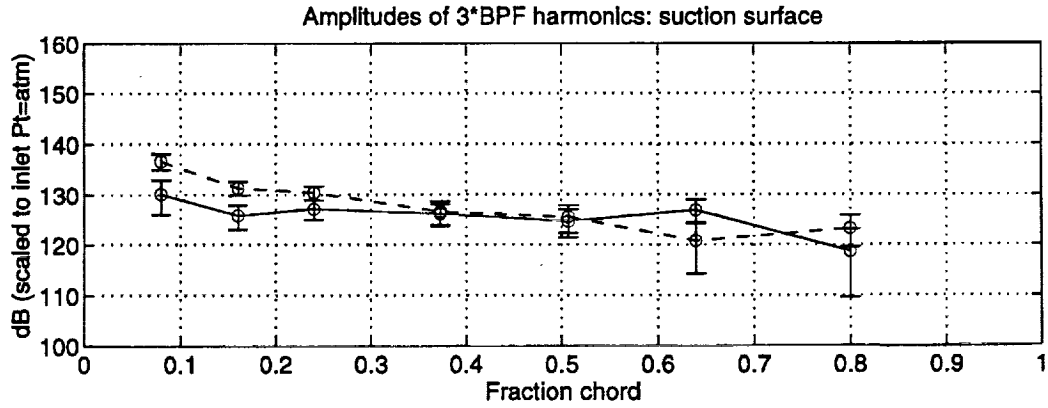

Figure C-1: Harmonic amplitudes of stator suction surface at 25% span. (—)w/o blowing, (- -)w/ blowing

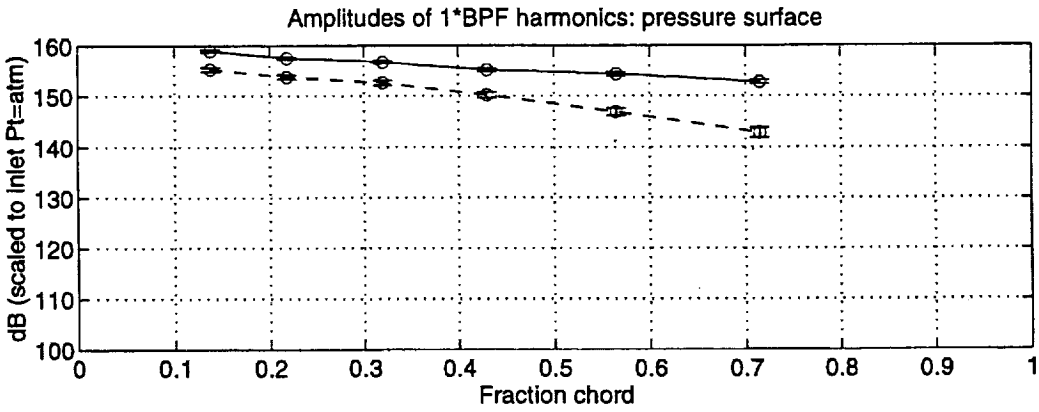

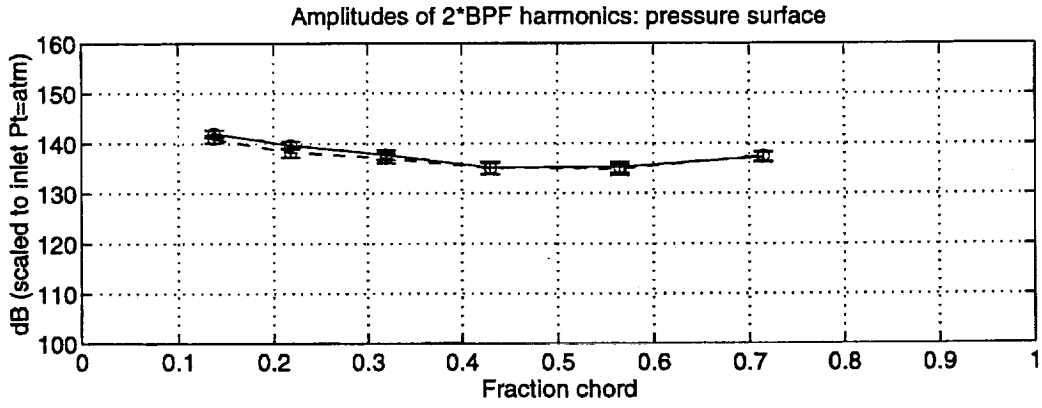

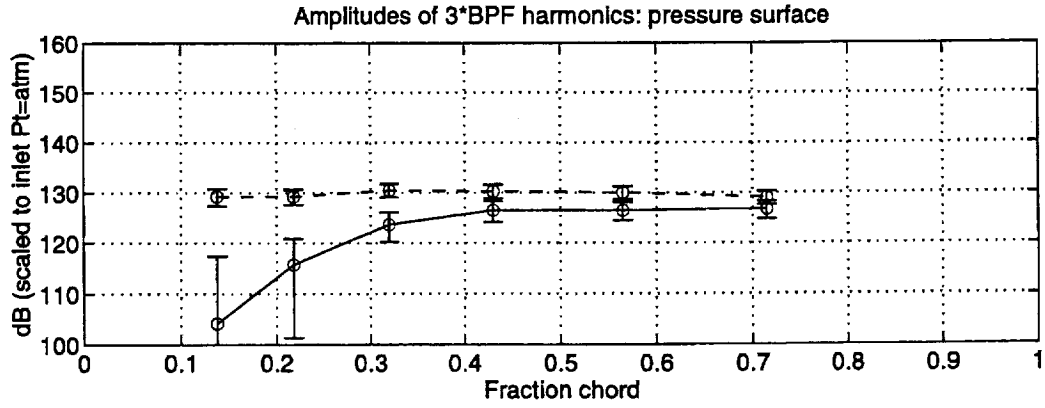

Figure C-2: Harmonic amplitudes of stator pressure surface at 25% span. (—)w/o blowing, (- -)w/ blowing

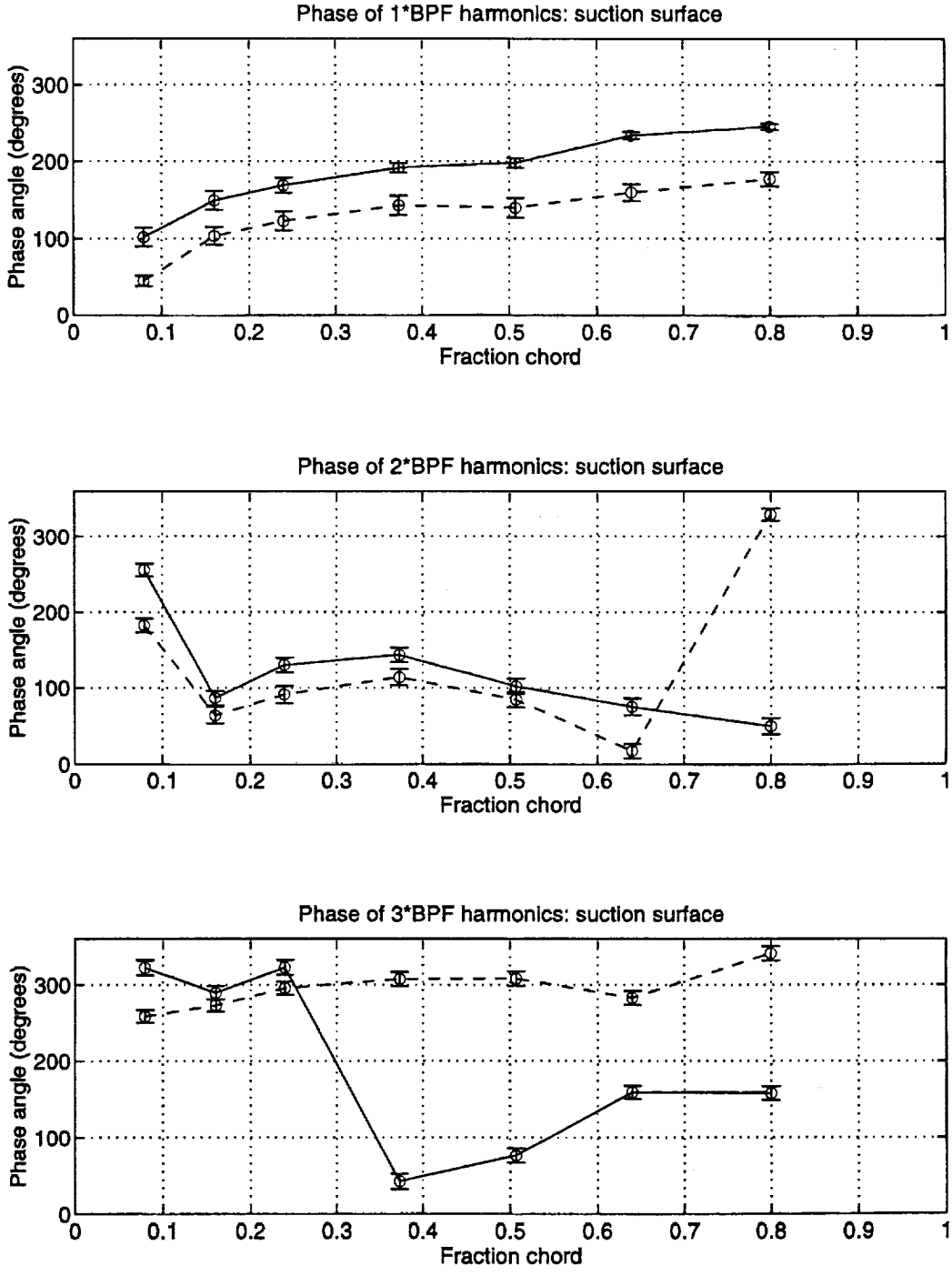

Figure C-3: Harmonic phases of stator suction surface at 25% span. (—)w/o blowing, (- -)w/ blowing

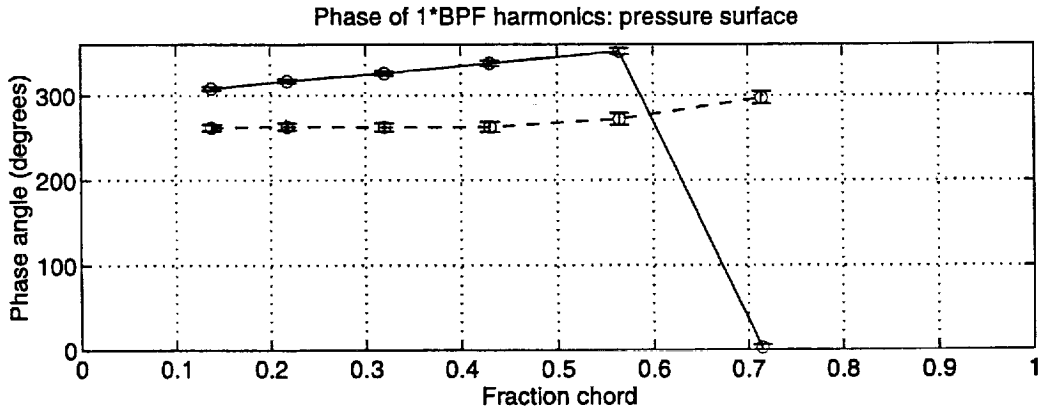

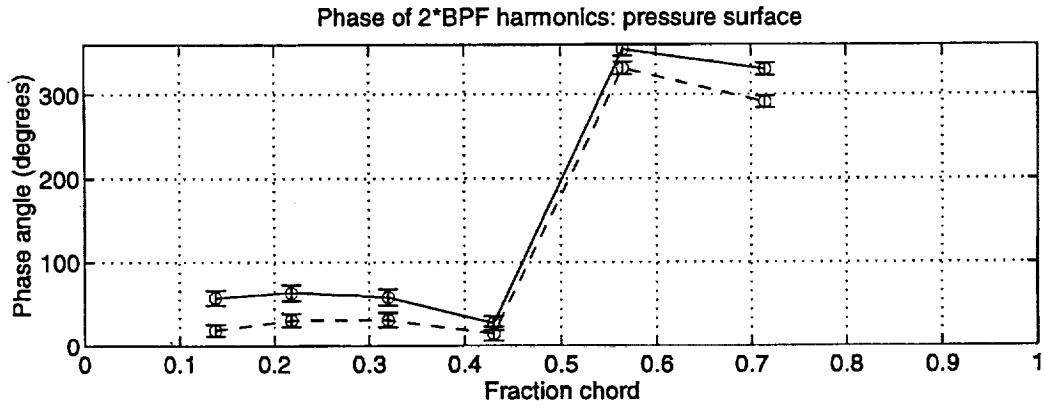

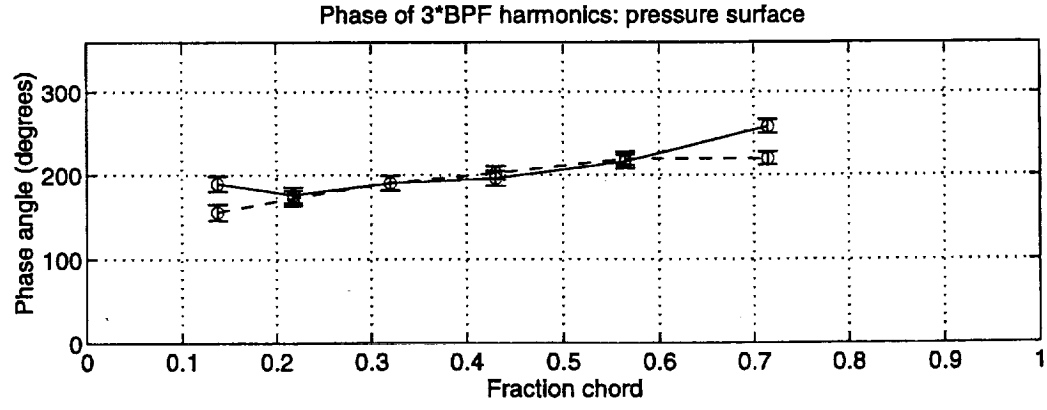

Figure C-4: Harmonic phases of stator pressure surface at 25% span. (—)w/o blowing, (- -)w/ blowing

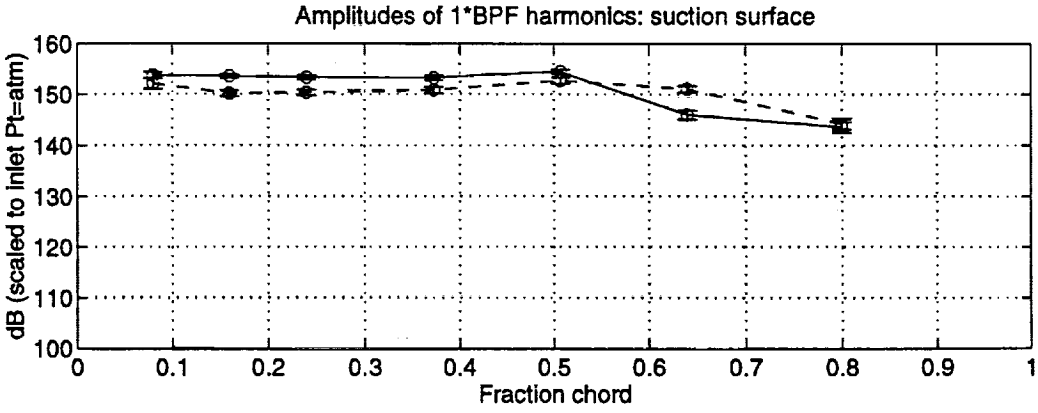

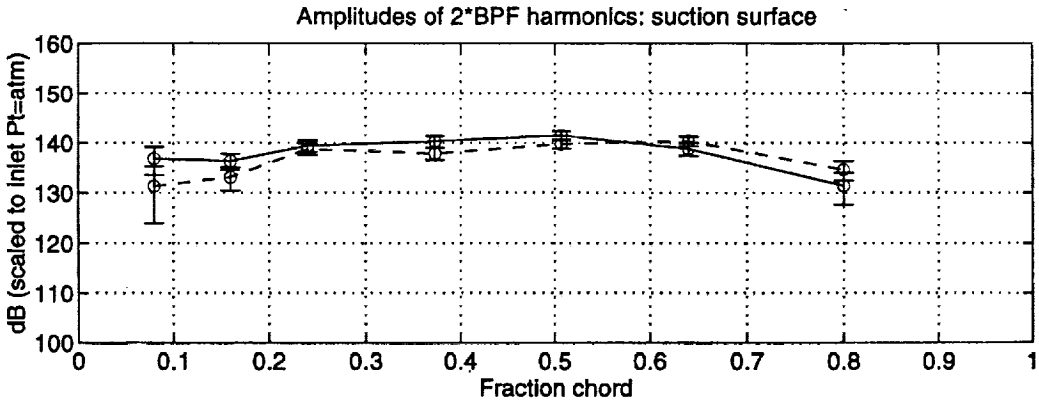

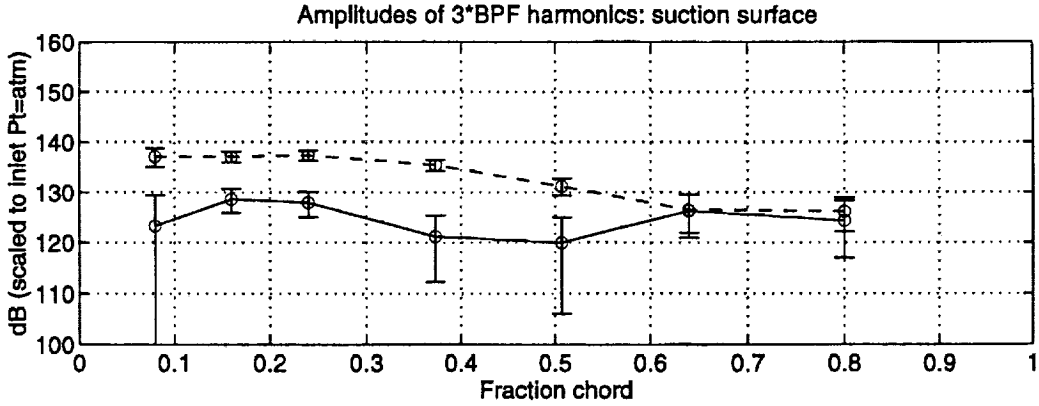

Figure C-5: Harmonic amplitudes of stator suction surface at 37.5% span. (—)w/o blowing, (- -)w/ blowing

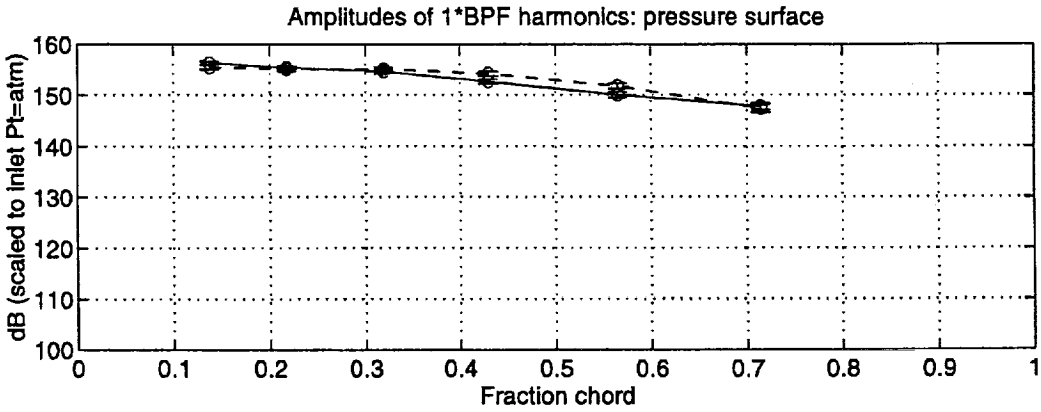

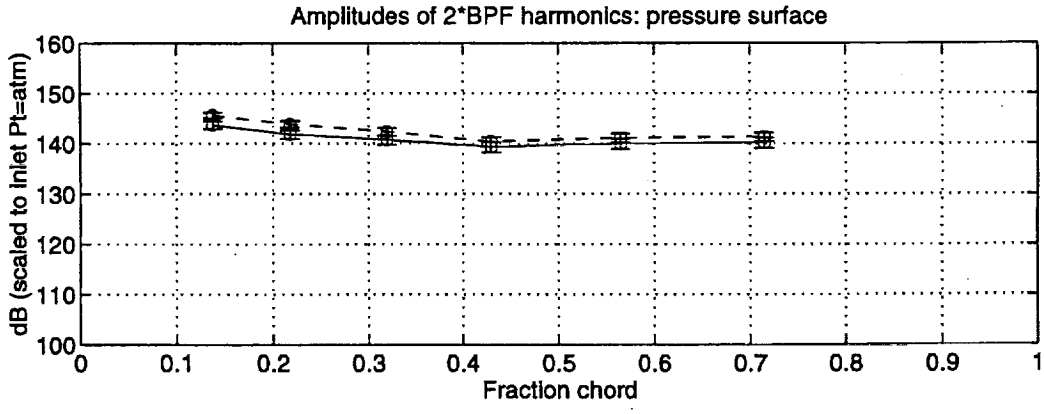

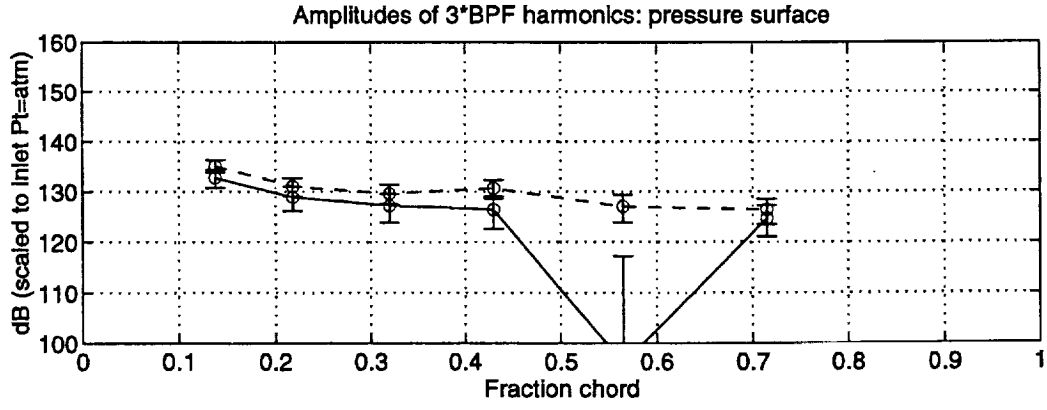

Figure C-6: Harmonic amplitudes of stator pressure surface at 37.5% span. (—)w/o blowing, (- -)w/ blowing

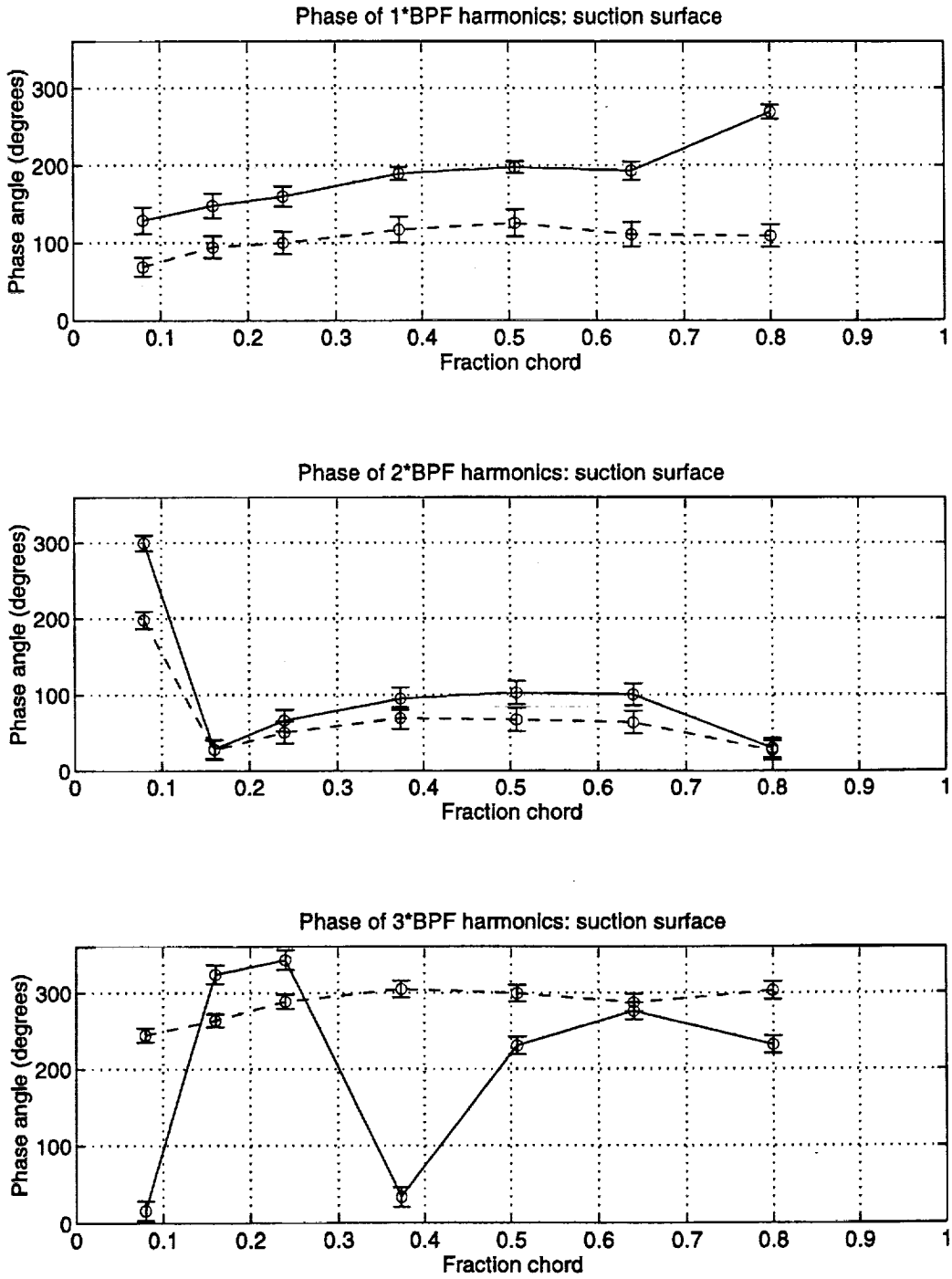

Figure C-7: Harmonic phases of stator suction surface at 37.5% span. (—)w/o blowing, (- -)w/ blowing

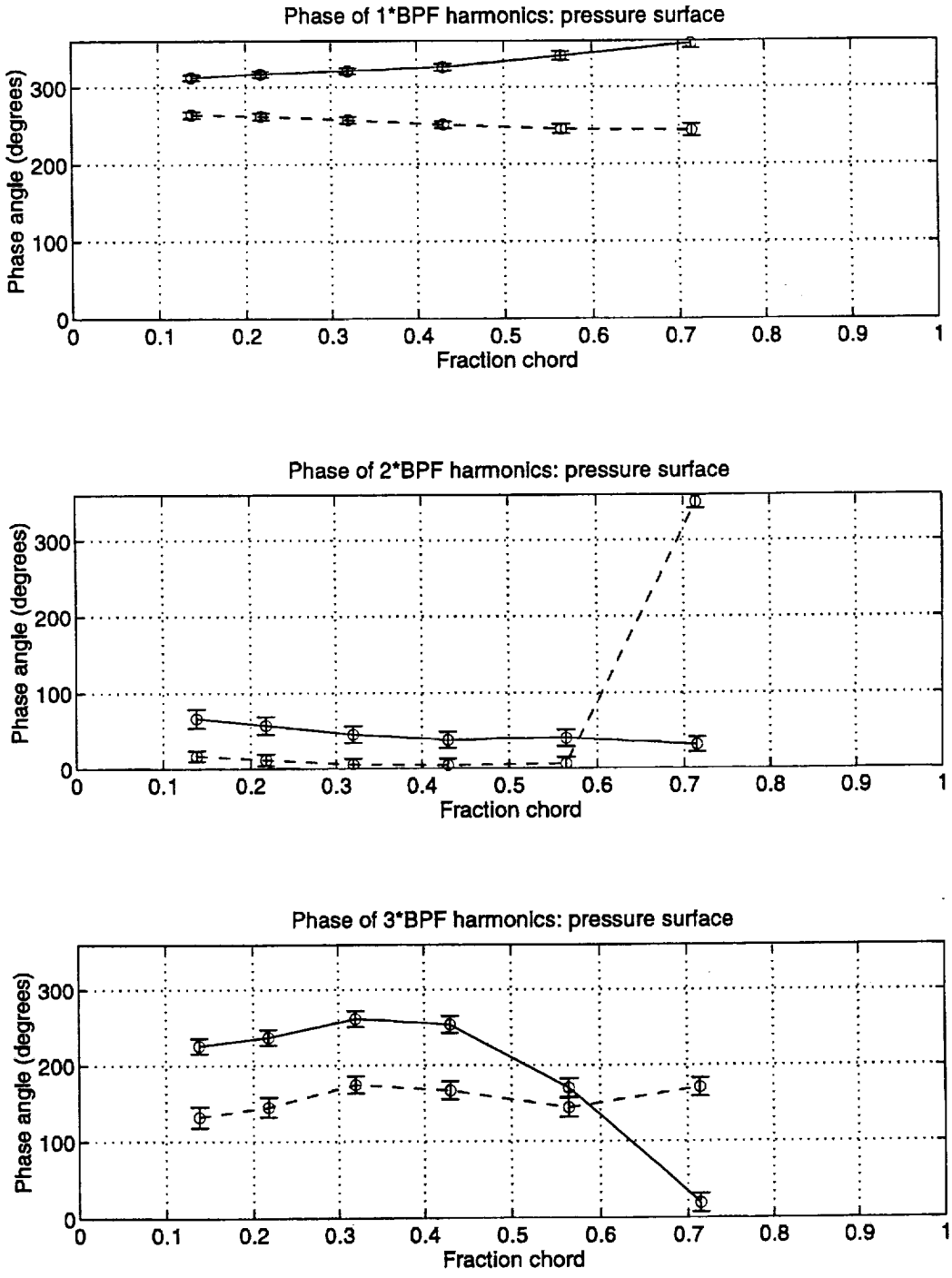

Figure C-8: Harmonic phases of stator pressure surface at 37.5% span. (—)w/o blowing, (- -)w/ blowing

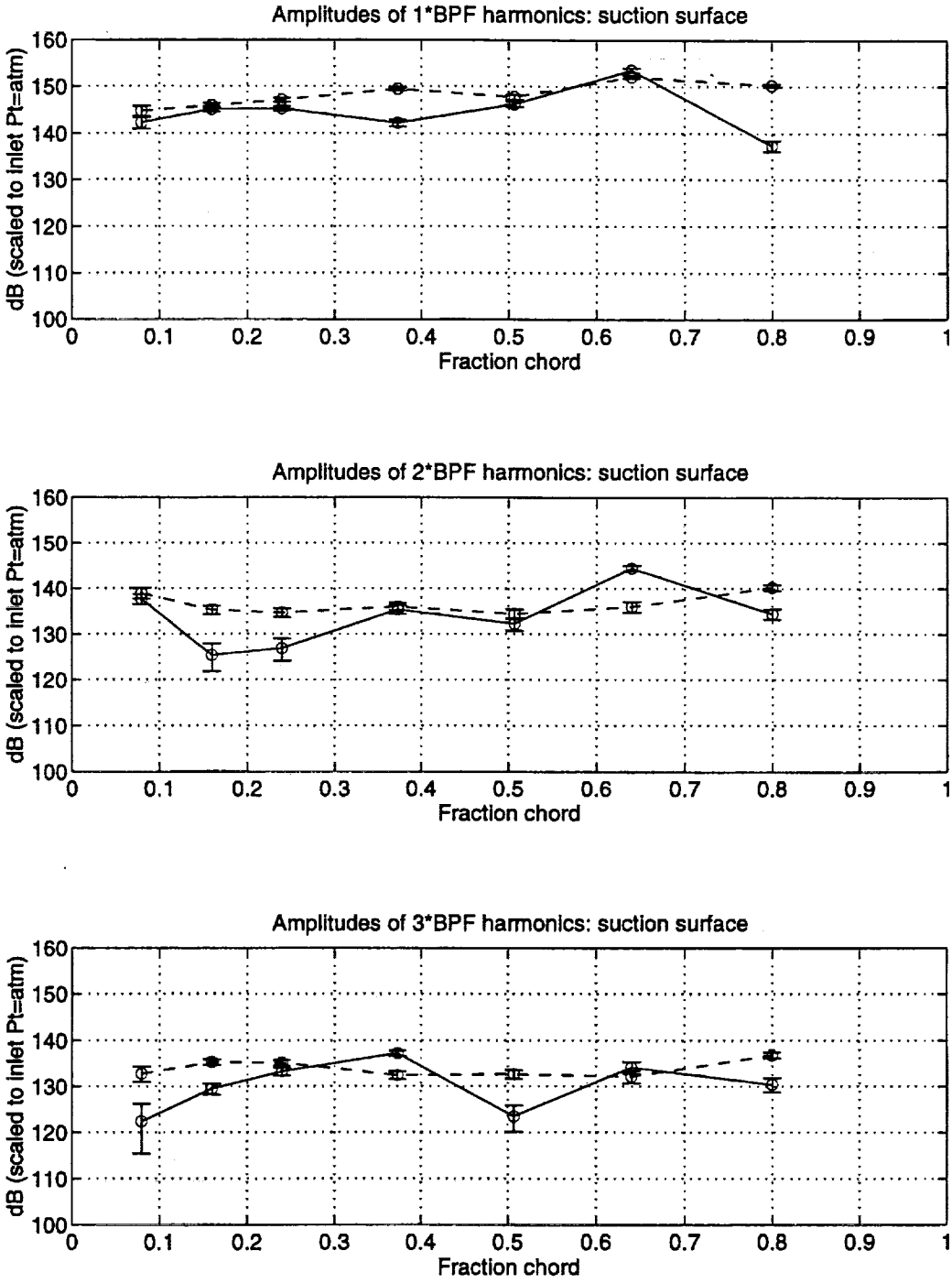

Figure C-9: Harmonic amplitudes of stator suction surface at 50% span. (—)w/o blowing, (- -)w/ blowing

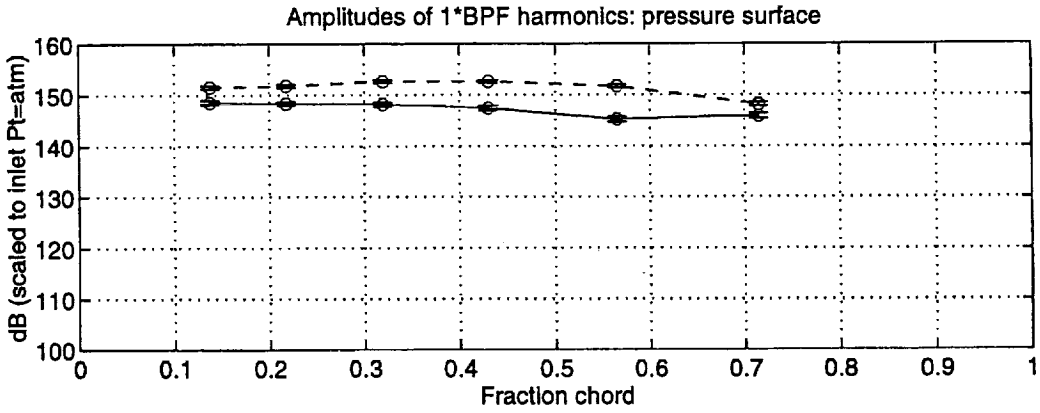

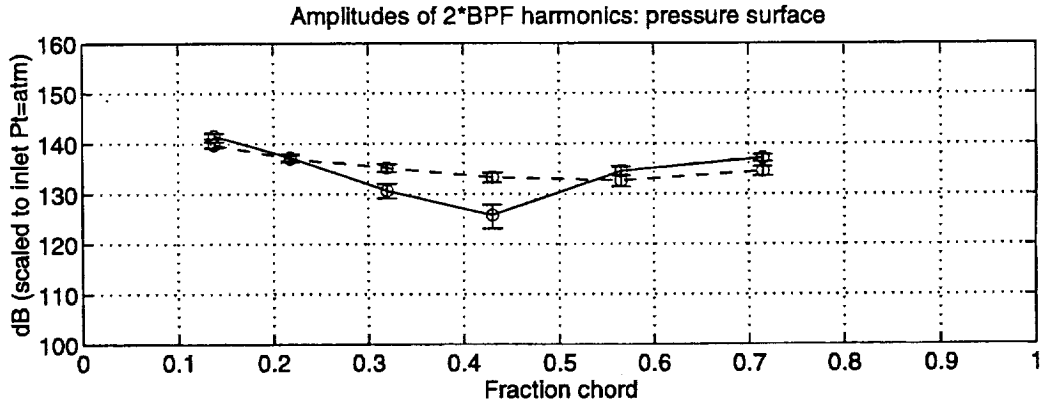

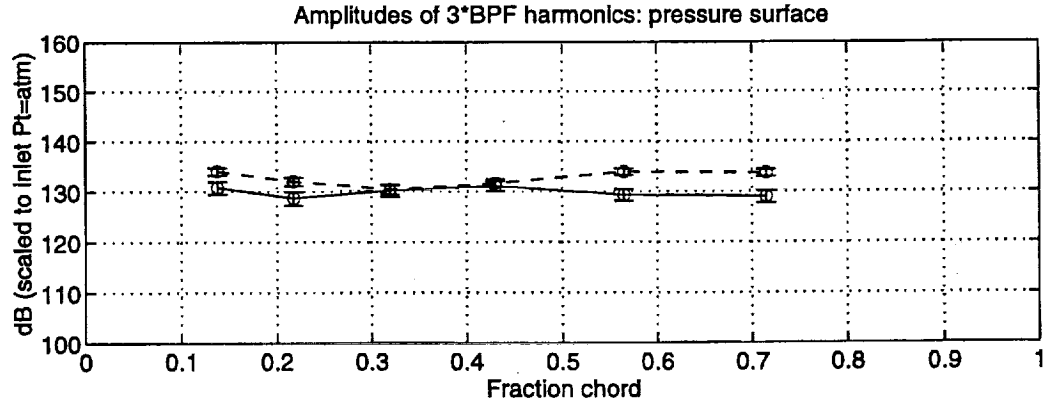

Figure C-10: Harmonic amplitudes of stator pressure surface at 50% span. (—)w/o blowing, (- -)w/ blowing

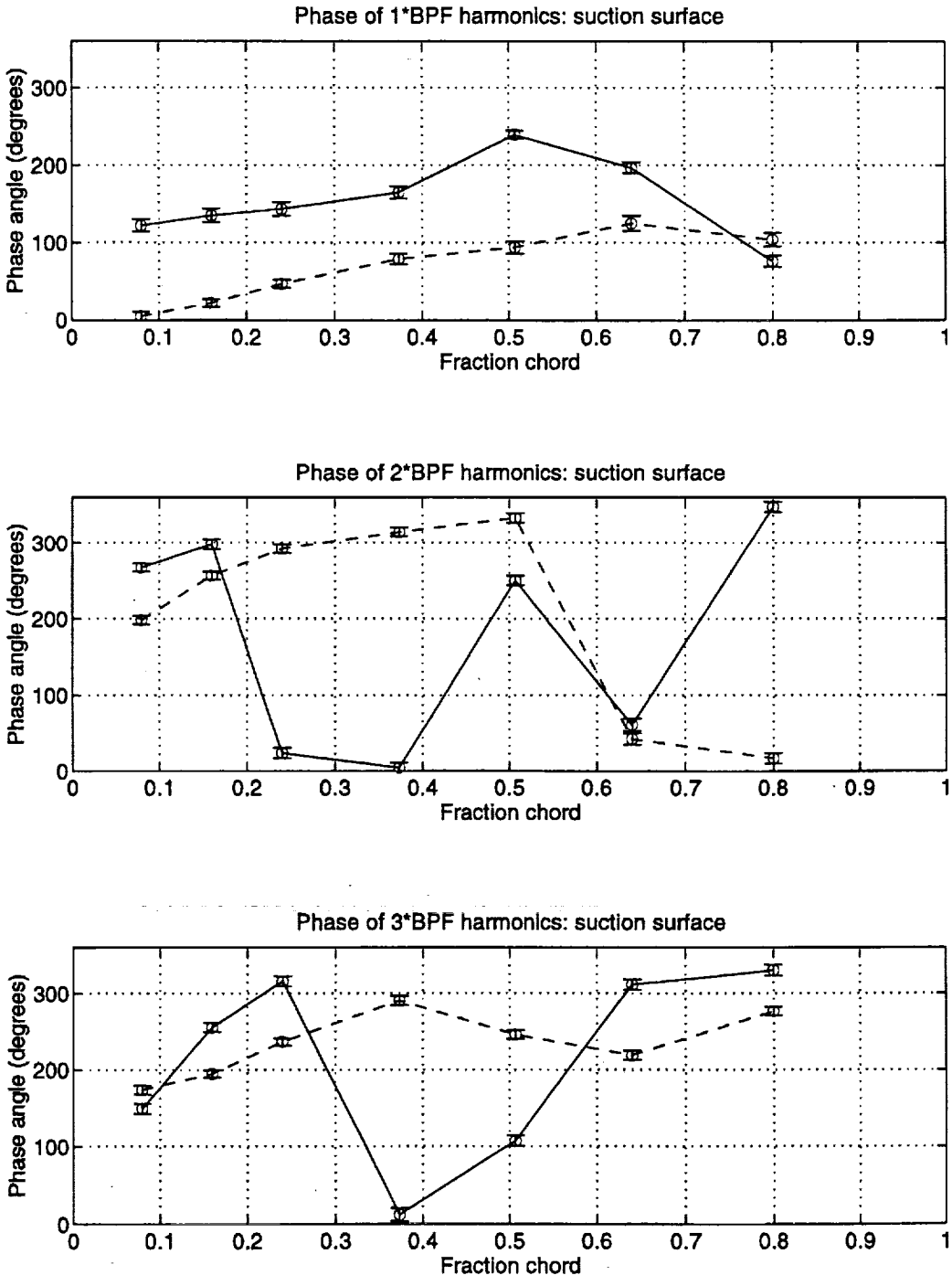

Figure C-11: Harmonic phases of stator suction surface at 50% span. (—)w/o blowing, (- -)w/ blowing

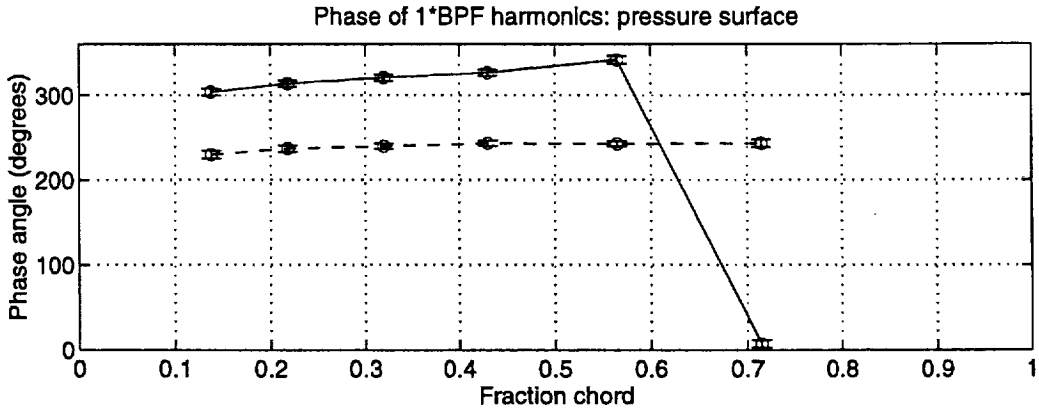

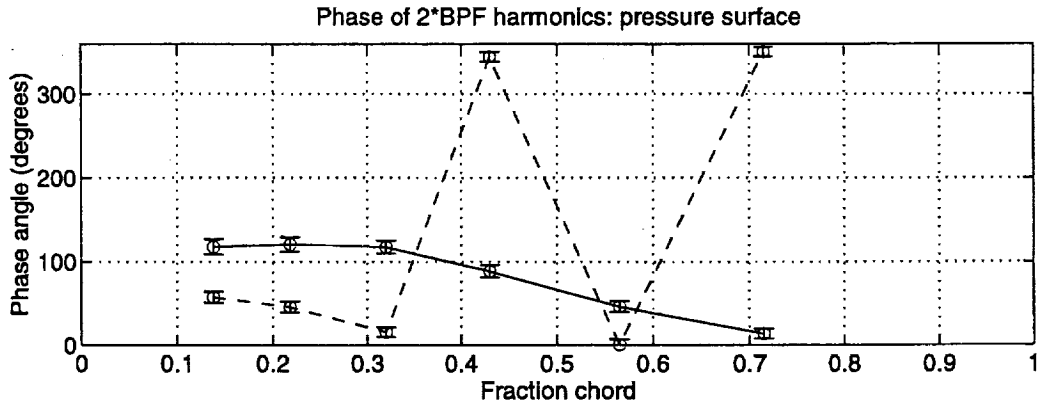

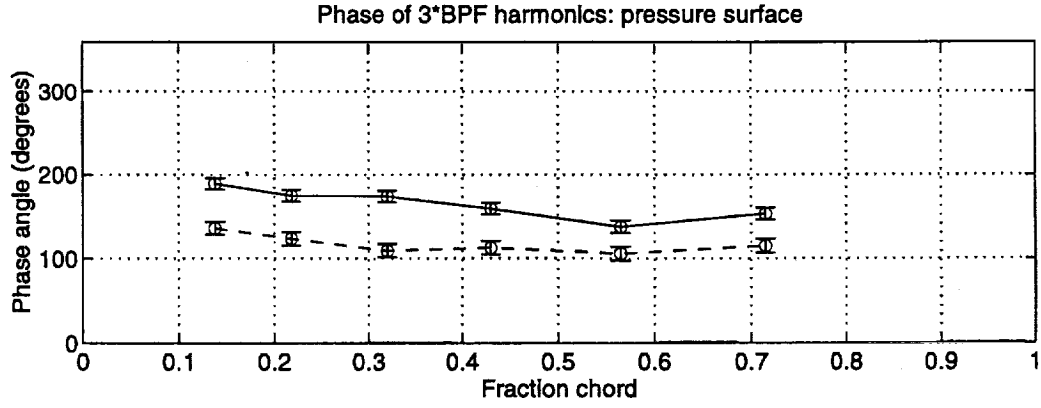

Figure C-12: Harmonic phases of stator pressure surface at 50% span. (—)w/o blowing, (- -)w/ blowing

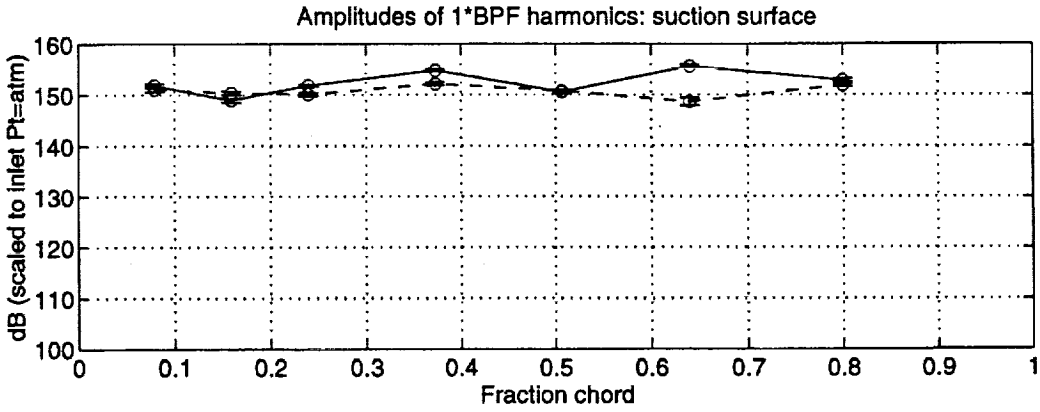

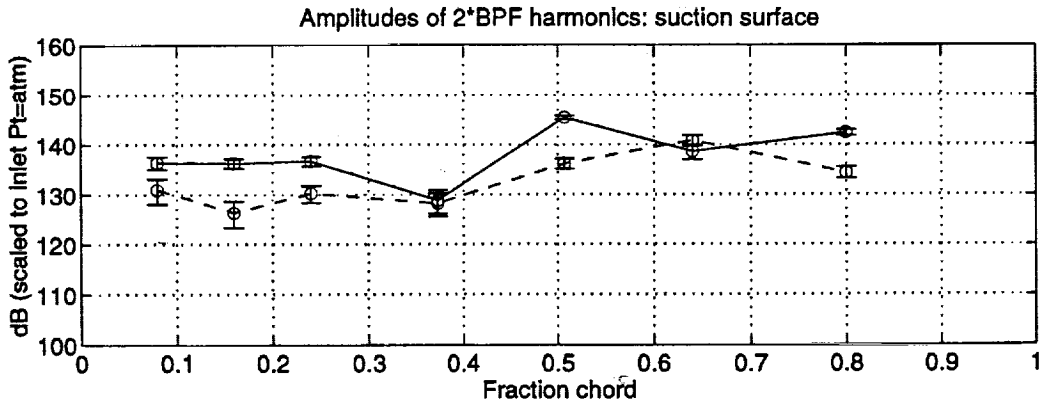

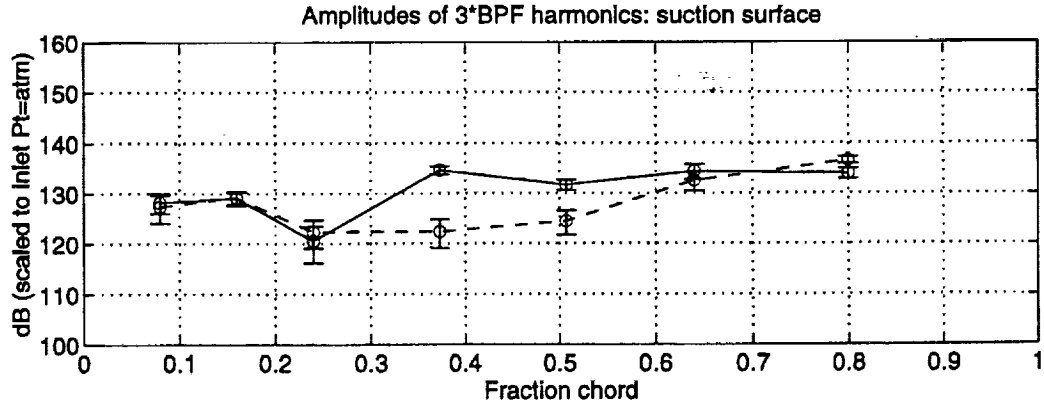

Figure C-13: Harmonic amplitudes of stator suction surface at 75% span. (—)w/o blowing, (- -)w/ blowing

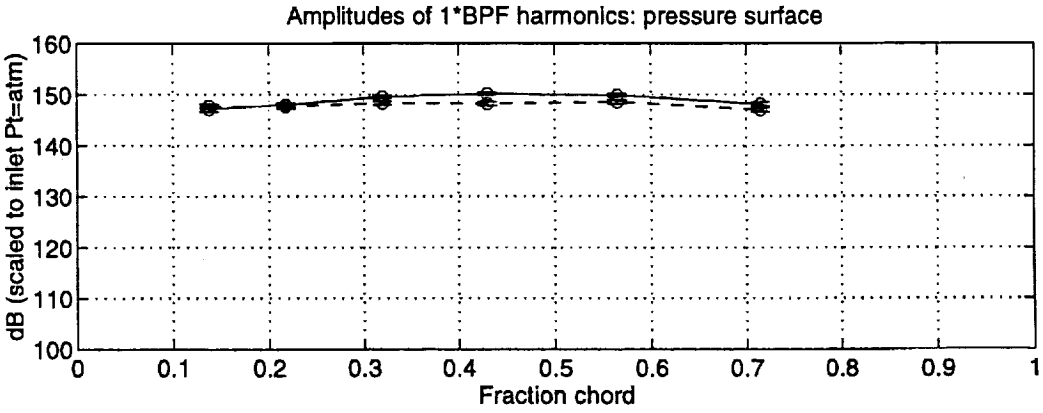

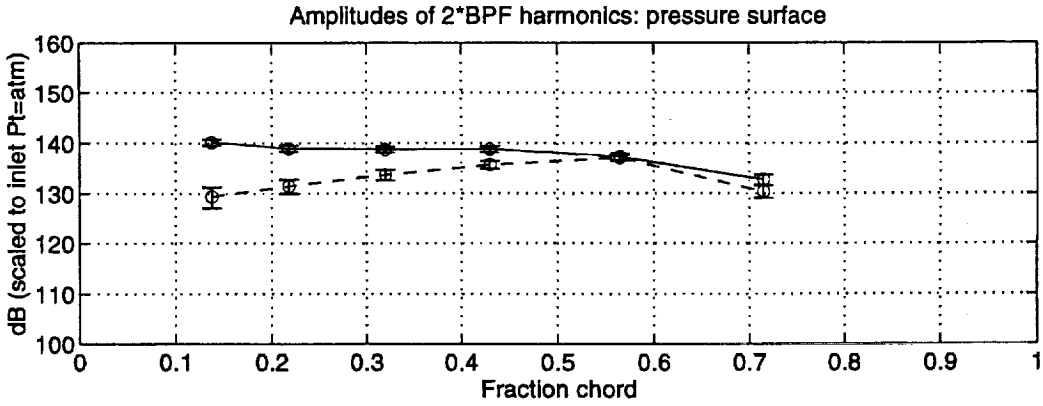

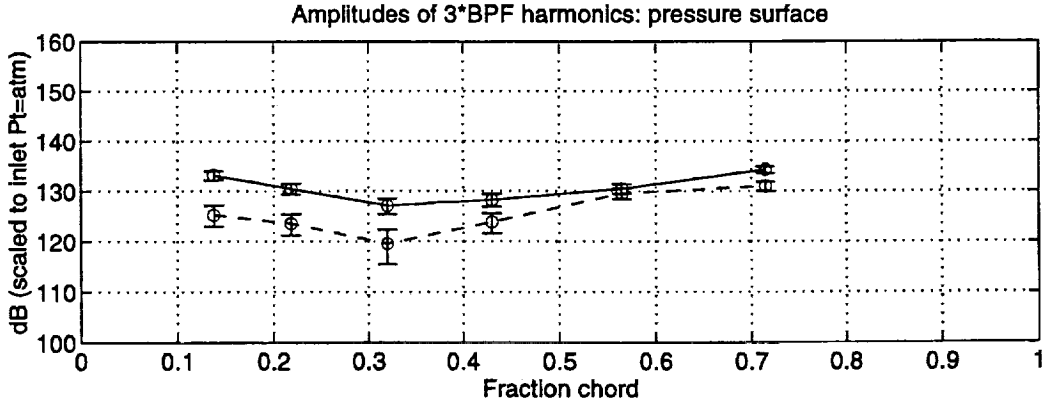

Figure C-14: Harmonic amplitudes of stator pressure surface at 75% span. (—)w/o blowing, (- -)w/ blowing

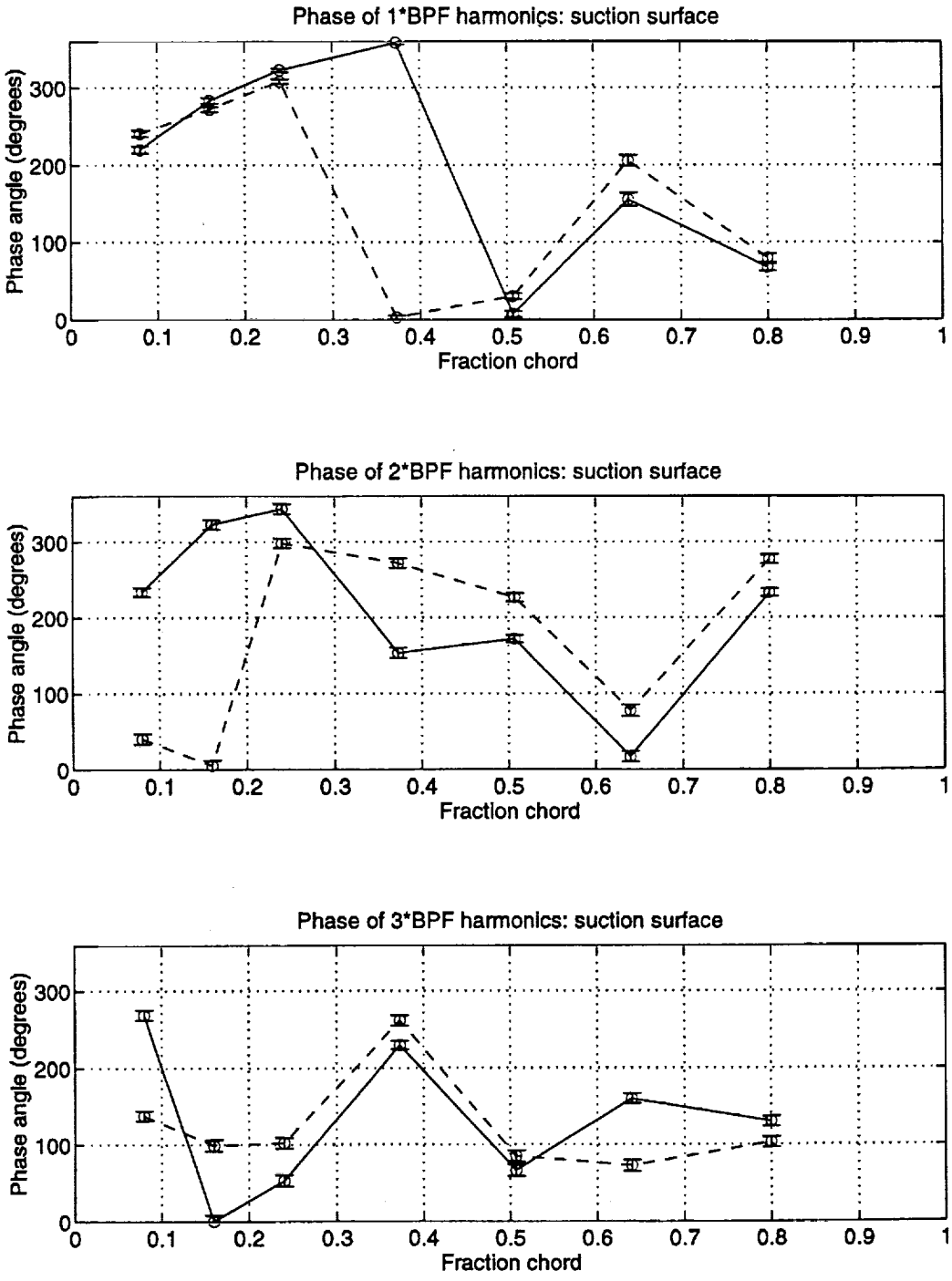

Figure C-15: Harmonic phases of stator suction surface at 75% span. (—)w/o blowing, (- -)w/ blowing

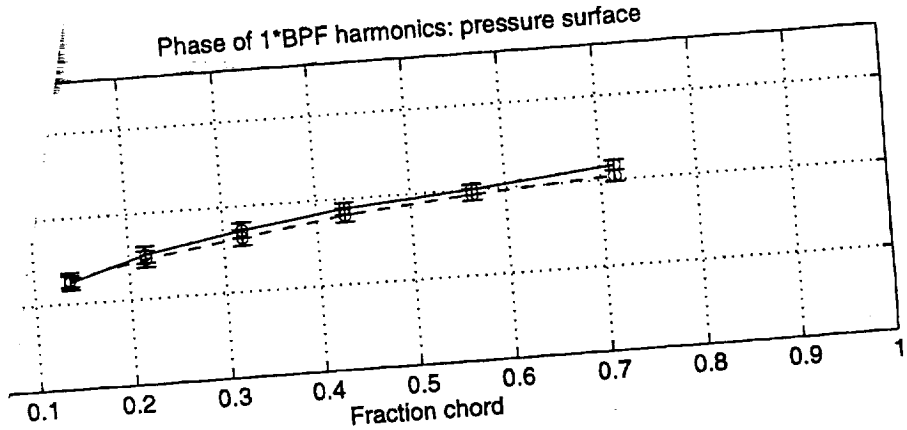

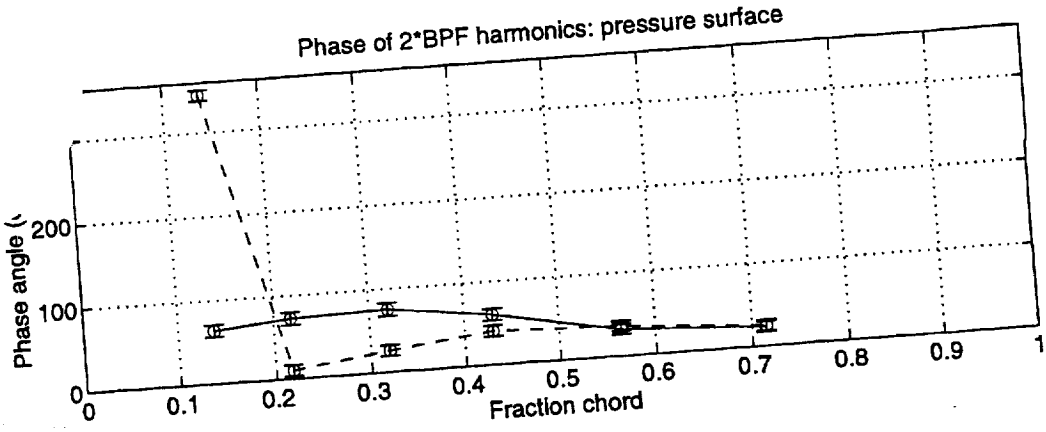

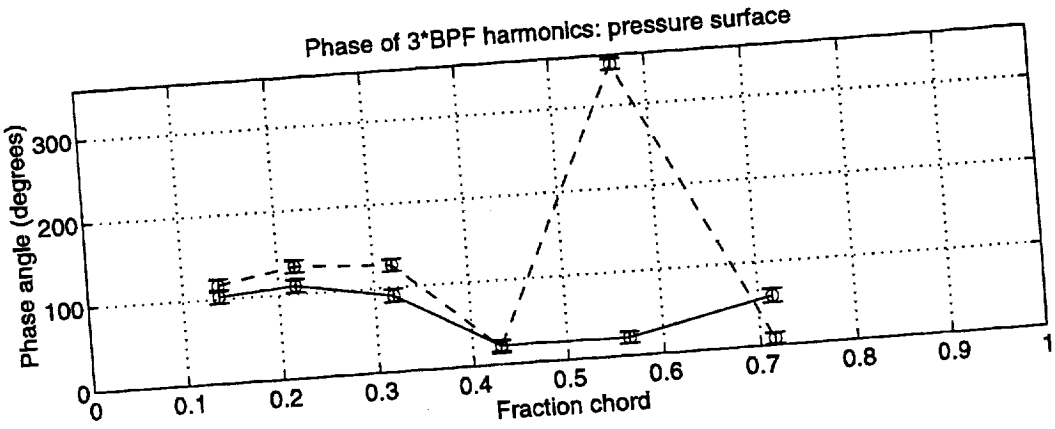

Figure C-16: Harmonic phases of stator pressure surface at 75% span. (—)w/o blowing, (- -)w/ blowing

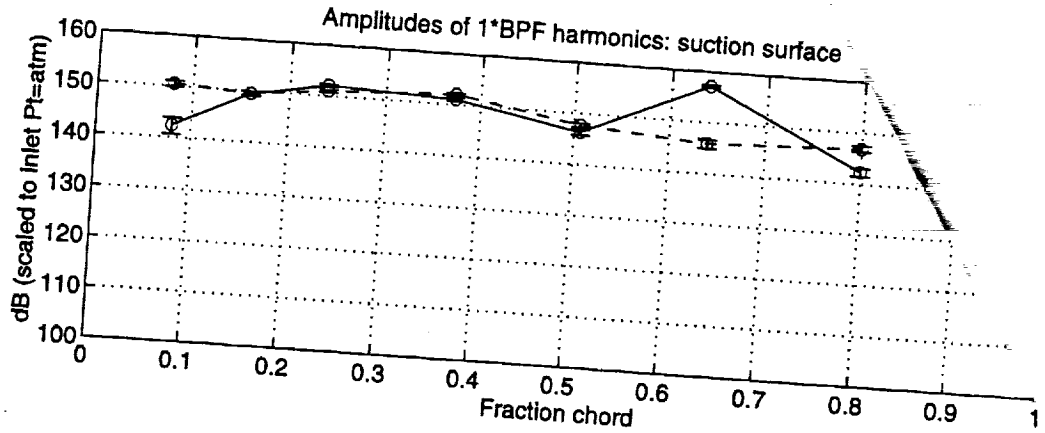

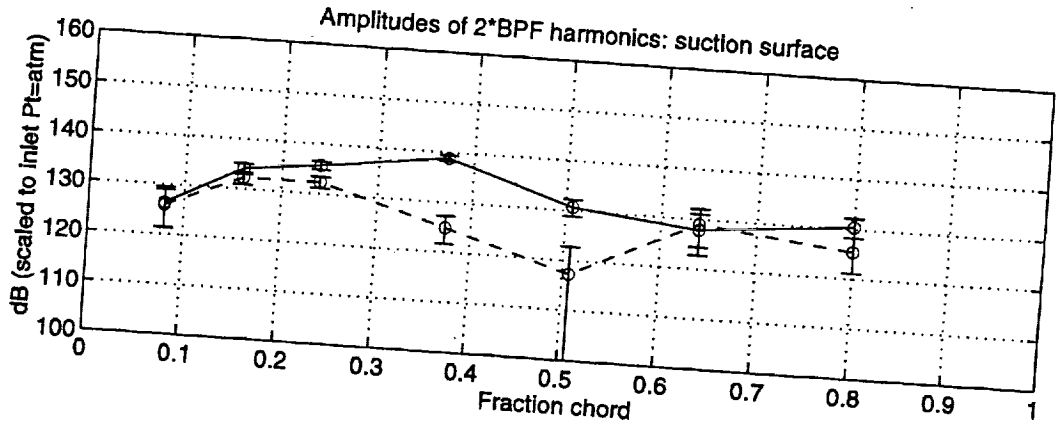

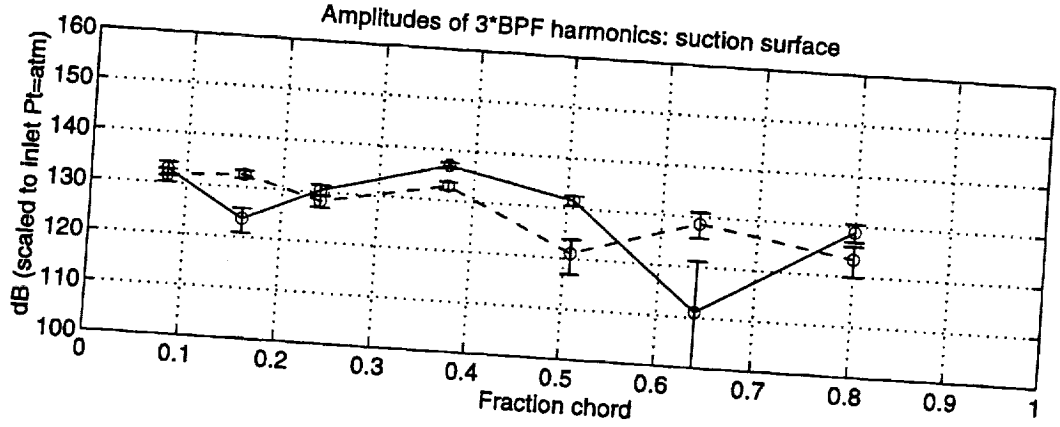

Figure C-17: Harmonic amplitudes of stator suction surface at 87.5% span. (—)w/o blowing, (- -)w/ blowing

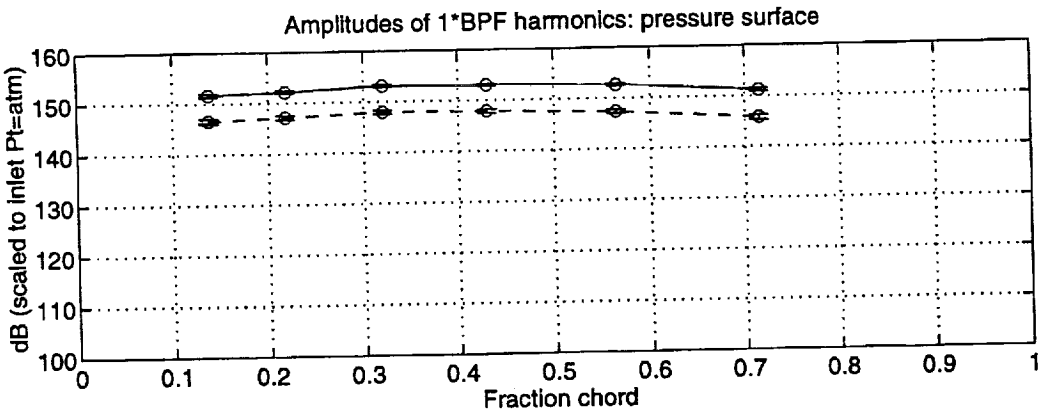

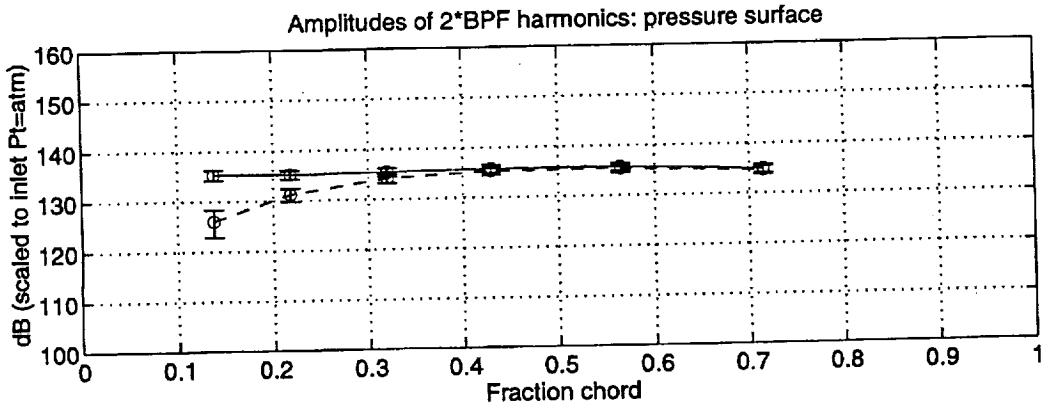

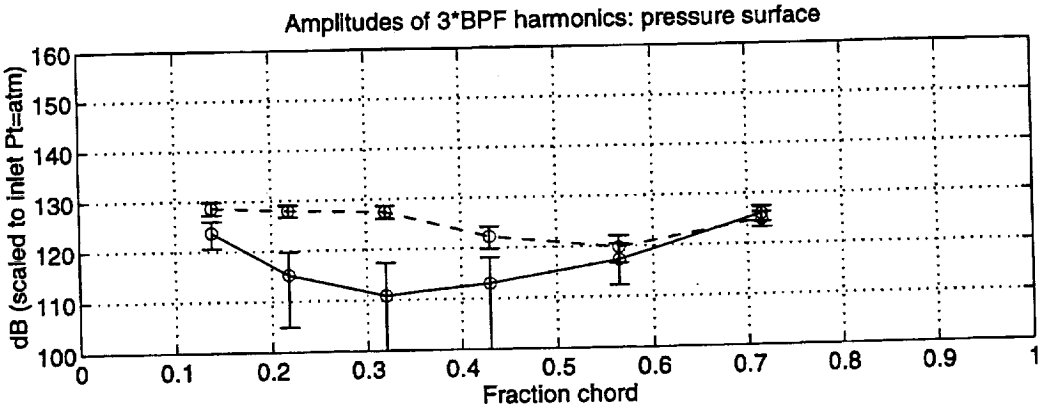

Figure C-18: Harmonic amplitudes of stator pressure surface at 87.5% span. (—)w/o blowing, (- -)w/ blowing

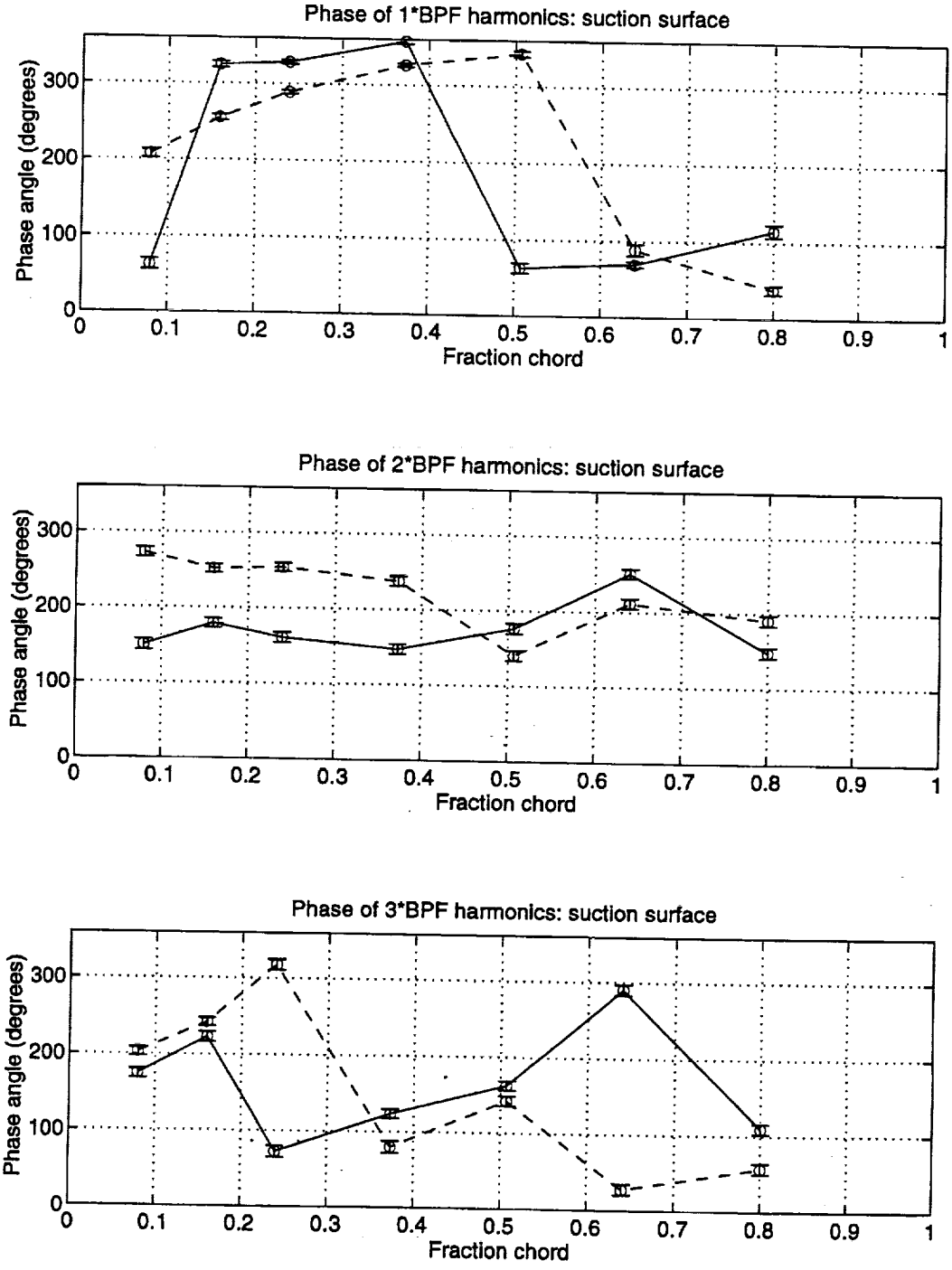

Figure C-19: Harmonic phases of stator suction surface at 87.5% span. (—)w/o blowing, (- -)w/ blowing

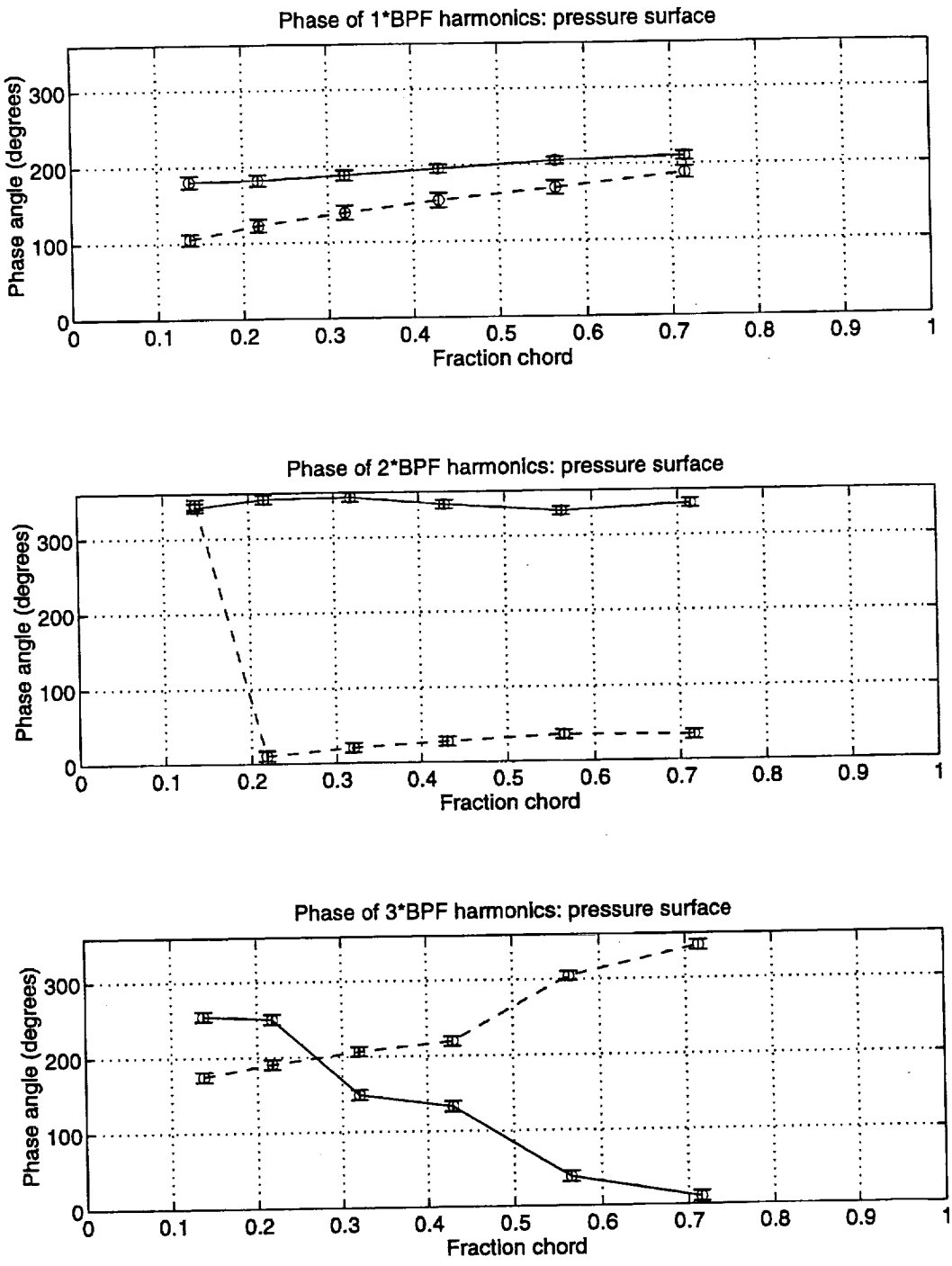

Figure C-20: Harmonic phases of stator pressure surface at 87.5% span. (—)w/o blowing, (- -)w/ blowing

BIBLIOGRAPHY

[1] *Current Market Outlook, 1999.* Boeing Aircraft Corporation, http://www.boeing.com/commercial/cmo.

[2] *Environmental Review, 1996.* International Air Transport Association.

[3] BROOKFIELD, J. *Turbofan Rotor/Stator Interaction Noise Reduction Through Trailing Edge Blowing.* PhD thesis, Massachusetts Institute of Technology, Cambridge, MA, June 1998.

[4] BROOKFIELD, J., AND WAITZ, I. "Trailing Edge Blowing for Reduction of Turbomachinery Fan Noise". AIAA 98-2321, 4th AIAA/CEAS Aeroacoustics Conference, Toulouse, France, June 1998.

[5] CORCORAN, T. "Control of the Wake from a Simulated Blade by Trailing Edge Blowing". Master's thesis, Lehigh University, Bethelem, PA, 1992.

[6] DRELA, M. "Two-Dimensional Transonic Aerodynamic Design and Analysis Using the Euler Equations". Gas Turbine Lab 187, Massachusetts Institute of Technology, Cambridge, MA, 1986.

[7] GOLDSTEIN, M., AND ATASSI, H. "A Complete Second-Order Theory for the Unsteady Flow About an Airfoil Due to a Periodic Gust". *Journal of Fluid Mechanics, Vol. 74* (1976).

[8] HANSON, D. "Influence of Lean and Sweep on Noise of Cascades with Turbulent Inflow". AIAA 99-1863, 5th AIAA/CEAS Aeroacoustics Conference, Bellevue, WA, May 1999.

[9] HORLOCK, J. "Fluctuating Lift Forces on Airfoils Moving Through Transverse and Chordwise Gusts". *ASME Journal of Basic Engineering, Vol. 90*, No. 4 (Dec. 1968).

[10] IDELCHIK, I. *Handbook of Hydraulic Resistance, 3rd Edition.* Begell House, Inc, 1996.

[11] KERREBROCK, J. "The MIT Blowdown Compressor Facility". Gas Turbine Lab 108, Massachusetts Institute of Technology, Cambridge, MA, 1972.

[12] LEITCH, T. "Reduction of Unsteady Rotor-Stator Interaction Using Trailing Edge Blowing". Master's thesis, Virginia Polytechnic Institute and State University, Blacksburg, VA, 1997.

[13] LEITCH, T., SAUNDERS, C., AND NG, W. "Reduction of Unsteady Stator-Rotor Interaction Using Trailing Edge Blowing". AIAA 99-1952, 5th AIAA/CEAS Aeroacoustics Conference, Bellevue, WA, May 1999.

[14] NALLASAMY, M., AND ENVIA, E. "Computation of Far-Field Tone Noise Levels for Radial and Swept and Leaned Stators". AIAA 99-186, 5th AIAA/CEAS Aeroacoustics Conference, Bellevue, WA, May 1999.

[15] NASA. *Aeroacoustics of Flight Vehicles: Theory Practice, Volumes 1&2, NASA RP-1258* (1991).

[16] NAUMANN, H., AND YEH, H. "Lift and Pressure Fluctuations of a Cambered Airfoil Under Periodic Gusts and Applications in Turbomachinery". *ASME Journal of Engineering for Power, Vol. 95* (Jan 1973), pp. 1–10.

[17] NAUMANN, R. "Control of the Wake from a Simulated Blade by Trailing Edge Blowing". Master's thesis, Lehigh University, Bethlehem, PA, 1992.

[18] PARK, W., AND CIMBALA, J. "The Effect of Jet Injection Geometry on Two-Dimensional Momentumless Wakes". *Journal of Fluid Mechanics, Vol. 224* (March 1991), pp. 29–47.

[19] REIJNEN, D. *An Experimental Study of Boundary Layer Suction in a Transonic Compressor.* PhD thesis, Massachusetts Institute of Technology, Cambridge, MA, Feb. 1997.

[20] SEARS, W. R. "Some Aspects of Non-Stationary Airfoil Theory and Its Practical Application". *Journal of the Aeronautical Sciences, Vol. 8*, No. 3 (1941).

[21] SELL, J. "Cascade Testing to Assess the Effectiveness of Mass Addition/Removal Wake Management Strategies for Reduction of Rotor-Stator Interaction Noise". Master's thesis, Massachusetts Institute of Technology, Cambridge, MA, Feb. 1997.

[22] WAITZ, I., BROOKFIELD, J., SELL, J., AND HAYDEN, B. "Preliminary Assessment of Wake Management Strategies for Reduction of Turbomachinery Fan Noise". *AIAA Journal of Propulsion and Power, Vol. 12*, No. 5 (Sept.-Oct. 1996), pp. 958–966.

[23] ZIMINSKY, W. "Design of a high pressure ratio transonic compressor stage with active boundary layer control". Master's thesis, Massachusetts Institute of Technology, 1996.